REPORT 1217

CONTENTS

REPORT 1217

THEORETICAL PREDICTION OF PRESSURE DISTRIBUTIONS ON NONLIFTING AIRFOILS AT HIGH SUBSONIC SPEEDS [1]

By JOHN R. SPREITER and ALBERTA ALKSNE

SUMMARY

Theoretical pressure distributions on nonlifting circular-arc airfoils in two-dimensional flows with high subsonic free-stream velocity are found by determining approximate solutions, through an iteration process, of an integral equation for transonic flow proposed by Oswatitsch. The integral equation stems directly from the small-disturbance theory for transonic flow. This method of analysis possesses the advantage of remaining in the physical, rather than the hodograph, variables and can be applied to airfoils having curved surfaces. After discussion of the derivation of the integral equation and qualitative aspects of the solution, results of calculations carried out for circular-arc airfoils in flows with free-stream Mach numbers up to unity are described. These results indicate most of the principal phenomena observed in experimental studies. At subcritical Mach numbers, the pressure distribution is symmetrical about the midchord position and the drag is zero. The magnitude of the pressure coefficient is found to increase more rapidly with increasing Mach number than the Prandtl-Glauert rule would indicate. When the critical Mach number is exceeded, compression shocks occur, the fore-and-aft symmetry of the pressure distribution is lost, and the airfoil experiences a drag force. As the Mach number is increased further, the shock wave becomes of greater intensity and moves rearward along the chord, thereby producing a rapid increase in the magnitude of the pressure drag coefficient. At Mach numbers close to unity, the variation of the pressure, local Mach number, and drag conforms, within the limitations of transonic small perturbation theory, to the known trends associated with the Mach number freeze. Some comparisons with experimental results are also included.

The solutions are obtained using an iteration process which differs from the classical methods in that the quadratic nature of the integral equation is recognized. If the iteration calculations are started using the linear-theory solution, it is shown that the retention of the quadratic feature has the interesting effect of forbidding shock-free supercritical second-order solutions. In order to obtain solutions for supercritical Mach numbers, it is necessary to start the iteration calculations with a velocity or pressure distribution which contains a compression shock. When this is done, it is found that the iteration procedure converges to a definite result.

[1] Supersedes NACA TN 3096 by John R. Spreiter and Alberta Alksne, March 1954.

INTRODUCTION

The theoretical problem of transonic flow about thin wings has been discussed by numerous authors in recent years. Since the basic equations are nonlinear and of mixed type, the difficulties are great, and progress has been made only through expenditure of considerable effort. At first, only the basic equations and the similarity rules were established. (See refs. 1 through 12.) More recently, a small number of actual solutions have been determined. At the present time, the most complete theoretical results are those of Guderley and Yoshihara, Vincenti and Wagoner, Cole, and Trilling (refs. 13 through 18) for the flow about wedge airfoils at both subsonic and supersonic speeds. These were all obtained by transforming the equations to hodograph variables whereby the differential equation becomes linear although still of mixed type. Superposition of solutions is then possible, but the boundary conditions generally become very complicated. It is because of the latter difficulty that all the solutions mentioned above are for wedge sections. A further disadvantage of the hodograph method is that it is definitely restricted to two-dimensional flows, there being no known transformation which linearizes the equation for three-dimensional compressible flows.

If the hodograph transformation is not introduced, there are available no direct methods of solution. However, various iteration methods have been used to study flows with high subsonic free-stream velocities. (See ref. 19 for a résumé.) Almost all these account for the compressibility effects by source distributions throughout the flow field and start with either the solution for incompressible flow or for linearized compressible flow as the first approximation. A second approximation is calculated from the first and so on. It was not found possible, however, to iterate starting with a typical shock-free subsonic flow solution and obtain a typical transonic flow field in which the supersonic region ends with a shock.

Oswatitsch has presented another method in references 20 and 21 for determining the transonic pressure distribution on thin airfoils in flows with subsonic free-stream velocity. The analysis is carried out in the physical rather than the

hodograph variables, and leads to a nonlinear integral equation in which the unknown velocity appears outside as well as inside the integral. Oswatitsch finds approximate solutions not by iteration, but by introducing various functions containing undetermined parameters into the integral equation and by determining the parameters so that the integral equation is satisfied at a small number of points on the airfoil. The method is applied to determine the pressure distribution on circular-arc and NACA symmetrical four-digit airfoils. The results show certain characteristics of transonic flow such as the appearance of shock waves and their rearward movement across the chord with increasing Mach number. It is disconcerting, however, that the method fails to give proper results at high subsonic Mach numbers (greater than about 0.88 for 6-percent-thick circular-arc sections), provides a multiplicity of solutions at supercritical Mach numbers, and permits the integral equation to be satisfied at only a very limited number of points.

The present work is based on the integral equation of Oswatitsch but an iteration process is used to obtain approximate solutions. This procedure permits the integral equation to be satisfied at a much larger number of points than in the original method of Oswatitsch, gives approximate solutions at all Mach numbers up to unity, and appears to avoid any multiplicity of solutions. The method is applied to determine the theoretical pressure distribution on symmetrical circular-arc airfoils at zero angle of attack. Except for phenomena that are primarily of viscous origin, such as boundary-layer separation, etc., these results exhibit most of the experimentally observed features of transonic flows.

Attention is also called to reference 22 by Gullstrand, an associate of Oswatitsch, in which transonic flows about thin air foils are investigated by still another extension of Oswatitsch's integral-equation theory. Gullstrand sought to determine approximate solutions by iteration, although his procedure differs considerably from that described herein. His method, however, succeeded in determining solutions only when the Mach number was less than about 0.90 for 6-percent-thick sections. Results were given for the pressure distribution at sonic speed in a second paper by Gullstrand (ref. 23), but they were obtained by introducing a new and more complicated integral equation than that of Oswatitsch used herein. In contrast to the present analysis in which the entire solution is obtained from the integral equation, Gullstrand uses the integral equation to determine only the solution for the forward part of the airfoil and uses the method of characteristics to complete the solution for the rear of the airfoil. Further work of Gullstrand is presented in references 24 and 25.

A list of symbols is contained in Appendix A.

BASIC EQUATIONS

The basic equations necessary for the discussion of inviscid transonic flow consist of a set of partial differential equations relating the velocity components and their gradients at every point, together with the auxiliary relation giving the velocity jump through a shock wave For thin airfoils inclined at zero or small angles of attack, the differential equations can be simplified by assuming that the shock waves are sufficiently weak that the flow is irrotational and isentropic, thereby permitting the introduction of a velocity potential Φ. The quasi-linear partial differential equation satisfied by Φ can be expressed in the form

$$(a^2-\Phi_x^2)\,\Phi_{xx}+(a^2-\Phi_y^2)\,\Phi_{yy}+(a^2-\Phi_z^2)\,\Phi_{zz}-2\Phi_x\Phi_y\Phi_{xy}-2\Phi_y\Phi_z\Phi_{yz}-2\Phi_z\Phi_x\Phi_{xz}=0 \quad (1)$$

where the subscript notation is used to indicate differentiation and a is the local speed of sound given by the relation

$$a^2=a_0^2-\frac{\gamma-1}{2}(\Phi_x^2+\Phi_y^2+\Phi_z^2-U_0^2) \quad (2)$$

In this latter equation U_o and a_o are, respectively, the free-stream velocity and the speed of sound in the free stream, and γ is the ratio of specific heats (for air, $\gamma=1.4$).

It is convenient to introduce the perturbation velocity potential φ, where

$$\varphi=-U_o x+\Phi \quad (3)$$

If it is assumed that all perturbation velocities and perturbation velocity gradients (represented by first and second derivatives, respectively, of φ) are small and that only the first-order terms in small quantities need be retained, equation (1) simplifies to the well-known Prandtl-Glauert equation of linear theory

$$(1-M_o^2)\varphi_{xx}+\varphi_{yy}+\varphi_{zz}=0 \quad (4)$$

where the free-stream velocity is directed along the positive x axis as shown in figure 1 and where $M_o=U_o/a_o$ is the Mach number of the free stream. It is well known that equation (4) leads to useful results in the study of subsonic and supersonic flow about thin wings and slender bodies but that it is incapable, in general, of treating transonic flows. The failure of linear theory in the transonic range is evidenced by the calculated values of φ_x growing to such magnitude that they can no longer be regarded as small quantities when compared with U_o.

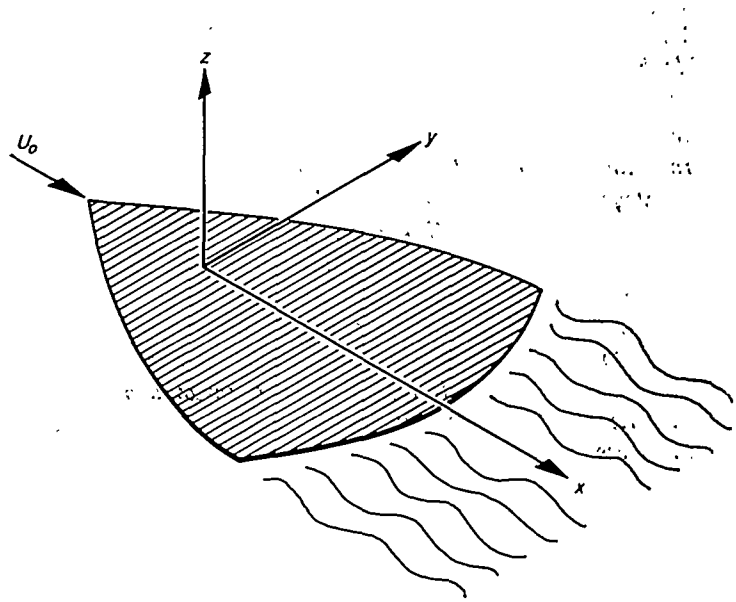

FIGURE 1.—View of wing and coordinate system.

Second-order theory for thin wings would involve solution of the equation

$$(1-M_0^2)\varphi_{xx}+\varphi_{yy}+\varphi_{zz}=M_0^2\left[\frac{\gamma+1}{U_0}\varphi_x\varphi_{xx}+\frac{\gamma-1}{U_0}\varphi_x(\varphi_{yy}+\varphi_{zz})+\frac{2}{U_0}(\varphi_y\varphi_{xy}+\varphi_z\varphi_{xz})\right] \tag{5}$$

(See ref. 26, p. 140.) Actually, we are interested in retaining higher-order terms only to the extent that is necessary to allow the study of transonic flow. Examination of the known properties of transonic flow fields indicates that the first term on the right can often become of importance and should be retained. It is assumed in the small-disturbance theory of transonic flow (refs. 1 through 25), however, that the remainder of the terms on the right can be safely disregarded. The simplified equation is

$$(1-M_0^2)\varphi_{xx}+\varphi_{yy}+\varphi_{zz}=M_0^2\frac{\gamma+1}{U_0}\varphi_x\varphi_{xx}=k\varphi_x\varphi_{xx} \tag{6}$$

where

$$k=M_o^2\frac{\gamma+1}{U_o} \tag{7}$$

As a result of minor differences in the perturbation analysis, recent papers have used at least three other expressions for k. This point will be discussed further at the conclusion of the present section.

Equation (6) is valid only in regions where the necessary derivatives exist and are continuous. Since these conditions do not hold where shock waves occur, an additional equation is needed for the transition through the shock. The necessary equation is provided by the classical relation for the shock polar (e. g., ref. 26, p. 108).

$$\tilde{v}_b^2+\tilde{w}_b^2=(\tilde{u}_a-\tilde{u}_b)^2\frac{\tilde{u}_a\tilde{u}_b-a^{*2}}{\frac{2}{\gamma+1}\tilde{u}_a^2-\tilde{u}_a\tilde{u}_b+a^{*2}} \tag{8}$$

where $\tilde{u}$, $\tilde{v}$, and $\tilde{w}$ refer to Cartesian velocity components with $\tilde{u}$ being parallel to the flow direction ahead of the shock, the subscripts a and b refer to conditions ahead of and behind the shock, and a^* is the critical sound velocity, which can be expressed in terms of U_o and M_o as follows:

$$\frac{a^*}{U_o}=\sqrt{\frac{\gamma-1}{\gamma+1}+\frac{2}{M_o^2(\gamma+1)}} \tag{9}$$

The appropriate simplified equation is obtained from equation (8) by resolving the velocities into components parallel to the axes of the coordinate system and carrying out a small-perturbation analysis analogous to that performed in the derivation of equation (6). In this way, the following relation is found between the perturbation velocity components on the two sides of the shock wave:

$$(1-M_o^2)(u_a-u_b)^2+(v_a-v_b)^2+(w_a-w_b)^2=M_o^2\frac{\gamma+1}{U_o}\left(\frac{u_a+u_b}{2}\right)(u_a-u_b)^2=k\left(\frac{u_a+u_b}{2}\right)(u_a-u_b)^2 \tag{10}$$

where u, v, and w are the perturbation velocity components parallel to the x, y, and z axes. This equation corresponds to the shock-polar curve for shock waves of small strength inclined at any angle between that of normal shock waves and that of the Mach lines. On either side of the shock wave, the perturbation velocity components are related to the perturbation velocity potential in the usual manner

$$u=\frac{\partial\varphi}{\partial x},\quad v=\frac{\partial\varphi}{\partial y},\quad w=\frac{\partial\varphi}{\partial z} \tag{11}$$

In addition to satisfying the differential equation and the shock-wave equation, the perturbation potential must provide flows compatible with the following physical requirements: (a) the perturbation velocities must vanish far ahead of the wing and (b) the flow must be tangential to the wing surface. Therefore, the following boundary conditions are to be specified for the perturbation potential:

at $x=-\infty$

$$\left(\frac{\partial\varphi}{\partial x}\right)_0=\left(\frac{\partial\varphi}{\partial y}\right)_0=\left(\frac{\partial\varphi}{\partial z}\right)_0=0 \tag{12}$$

at the wing surface W

$$\frac{1}{U_o}\left(\frac{\partial\varphi}{\partial z}\right)_W=\frac{\partial Z}{\partial x} \tag{13}$$

where $\partial Z/\partial x$ is the local slope of the wing surface in the x direction. Furthermore, it is consistent with the assumption of small disturbances to satisfy the second boundary condition on the two sides of the xy plane rather than on the actual wing surface. Equation (13) thus becomes

$$\frac{1}{U_o}\left(\frac{\partial\varphi}{\partial z}\right)_W\approx\frac{1}{U_o}\left(\frac{\partial\varphi}{\partial z}\right)_{z=0}=\frac{\partial Z}{\partial x}=\tau\frac{\partial}{\partial(x/c)}f\left(\frac{x}{c},\frac{y}{s}\right) \tag{14}$$

where the shape of the wing profile is given by

$$\frac{Z}{c}=\tau f\left(\frac{x}{c},\frac{y}{s}\right) \tag{15}$$

In addition, it is presumed necessary to prescribe that the direct influence of a disturbance in the supersonic region proceeds only in the downstream direction and that the Kutta condition applies whenever the flow velocity at the trailing edge is subsonic.

Upon solving the above boundary-value problem for the potential, one may determine the pressure coefficient for planar systems by means of the formula

$$C_p\equiv\frac{p-p_o}{\frac{\rho_o}{2}U_o^2}=-\frac{2}{U_o}\frac{\partial\varphi}{\partial x} \tag{16}$$

COMPARISON WITH OTHER STATEMENTS OF THE TRANSONIC-FLOW EQUATIONS

As a result of minor variations in the perturbation analysis, recent papers have used at least four different relations for k, the coefficient of the nonlinear term in the simplified equation for the perturbation velocity potential. As indicated in the

preceding paragraphs, straightforward development of second-order theory leads to the relation

$$k=M_o^2\frac{\gamma+1}{U_o} \tag{7}$$

This is sometimes simplified (e. g., refs. 8, 10, and 12) to

$$k=\frac{\gamma+1}{U_o} \tag{17}$$

by arguing that M_o can be set equal to unity in this term without any loss in accuracy since the right-hand side of equation (6) is merely an approximation to allow the treatment of transonic flows and rapidly diminishes in magnitude as M_o departs from unity. In some treatments (e. g., refs. 7 and 23), equation (1) is divided by a^2 and the quotient $1/a^2$ in each term is expanded in a binomial series. When this is done, the coefficient k of the term involving $\varphi_x\varphi_{xx}$ is

$$k=M_o^2\left[\frac{2+(\gamma-1)M_o^2}{U_o}\right] \tag{18}$$

Still another expression for k is used by Oswatitsch in the papers that form the principal references for the present work. Two derivations are given, one based on mass-flow considerations (ref. 21) and the other (ref. 20) on simplifying equation (1) under the assumption of nearly parallel flow to

$$(1-M^2)\varphi_{xx}+\varphi_{yy}+\varphi_{zz}=0 \tag{19}$$

and substituting the following series for the variable coefficient $(1-M^2)$:

$$1-M^2=1-M_o^2-\frac{1-M_o^2}{a^*-U_o}\frac{\partial\varphi}{\partial x}+\cdots \tag{20}$$

where M is the local Mach number and a^* is the critical sound velocity as defined in equation (9). Comparison of equations (19) and (20) with equation (6) shows that the coefficient k in this approximation is

$$k=\frac{1-M_o^2}{a^*-U_o} \tag{21}$$

A similar situation arises in the derivation of the simplified equation for the shock polar. Here again the precise form of the expression for the coefficient k of equation (10) depends on the details of the perturbation analysis. The most important point from the present point of view is that the same expression for k is used in both the equation for the potential and that for the shock polar, namely, equations (6) and (10). While this point has not always been explicitly stated, it is actually a necessary condition for the existence of the well-known transonic similarity rules.

The foregoing discussion has been based on equations obtained by assuming that the local velocities are only slightly different from the free-stream velocity. On the other hand, many of the recent papers on transonic flow about wings and bodies have been based on equations obtained by assuming that the local velocities are only slightly different from the critical sound velocity a^*. (See refs. 1 through 6, 9, and 13 through 18.) It is shown in reference 12, however, that the pressure, force, and moment results obtained using these equations are identical with those obtained using the present equations if k is selected as given in equation (17). These results, however, can be easily converted to those that would be obtained using any of the other expressions for k by simply replacing $(\gamma+1)/U_o$ by k wherever it occurs.

In order to facilitate comparison with previous results and to achieve an economy of notation, the present analysis is carried as far as possible without specifying a particular relation for k. That is, the equations of the analysis and the reduced parameters with which the results are expressed are written containing k which may be equated to any of the four stated expressions. However, the actual values of the pressure coefficient and Mach number for an airfoil of specific thickness ratio depend on which relation is selected for k. The present calculations have been made using the expression for k given in equation (7). The principal reason for this choice is that it appears to provide a set of equations, or a mathematical model, which approximates certain essential features of transonic flow with superior accuracy. Before proceeding with discussion of this point, it should be noted that the four alternative expressions for k are identical for $M_o=1$, and all but that given by equation (17) are zero for $M_o=0$.

A significant case where the four relations lead to different results is the prediction of the variation with free-stream Mach number of the critical pressure coefficient $C_{p_{cr}}$, defined as the value of the pressure coefficient C_p at a point where the local Mach number is unity. It is important that a reasonably good approximation be maintained for the variation of $C_{p_{cr}}$ with M_o because shock waves make their first appearance and the airfoil first experinces a pressure drag when C_p becomes more negative than $C_{p_{cr}}$ somewhere on the airfoil surface. In the present approximation, $C_{p_{cr}}$ corresponds to that value of C_p and, hence, of φ_x, at which equation (6) changes locally from elliptic to hyperbolic type. This condition is recognized by the vanishing of the coefficient of φ_{xx}, thus

$$1-M_o^2-k(\varphi_x)_{cr}=0$$

or, in view of equation (16)

$$C_{p_{cr}}=-\frac{2}{U_o}(\varphi_x)_{cr}=-\frac{2}{kU_o}(1-M_o^2) \tag{22}$$

The exact relation for isentropic flow is (e. g., ref. 27, p. 28)

$$C_{p_{cr}}=\frac{2}{\gamma M_o^2}\left[\left(\frac{2}{\gamma+1}+\frac{\gamma-1}{\gamma+1}M_o^2\right)^{\frac{\gamma}{\gamma-1}}-1\right] \tag{23}$$

The variation of $C_{p_{cr}}$ with M_o has been computed using the exact relation and each of the four approximate relations. The results are presented graphically in figure 2. It may be seen that a reasonably good approximation for $C_{p_{cr}}$ is obtained over a wide Mach number range when k is taken as $Mo^2(\gamma+1)/U_o$ or $(1-M_o^2)/(a^*-U_o)$, and that a somewhat greater error is incurred when k is equated to $M_o^2[2+$

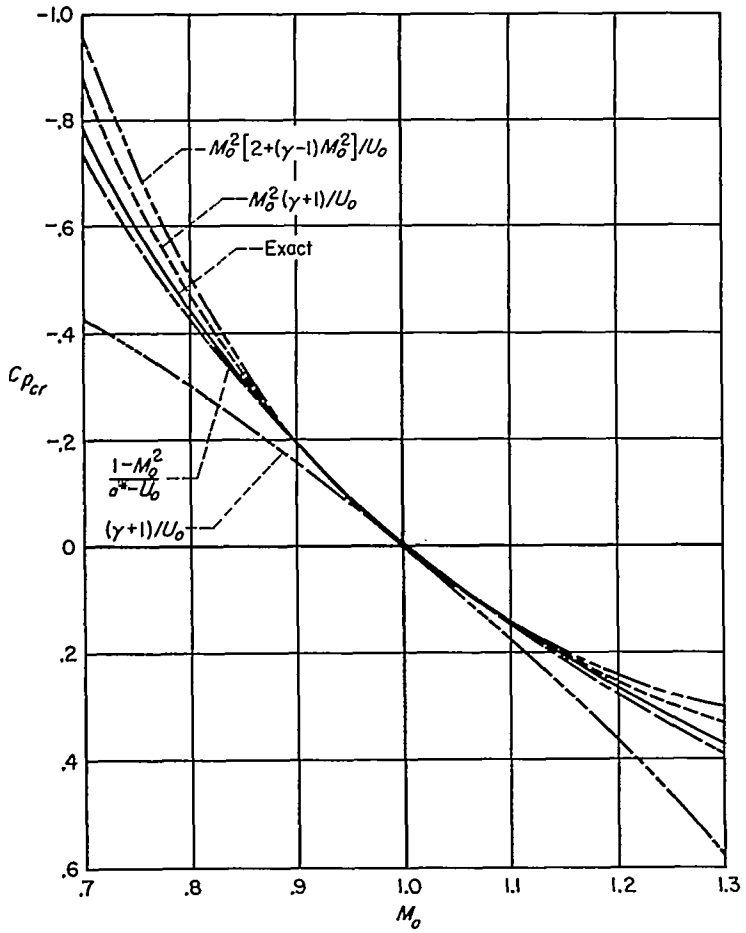

FIGURE 2.—Variation, approximate and exact, of critical pressure coefficient with free-stream Mach number.

$(\gamma-1)M_o^2]/U_o$. On the other hand, a very poor approximation results if k is equated to $(\gamma+1)/U_o$.

Similar comparisons can be made for local Mach numbers M other than unity by noting that the coefficient $(1-M_o^2-k\varphi_x)$ of φ_{xx} in equation (6) corresponds, in the present approximation, to $1-M^2$, thus,

$$1-M^2=1-M_o^2-k\varphi_x=1-M_o^2+\frac{kU_o}{2}C_p \tag{24}$$

The corresponding exact relation for isentropic flow is

$$C_p=\frac{2}{\gamma M_o^2}\left[-1+\left(\frac{1+\frac{\gamma-1}{2}M_o^2}{1+\frac{\gamma-1}{2}M^2}\right)^{\frac{\gamma}{\gamma-1}}\right] \tag{25}$$

The results so obtained are generally similar to those indicated in Figure 2 although the relative accuracy of the better approximations changes somewhat with the situation. All the approximations are exact, of course, when $C_p=0$. On the other hand, none of the approximations are exact, except for isolated cases, when C_p is different from zero, even though all of the approximations agree among themselves when the free-stream Mach number is unity. In order to provide some information regarding the errors that are likely to be incurred when C_p is not very small, figure 3 has been prepared illustrating the variation of local Mach

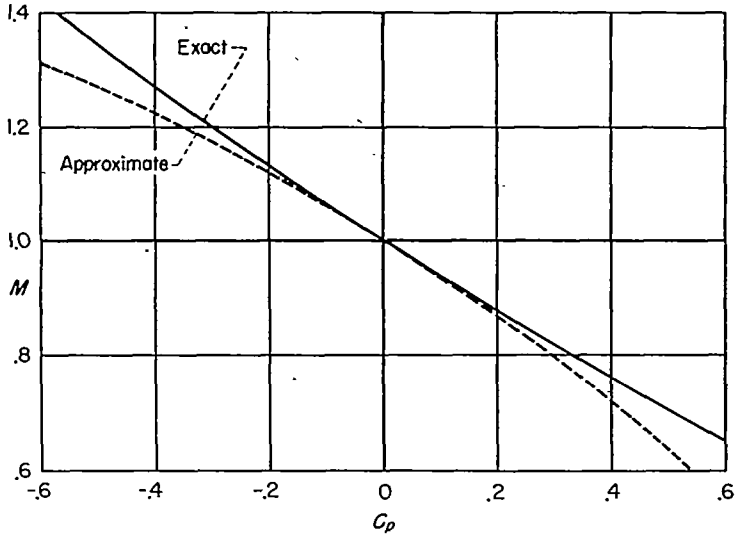

FIGURE 3.—Variation, approximate and exact, of local Mach number with pressure coefficient, $M_o=1$.

number with pressure coefficient for a free-stream Mach number of unity.

A second case where the exact and approximate relations can be compared is furnished by considering the velocity jump through a shock wave. If the flow ahead of the shock wave is uniform and parallel to the x axis, the results may conveniently be represented by the shock-polar diagram in which $\sqrt{\tilde{v}_b^2+\tilde{w}_b^2}$ is plotted as a function of $\tilde{u}_b$. The exact relation is furnished by equation (8). The corresponding approximate relations are determined from equation (10) by setting u_a, v_a, and w_a to zero, whereby

$$v_b^2+w_b^2=\left[-(1-M_o^2)+\frac{k}{2}u_b\right]u_b^2 \tag{26}$$

Once the variation of $(v_b^2+w_b^2)$ with u_b is determined for a given M_o, the corresponding variation of $(\tilde{v}_b^2+\tilde{w}_b^2)$ with $\tilde{u}_b$ may be readily determined since, for this case,

$$\tilde{u}_b=U_o+u_b, \qquad \tilde{v}_b=v_b, \qquad \tilde{w}_b=w_b \tag{27}$$

The variation of $\sqrt{\tilde{v}_b^2+\tilde{w}_b^2}$ with $\tilde{u}_b$ for $M_o=1.2$ has been computed using both the exact and approximate relations, and the results are presented graphically in conventional shock-polar form in figure 4.

It is evident from this comparison that the best approximation to the shock-polar curve is that obtained by equating k to $M_o^2(\gamma+1)/U_o$. Since all shock waves are assumed to be normal to the flow direction in the course of the present

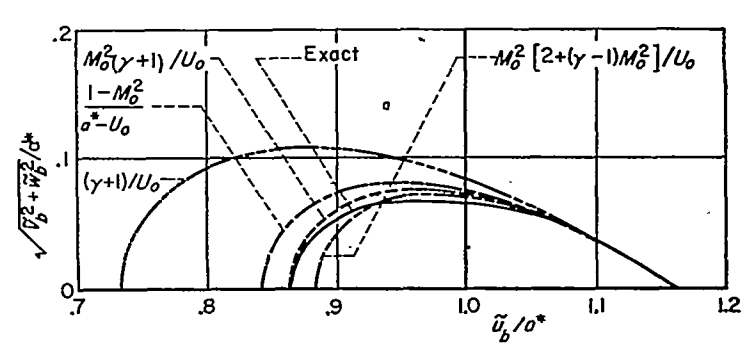

FIGURE 4.—Approximate and exact shock polar diagram, $M_o=1.2$.

analysis, a notable point is that this expression for k leads to the exact relation for the velocity jump through a normal shock wave.

In problems such as we are considering here, the final test is provided by comparison with experimental results. Although both experimental and theoretical results for the transonic speed range are limited, complete information does exist at the present time for the drag of a single-wedge section followed by a straight section extending far downstream. (See refs. 13, 14, 16, 28, and 29.) The theoretical results were determined originally using equations obtained by assuming that the local velocities are only slightly different from the critical sound velocity a^* and are therefore identical with those that would be obtained using the present equations, provided k is equated to $(\gamma+1)U_o$. Figure 5 shows the theoretical and experimental results plotted in

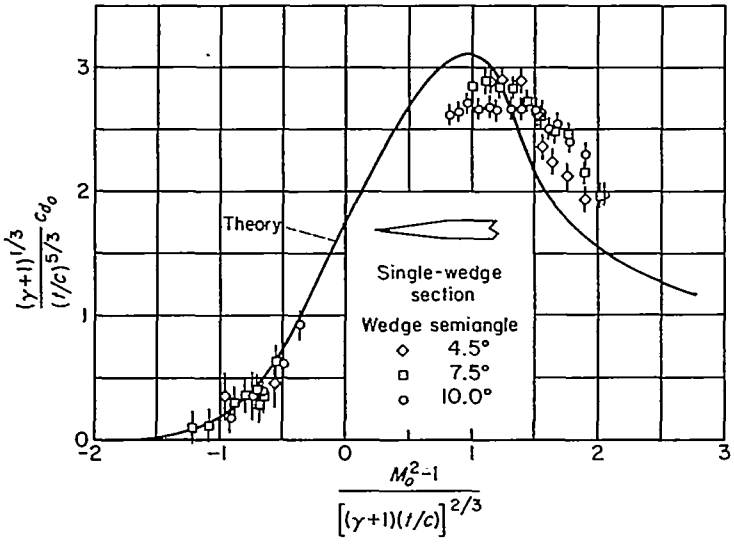

FIGURE 5.—Theoretical and experimental drag results for a single wedge section, $k=\frac{\gamma+1}{U_o}$.

the same manner as in the original papers. The small vertical lines on the experimental data points represent the uncertainty of the values. This figure indicates that the theoretical and experimental results are only in general qualitative agreement when $k=(\gamma+1)U_o$.

The same results are replotted in figure 6 with k equated to $M_o^2(\gamma+1)/U_o$ rather than $(\gamma+1)/U_o$. It can be seen that the theoretical and experimental results are now in nearly perfect agreement. Comparison of figures 5 and 6 provides striking evidence supporting the contention that k should be equated to $M_o^2(\gamma+1)/U_o$ rather than $(\gamma+1)/U_o$.

DERIVATION OF INTEGRAL EQUATIONS FOR TRANSONIC FLOW

In order to make the present work more self-contained, a derivation of the integral equations for transonic flows having subsonic free-stream velocities will be presented even though this has been done previously by both Oswatitsch and Gullstrand (refs. 20, 21, and 22). The present derivation, in common with that of Gullstrand, proceeds through the application of Green's theorem in a manner closely analogous to that employed in linearized wing theory (e. g.,

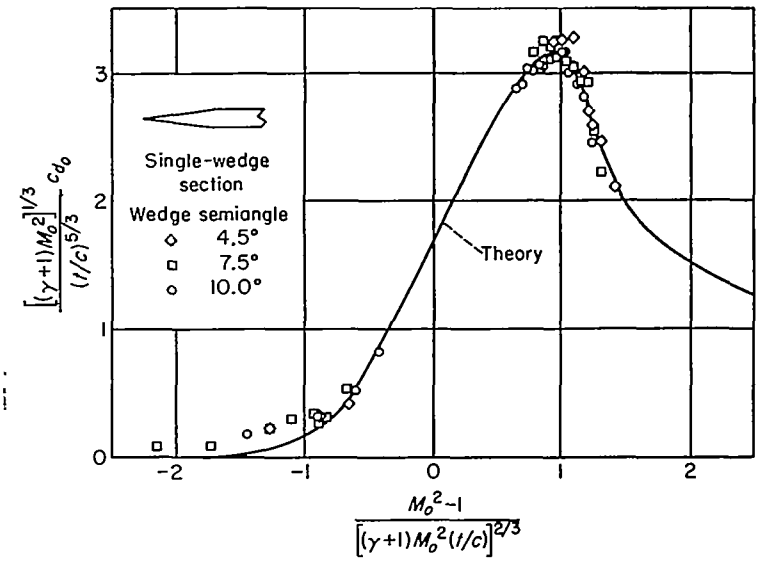

FIGURE 6.—Theoretical and experimental drag results for a single wedge section, $k=\frac{M_o^2(\gamma+1)}{U_o}$.

ref. 30), except that proper cognizance must be taken of the shock discontinuities and of the additional nonlinear term in the differential equation for the perturbation velocity potential. For the sake of completeness and to illustrate the simplifications introduced by making additional restrictions and assumptions, the derviation will be carried through for lifting wings of finite thickness and span, even though the applications contained herein will be confined to two-dimensional flow about symmetrical airfoil sections at zero angle of attack.

The differential equation fundamental to the following discussion is equation (6).

$$(1-M_o^2)\frac{\partial^2\varphi}{\partial x^2}+\frac{\partial^2\varphi}{\partial y^2}+\frac{\partial^2\varphi}{\partial z^2}=k\frac{\partial\varphi}{\partial x}\frac{\partial^2\varphi}{\partial x^2} \tag{6}$$

Since the principal object of the following analysis is to determine the pressure which, according to equation (16), is linearly proportional to the perturbation velocity component u, it is convenient to work with an equivalent equation for u obtained by differentiating equation (6) with respect to x; it is

$$(1-M_o^2)\frac{\partial^2 u}{\partial x^2}+\frac{\partial^2 u}{\partial y^2}+\frac{\partial^2 u}{\partial z^2}=k\frac{\partial^2}{\partial x^2}\left(\frac{u^2}{2}\right) \tag{28}$$

It is advantageous to normalize the equations by letting

$$\bar{x}=x, \quad \bar{y}=\beta y, \quad \bar{z}=\beta z, \quad \bar{\varphi}=\frac{k}{\beta^2}\varphi$$

$$\bar{u}=\frac{\partial\bar{\varphi}}{\partial\bar{x}}=\frac{k}{\beta^2}u, \quad \bar{v}=\frac{\partial\bar{\varphi}}{\partial\bar{y}}=\frac{k}{\beta^3}v, \quad \bar{w}=\frac{\partial\bar{\varphi}}{\partial\bar{z}}=\frac{k}{\beta^3}w \tag{29}$$

where

$$\beta=\sqrt{1-M_o^2}$$

In this way, equations (6) and (28) reduce to the following:

$$\frac{\partial^2\bar{\varphi}}{\partial\bar{x}^2}+\frac{\partial^2\bar{\varphi}}{\partial\bar{y}^2}+\frac{\partial^2\bar{\varphi}}{\partial\bar{z}^2}=\nabla^2\bar{\varphi}=\frac{\partial\bar{\varphi}}{\partial\bar{x}}\frac{\partial^2\bar{\varphi}}{\partial\bar{x}^2} \tag{30}$$

$$\frac{\partial^2\bar{u}}{\partial\bar{x}^2}+\frac{\partial^2\bar{u}}{\partial\bar{y}^2}+\frac{\partial^2\bar{u}}{\partial\bar{z}^2}=\nabla^2\bar{u}=\frac{\partial^2}{\partial\bar{x}^2}\left(\frac{\bar{u}^2}{2}\right) \tag{31}$$

Before proceeding, it should be noted that the introduction of the reduced perturbation velocity component $\bar{u}$ permits the ready recognition of regions of subsonic and supersonic velocities and emphasizes the points at which sonic velocity occurs. This relationship becomes immediately apparent upon substituting the definition of $\bar{u}$ into equation (24). Thus,

$$\frac{1-M^2}{1-M_o^2}=1-\frac{k}{1-M_o^2}u=1-\bar{u} \tag{32}$$

from which it is clear, for flows having subsonic free-stream Mach numbers ($M_o<1$), that $\bar{u}<1$ when the local velocity is subsonic, $\bar{u}=1$ when it is sonic, and $\bar{u}>1$ when it is supersonic.

As noted above, the derivation proceeds from Green's theorem which relates a volume integral over a region R to a surface integral over the surface Σ enclosing R. If σ and Ω are any two functions which, together with their first and second derivatives, are finite and single-valued throughout R, Green's theorem states

$$\iint_{\Sigma}\left(\sigma\frac{\partial\Omega}{\partial n}-\Omega\frac{\partial\sigma}{\partial n}\right)d\Sigma=-\iiint_{R}(\sigma\nabla^2\Omega-\Omega\nabla^2\sigma)\,dR \tag{33}$$

where the directional derivatives on the left side are taken along the normal n, drawn inward, to the surface Σ. It is convenient to let $\Omega=\bar{u}$ and to choose σ as the fundamental solution $1/r_3$ of the equation $\nabla^2\sigma=0$

$$\sigma=\frac{1}{r_3}=\frac{1}{[(\bar{x}-\bar{\xi})^2+(\bar{y}-\bar{\eta})^2+(\bar{z}-\bar{\zeta})^2]^{1/2}} \tag{34}$$

whereby equation (33) becomes

$$\iint_{\Sigma}\left[\frac{1}{r_3}\frac{\partial\bar{u}}{\partial n}-\bar{u}\frac{\partial}{\partial n}\left(\frac{1}{r_3}\right)\right]d\Sigma=-$$

$$\iiint_{R}\frac{1}{r_3}\nabla^2\bar{u}\,dR=-\iiint_{R}\frac{1}{r_3}\frac{\partial^2}{\partial\bar{\xi}^2}\left(\frac{\bar{u}^2}{2}\right)dR \tag{35}$$

The variables of integration in the equation are $\bar{\xi}$, $\bar{\eta}$, $\bar{\zeta}$ while $\bar{x}$, $\bar{y}$, $\bar{z}$ are the coordinates of a point P. It must be observed that $1/r_3$ is singular at $r_3=0$ and $\bar{u}$ is discontinuous at the shock wave. The point P and the shock wave must, therefore, be excluded from the region R. The exclusion of P from the region R is accomplished by enclosing it within a small sphere. The shock wave is excluded by altering the boundary of the region so that it goes around the shock wave. In this way, equation (35) may be applied to the region R_u bounded by the $\bar{x}\bar{y}$ plane and a hemispherical dome of infinite radius lying above this plane, exclusive of the subregions surrounding P and the shock wave (see fig. 7). Since, furthermore, the values of $\bar{u}$ may be assumed to diminish sufficiently rapidly with distance that the contributions of

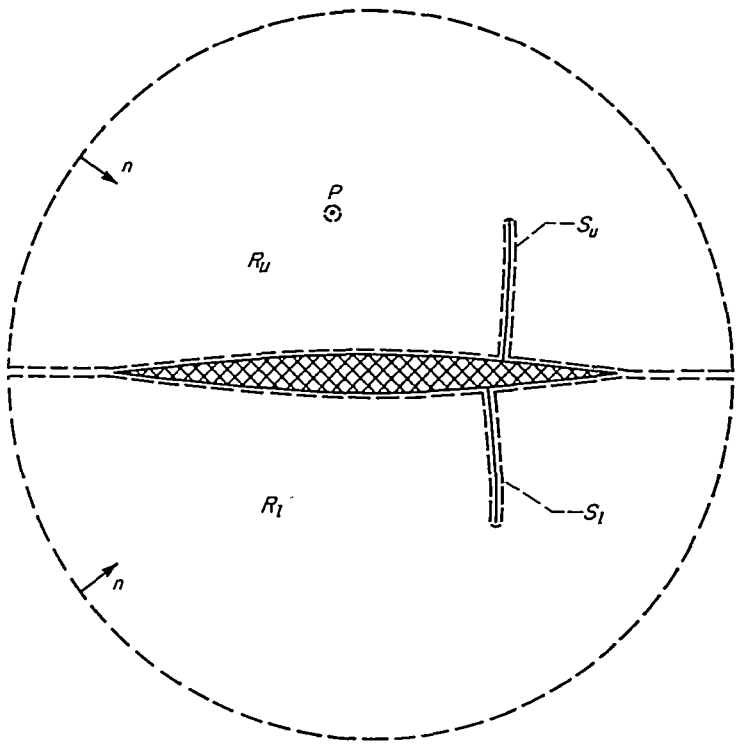

FIGURE 7.—Region of integration.

the integrals over the hemisphere vanish, the following result is obtained:

$$\bar{u}(\bar{x},\bar{y},\bar{z})=-\frac{1}{4\pi}\int_{-\infty}^{+\infty}\iint\left[\frac{1}{r_3}\frac{\partial\bar{u}_u}{\partial\bar{\zeta}}-\bar{u}_u\frac{\partial}{\partial\bar{\zeta}}\left(\frac{1}{r_3}\right)\right]d\bar{\xi}d\bar{\eta}-$$

$$\frac{1}{4\pi}\iint_{S_u}\left\{\left[\frac{1}{r_3}\frac{\partial\bar{u}}{\partial n}-\bar{u}\frac{\partial}{\partial n}\left(\frac{1}{r_3}\right)\right]_a+\right.$$

$$\left.\left[\frac{1}{r_3}\frac{\partial\bar{u}}{\partial n}-\bar{u}\frac{\partial}{\partial n}\left(\frac{1}{r_3}\right)\right]_b\right\}dS-\frac{1}{4\pi}\iiint_{R_u}\frac{1}{r_3}\frac{\partial^2}{\partial\bar{\xi}^2}\left(\frac{\bar{u}^2}{2}\right)dR \tag{36}$$

where the subscript u denotes conditions on the upper side of the $\bar{x}\bar{y}$ plane, the subscripts a and b denote values immediately ahead of and behind the shock wave, and S is the surface of the shock wave. The volume integral is defined as follows when P is ahead of S. (For sake of brevity, ψ is written in place of $\frac{1}{r_3}\frac{\partial^2}{\partial\bar{\xi}^2}\left(\frac{\bar{u}^2}{2}\right)$.)

$$\iiint_{R_u}\frac{1}{r_3}\frac{\partial^2}{\partial\bar{\xi}^2}\left(\frac{\bar{u}^2}{2}\right)dR\equiv\iiint_{R_u}\psi dR=$$

$$\lim_{\substack{\epsilon_1\to 0\\ \epsilon_2\to 0}}\int_{-\infty}^{+\infty}d\bar{\eta}\int_{0}^{+\infty}d\bar{\zeta}\left(\int_{-\infty}^{x_P-\epsilon_1}\psi d\bar{\xi}+\int_{x_P+\epsilon_1}^{x_S-\epsilon_2}\psi d\bar{\xi}+\int_{x_S+\epsilon_2}^{+\infty}\psi d\bar{\xi}\right) \tag{37}$$

It is clear that the corresponding definition of the volume integral when P is behind S can be obtained by rearranging the limits of integration. If P is kept fixed in the upper

half space and the region R_l bounded by the $\bar{x}\bar{y}$ plane and a hemispherical dome of infinite radius lying below this plane is considered, it follows in a similar manner that

$$0=\frac{1}{4\pi}\int_{-\infty}^{+\infty}\iint\left[\frac{1}{r_3}\frac{\partial\bar{u}_l}{\partial\bar{\zeta}}-\bar{u}_l\frac{\partial}{\partial\bar{\zeta}}\left(\frac{1}{r_3}\right)\right]d\bar{\xi}d\bar{\eta}-\frac{1}{4\pi}\iint_{S_l}\left\{\left[\frac{1}{r_3}\frac{\partial\bar{u}}{\partial n}-\bar{u}\frac{\partial}{\partial n}\left(\frac{1}{r_3}\right)\right]_a+\left[\frac{1}{r_3}\frac{\partial\bar{u}}{\partial n}-\bar{u}\frac{\partial}{\partial n}\left(\frac{1}{r_3}\right)\right]_b\right\}dS-\frac{1}{4\pi}\iiint_{R_l}\frac{1}{r_3}\frac{\partial^2}{\partial\bar{\xi}^2}\left(\frac{\bar{u}^2}{2}\right)dR \tag{38}$$

where the subscript l denotes conditions on the lower side of the $\bar{x}\bar{y}$ plane and the volume integral is defined as follows:

$$\iiint_{R_l}\frac{1}{r_3}\frac{\partial^2}{\partial\bar{\xi}^2}\left(\frac{\bar{u}^2}{2}\right)dR\equiv\iiint_{R_l}\psi dR=\lim_{\epsilon_2\to 0}\int_{-\infty}^{+\infty}d\bar{\eta}\int_{-\infty}^{0}d\bar{\zeta}\left\{\int_{-\infty}^{x_S-\epsilon_2}\psi d\bar{\xi}+\int_{x_S+\epsilon_2}^{+\infty}\psi d\bar{\xi}\right\} \tag{39}$$

Introducing the notation

$$\Delta\bar{u}=\bar{u}_u-\bar{u}_l,\quad \Delta\frac{\partial\bar{u}}{\partial\bar{\zeta}}=\frac{\partial\bar{u}_u}{\partial\bar{\zeta}}-\frac{\partial\bar{u}_l}{\partial\bar{\zeta}} \tag{40}$$

and adding equations (36) and (38), we have

$$\bar{u}(\bar{x},\bar{y},\bar{z})=-\frac{1}{4\pi}\iint_{W}\left[\frac{1}{r_3}\Delta\frac{\partial\bar{u}}{\partial\bar{\zeta}}-\Delta\bar{u}\frac{\partial}{\partial\bar{\zeta}}\left(\frac{1}{r_3}\right)\right]d\bar{\xi}d\bar{\eta}-\frac{1}{4\pi}\iint_{S}\left\{\left[\frac{1}{r_3}\frac{\partial\bar{u}}{\partial n}-\bar{u}\frac{\partial}{\partial n}\left(\frac{1}{r_3}\right)\right]_a+\left[\frac{1}{r_3}\frac{\partial\bar{u}}{\partial n}-\bar{u}\frac{\partial}{\partial n}\left(\frac{1}{r_3}\right)\right]_b\right\}dS-\frac{1}{4\pi}\iiint_{R}\frac{1}{r_3}\frac{\partial^2}{\partial\bar{\xi}^2}\left(\frac{\bar{u}^2}{2}\right)dR \tag{41}$$

where the surface integral over S represents the sum of the corresponding integrals over S_u and S_l and the volume integral over R represents the sum of the integrals over R_u and R_l. The integrand of the first integral of equation (41) is zero over all of the $\bar{x}\bar{y}$ plane except the surface W of the wing sufficiently extended to include the effect of the edge singularities and is, in certain cases, exactly equal to the value of $\bar{u}$ given by the linearized theory of subsonic flow about thin wings (e. g., ref. 30).

$$\bar{u}_L=-\frac{1}{4\pi}\iint_{W}\left[\frac{1}{r_3}\Delta\frac{\partial\bar{u}_L}{\partial\bar{\zeta}}-\Delta\bar{u}_L\frac{\partial}{\partial\bar{\zeta}}\left(\frac{1}{r_3}\right)\right]d\bar{\xi}d\bar{\eta} \tag{42}$$

It can be seen that the first integral of equation (41) may be equated to $\bar{u}_L$ when the problem is one in which

$$\Delta\bar{u}=\Delta\bar{u}_L$$

and

$$\Delta(\partial\bar{u}/\partial\bar{\zeta})=\Delta(\partial\bar{u}/\partial\bar{\zeta})_L$$

This condition exists in those problems where $\Delta\bar{u}$ and $\Delta(\partial\bar{u}/\partial\bar{\zeta})$ are prescribed at the outset by the boundary conditions; for example, (a) given the loading on a lifting surface, find the camber distribution; (b) given the shape of a symmetrical nonlifting airfoil, find the pressure distribution.

Equation (41) can be regarded as the final integral equation for $\bar{u}$, but it is advantageous for the forthcoming analysis to perform two more operations. They are to integrate the volume integral twice by parts with respect to $\bar{\xi}$, taking proper cognizance of the definitions given in equations (37) and (39), and to decompose the surface integral over the shock wave into components parallel to the axes of the coordinate system. In this way, the following equation is obtained:

$$\bar{u}=-\frac{1}{4\pi}\iint_{W}\left[\frac{1}{r_3}\Delta\frac{\partial\bar{u}}{\partial\bar{\zeta}}-\Delta\bar{u}\frac{\partial}{\partial\bar{\zeta}}\left(\frac{1}{r_3}\right)\right]d\bar{\xi}d\bar{\eta}+\frac{\bar{u}^2}{2}-\frac{1}{4\pi}\iiint_{R}\frac{\bar{u}^2}{2}\frac{\partial^2}{\partial\bar{\xi}^2}\left(\frac{1}{r_3}\right)d\bar{\xi}d\bar{\eta}d\bar{\zeta}+\frac{1}{4\pi}\iint_{S}\left[\left[\frac{1}{r^3}\frac{\partial}{\partial\bar{\xi}}\left(\bar{u}-\frac{\bar{u}^2}{2}\right)-\left(\bar{u}-\frac{\bar{u}^2}{2}\right)\frac{\partial}{\partial\bar{\xi}}\left(\frac{1}{r_3}\right)\right]_a-\left[\frac{1}{r_3}\frac{\partial}{\partial\bar{\xi}}\left(\bar{u}-\frac{\bar{u}^2}{2}\right)-\left(\bar{u}-\frac{\bar{u}^2}{2}\right)\frac{\partial}{\partial\bar{\xi}}\left(\frac{1}{r_3}\right)\right]_b+\left\{\left[\frac{1}{r_3}\frac{\partial\bar{u}}{\partial\bar{\eta}}-\bar{u}\frac{\partial}{\partial\bar{\eta}}\left(\frac{1}{r_3}\right)\right]_a-\left[\frac{1}{r_3}\frac{\partial\bar{u}}{\partial\bar{\eta}}-\bar{u}\frac{\partial}{\partial\bar{\eta}}\left(\frac{1}{r_3}\right)\right]_b\right\}\left[\frac{\cos(n,\bar{\eta})}{\cos(n,\bar{\xi})}\right]_b+\left\{\left[\frac{1}{r_3}\frac{\partial\bar{u}}{\partial\bar{\zeta}}-\bar{u}\frac{\partial}{\partial\bar{\zeta}}\left(\frac{1}{r_3}\right)\right]_a-\left[\frac{1}{r_3}\frac{\partial\bar{u}}{\partial\bar{\zeta}}-\bar{u}\frac{\partial}{\partial\bar{\zeta}}\left(\frac{1}{r_3}\right)\right]_b\right\}\left[\frac{\cos(n,\bar{\zeta})}{\cos(n,\bar{\xi})}\right]_b\right]d\bar{\eta}d\bar{\zeta} \tag{43}$$

Although the integration by parts of the triple integral performed in going from equation (41) to (43) may seem somewhat arbitrary, the resulting equation is superior from the point of view of obtaining approximate solutions. For example, the triple integral of equation (41) shows a very strong influence of the velocities in the region immediately surrounding P since they are multiplied by $1/r_3$. This influence is largely nullified in the triple integral of equation (43) because part of the region has a negative influence and part has a positive influence. The predominant influence in the latter case is furnished by the term $\bar{u}^2/2$ standing outside the integral. The contribution of distant regions is also diminished in importance in the triple integral of equation (43) since their influence varies inversely with the third power of the distance, rather than the first power as in equation (41). The advantages of using the formulation provided by equation (43) will become more evident on examining Appendix B and the section entitled "Subcritical flows."

A further advantage is that the value of the triple integral of equation (43) is continuous through a shock wave rather than discontinuous as is the case with equation (41). A point of great importance in the approximate solution described herein arises from the fact that the integration by parts provides extra terms (those containing $\bar{u}^2/2$) in the integrals along the shock surface S which combine with those already present in such a way that the contribution of these integrals becomes very small when the shock waves approach normal waves, as is usually the case at high subsonic speeds.

In addition to satisfying the integral equation for $\bar{u}$ given in equation (43), the velocity components on opposite sides of shock waves must be in accord with the simplified relation for the shock polar given in equation (10). This equation may be rewritten in normalized form by introducing the quantities defined in equation (29), thus

$$(\bar{u}_a-\bar{u}_b)^2+(\bar{v}_a-\bar{v}_b)^2+(\bar{w}_a-\bar{w}_b)^2=\left(\frac{\bar{u}_a+\bar{u}_b}{2}\right)(\bar{u}_a-\bar{u}_b)^2 \tag{44}$$

Two alternative forms of equation (44) are the following:

$$\left(1-\frac{\bar{u}_a+\bar{u}_b}{2}\right)(\bar{u}_a-\bar{u}_b)^2+(\bar{v}_a-\bar{v}_b)^2+(\bar{w}_a-\bar{w}_b)^2=0 \tag{45}$$

and

$$(\bar{u}_a-\bar{u}_b)\left[\left(\bar{u}_a-\frac{\bar{u}_a^2}{2}\right)-\left(\bar{u}_b-\frac{\bar{u}_b^2}{2}\right)\right]+(\bar{v}_a-\bar{v}_b)^2+(\bar{w}_a-\bar{w}_b)^2=0 \tag{46}$$

If the shock wave is a normal wave and the flow is parallel to the $\bar{x}$ axis (i.e., $\bar{v}_a=\bar{v}_b=\bar{w}_a=\bar{w}_b=0$, but $\bar{u}_a\neq\bar{u}_b$), it can be seen from equation (45) that the normalized perturbation velocity component $\bar{u}$ jumps from $1+\Delta$ immediately ahead of the shock to $1-\Delta$ immediately behind the shock. On the other hand, equation (46) shows that the quantity $\bar{u}-\bar{u}^2/2$ is equal on the two sides of the shock. This is consistent with the fact that the latter quantity corresponds, in the transonic approximation, to the mass flow, which is continuous through a normal shock.

The solution, by the present method, of the general problem of transonic flow about thin wings requires the solution of equation (43) while taking proper account of the shock relations given in equation (44). This represents a formidable task well beyond the reach of the present analysis. Simplification can be achieved in two ways: by restricting attention to a less general class of problems and by introducing additional simplifying approximations. The first way is, of course, much to be preferred. Accordingly, in most of the following analysis, attention will be confined to two-dimensional flows. The necessary equations can be obtained from equations (42) through (44) above by integrating in the $\bar{\eta}$ direction from $\bar{\eta}=-\infty$ to $\bar{\eta}=+\infty$, noting that $\bar{v}=0$ and that $\bar{u}$ and $\bar{w}$ are independent of $\bar{\eta}$. They are as follows:

$$\bar{u}_L=-\frac{1}{2\pi}\int_W\left(\Delta\frac{\partial\bar{u}_L}{\partial\bar{\zeta}}\ln\frac{1}{r_2}-\Delta\bar{u}_L\frac{\partial}{\partial\bar{\xi}}\ln\frac{1}{r_2}\right)d\bar{\xi} \tag{47}$$

$$\begin{aligned}\bar{u}=&-\frac{1}{2\pi}\int_W\left(\Delta\frac{\partial\bar{u}}{\partial\bar{\zeta}}\ln\frac{1}{r_2}-\Delta\bar{u}\frac{\partial}{\partial\bar{\xi}}\ln\frac{1}{r_2}\right)d\bar{\xi}+\frac{\bar{u}^2}{2}-\\&\frac{1}{2\pi}\iint_R\frac{\bar{u}^2}{2}\frac{\partial^2}{\partial\bar{\xi}^2}\ln\frac{1}{r_2}d\bar{\xi}d\bar{\zeta}+\frac{1}{2\pi}\int_S\left\{\left[\ln\frac{1}{r_2}\frac{\partial}{\partial\bar{\xi}}\left(\bar{u}-\frac{\bar{u}^2}{2}\right)-\right.\right.\\&\left(\bar{u}-\frac{\bar{u}^2}{2}\right)\frac{\partial}{\partial\bar{\xi}}\ln\frac{1}{r_2}\Big]_a-\left[\ln\frac{1}{r_2}\frac{\partial}{\partial\bar{\xi}}\left(\bar{u}-\frac{\bar{u}^2}{2}\right)-\right.\\&\left.\left(\bar{u}-\frac{\bar{u}^2}{2}\right)\frac{\partial}{\partial\bar{\xi}}\ln\frac{1}{r_2}\Big]_b+\left[\left(\ln\frac{1}{r_2}\frac{\partial\bar{u}}{\partial\bar{\zeta}}-\bar{u}\frac{\partial}{\partial\bar{\zeta}}\ln\frac{1}{r_2}\right)_a-\right.\\&\left.\left.\ln\frac{1}{r_2}\frac{\partial\bar{u}}{\partial\bar{\zeta}}-\bar{u}\frac{\partial}{\partial\bar{\zeta}}\ln\frac{1}{r_2}\right)_b\Big]\left[\frac{\cos(n,\bar{\zeta})}{\cos(n,\bar{\xi})}\right]_b\right\}d\bar{\zeta}\end{aligned} \tag{48}$$

where

$$\frac{1}{r_2}=\frac{1}{[(\bar{x}-\bar{\xi})^2+(\bar{z}-\bar{\zeta})^2]^{1/2}} \tag{49}$$

and

$$(\bar{u}_a-\bar{u}_b)^2+(\bar{w}_a-\bar{w}_b)^2=\left(\frac{\bar{u}_a+\bar{u}_b}{2}\right)(\bar{u}_a-\bar{u}_b)^2 \tag{50}$$

As remarked following equation (42), considerable simplification results in both two- and three-dimensional problems if attention is confined to the determination of the pressure distribution on symmetrical nonlifting wings of specified geometry. This restriction permits the introduction of the relations

$$\begin{gathered}\Delta\bar{u}=\Delta\bar{u}_L=0\\ \Delta\frac{\partial\bar{u}}{\partial\bar{\zeta}}=\Delta\frac{\partial\bar{w}}{\partial\bar{\xi}}=\Delta\left(\frac{\partial\bar{w}}{\partial\bar{\xi}}\right)_L\equiv\text{given}\end{gathered} \tag{51}$$

into the integral over W in either equation (43) or (48). This integral is then equal to the linear-theory solution $\bar{u}_L$ given in equation (42) or (47) and can be determined completely at the outset of the analysis.

SIMPLIFICATION AND APPROXIMATE SOLUTION OF INTEGRAL EQUATIONS FOR TRANSONIC FLOW ABOUT NONLIFTING WINGS

QUALITATIVE DISCUSSION OF INTEGRAL EQUATIONS

The integral equations and the auxiliary relations developed in the preceding section provide a means for the discussion of the aerodynamics of symmetrical nonlifting thin wings of specified geometry in flows with free-stream Mach numbers up to unity. At the present stage of development, however, it is necessary to introduce some further approximations before solutions can be obtained. One of the more accurate of these involves two statements about the nature of the shock waves. They are: (a) all shock waves are assumed to lie in a plane perpendicular to the x axis, and (b) the shock waves are assumed to be normal shock waves (i. e., normal to the local flow direction). These two statements are slightly contradictory in themselves but might be expected to approach the true conditions quite closely for flows about smoothly curved thin airfoils. The first statement corresponds to setting $\cos(n,\bar{\eta})$ and $\cos(n,\bar{\zeta})$ to zero, thereby eliminating part of the integrals over S of equations (43) and (48). The second permits an advantageous introduction of equations (30) and (46) to eliminate the remainder of the integrals over S. The above assumptions correspond to setting $\bar{v}$ and $\bar{w}$ to zero both before and after the shock wave and lead to the following relations:

$$\left(\bar{u}-\frac{\bar{u}^2}{2}\right)_a=\left(\bar{u}-\frac{\bar{u}^2}{2}\right)_b,\qquad\frac{\partial}{\partial\bar{\xi}}\left(\bar{u}-\frac{\bar{u}^2}{2}\right)_a=\frac{\partial}{\partial\bar{\xi}}\left(\bar{u}-\frac{\bar{u}^2}{2}\right)_b=0 \tag{52}$$

Equations (43) and (48) thereby simplify to

$$\bar{u}=\bar{u}_L+\frac{\bar{u}^2}{2}-\frac{1}{4\pi}\iiint_R\frac{\bar{u}^2}{2}\frac{\partial^2}{\partial\bar{\xi}^2}\left(\frac{1}{r_3}\right)d\bar{\xi}\,d\bar{\eta}d\bar{\zeta} \tag{53}$$

for three-dimensional flows, and

$$\bar{u}=\bar{u}_L+\frac{\bar{u}^2}{2}-\frac{1}{2\pi}\iint_R\frac{\bar{u}^2}{2}\frac{\partial^2}{\partial\bar{\xi}^2}\ln\left(\frac{1}{r_2}\right)d\bar{\xi}d\bar{\zeta} \tag{54}$$

for two-dimensional flows. These equations correspond to those used by Oswatitsch and Gullstrand (refs. 20, 21, and 22) although a number of further assumptions were necessary before approximate solutions could be obtained for the velocity distribution on an airfoil surface. The present analysis also requires many of the same or similar assumptions, but there are a number of general points which should be discussed before any further approximations are introduced. These points were not observed in the previous papers and the results suffer by lacking uniqueness in some cases and failing to converge in other cases.

Before proceeding further, it should be observed that the solutions of equations (53) and (54) must approach those of linear theory when the free-stream Mach number is much less than unity, since $\bar{u} \ll 1$ and the terms involving the square of $\bar{u}$ become negligible with respect to those linear in $\bar{u}$, thereby leaving only

$$(\bar{u})_{M_0 \ll 1} \approx \bar{u}_L \tag{55}$$

In the interest of brevity, the integral equations for $\bar{u}$ given in equations (53) and (54) may be rewritten as follows:

$$\bar{u} = \bar{u}_L + \frac{\bar{u}^2}{2} - \frac{I}{2} \tag{56}$$

where

$$I = 2\left[\frac{1}{4\pi}\iiint_R \frac{\bar{u}^2}{2}\frac{\partial^2}{\partial \bar{\xi}^2}\left(\frac{1}{r_3}\right) d\bar{\xi}\, d\bar{\eta}\, d\bar{\zeta}\right] \tag{57}$$

for three-dimensional flows, and

$$I = 2\left[\frac{1}{2\pi}\iint_R \frac{\bar{u}^2}{2}\frac{\partial^2}{\partial \bar{\xi}^2}\ln\left(\frac{1}{r_2}\right) d\bar{\xi}\, d\bar{\zeta}\right] \tag{58}$$

for two-dimensional flows. Although I is a function of $\bar{u}$ and is therefore unknown, it is informative to rewrite equation (56) by solving for $\bar{u}$ in terms of I and $\bar{u}_L$, thus

$$\bar{u} = 1 \pm \sqrt{I - (2\bar{u}_L - 1)} = 1 \pm \sqrt{I - L} \tag{59}$$

where

$$L = 2\bar{u}_L - 1$$

Several points are to be observed at once with regard to equation (59). First of all, the discriminant must always be positive in order to obtain real values for $\bar{u}$, thus

$$I \geq L \tag{60}$$

Furthermore, the choice of the plus or minus sign determines whether the local velocities are subsonic or supersonic. A change in sign at a point where the radical is zero corresponds to a smooth transition through sonic velocity. A change in sign at a point where the radical is not zero corresponds to a discontinuous jump in velocity. As pointed out following equation (46), such discontinuities correspond to normal shock waves and are permissible when they proceed from supersonic to subsonic velocities (or from plus to minus sign in equation (59)) when progressing in the flow direction. Discontinuities in the reverse direction are inadmissible since they correspond to expansion shocks, a phenomenon which violates the second law of thermodynamics.

The values of $\bar{u}_L$, and hence L, can be calculated for any given wing and are generally characterized by certain regions in which $\bar{u}_L$ is positive and other regions in which it is negative. The absolute values increase continuously with increasing Mach number and the maximum positive values may considerably exceed unity as sonic velocity is approached in the free stream. Not very much can be stated at this point about the values of I, except that they depend on the distribution as well as magnitude of $\bar{u}$ and that the above inequality must be satisfied. The relation between the two curves is of utmost importance, however, and will be discussed qualitatively in the following paragraphs.

In order to remove unnecessary complications and to facilitate the discussion, the following remarks will be confined to the relations in two-dimensional flow between the functions I, L, $\bar{u}$, and $\bar{u}_L$ evaluated at the airfoil surface. In this way, each of the four functions reduces to a function of a single variable $\bar{x}$ and can be illustrated simply by curves rather than surfaces or hypersufaces. The subscript W is appended to $\bar{u}$ and $\bar{u}_L$ to denote that the values are those at the wing surface. In that which follows, the curves will be shown on two separate plots, one containing the L and I curves representing the components involved in the solution of equation (59) and the other containing the $\bar{u}_W$ and $\bar{u}_{L_W}$ curves representing, respectively, the velocity distributions given by transonic theory and by linear theory. In order to make the discussion more definite, the curves will be drawn qualitatively as they would appear for a circular-arc airfoil having its maximum thickness at the midchord position. A quantitative discussion of these characteristics will be taken up for the same airfoil in a later section.

The linear-theory solution $\bar{u}_{L_W}$ for subsonic flow about circular-arc airfoils can be easily derived through application of the expression given in equation (47). It is found that the values of $\bar{u}_{L_W}$ are symmetrical about the midchord position at all free-stream Mach numbers less than unity. It follows directly that the L curves possess the same symmetry.

For pure subsonic flows about such an airfoil, it is well known that the more exact treatments, such as the Kármán-Tsien or the classical iteration methods reviewed in reference 19, indicate that the nonlinear-theory solutions and, hence, the $\bar{u}_W$ and I curves, are also symmetrical about the midchord position. Since sonic velocity is not attained at any point, the L and I curves never touch. Sketches of the curves for this condition are shown in figure 8. The second part of this figure illustrates the fact that $\bar{u}_W$ possesses larger values over the middle of the airfoil chord than does $\bar{u}_{L_W}$

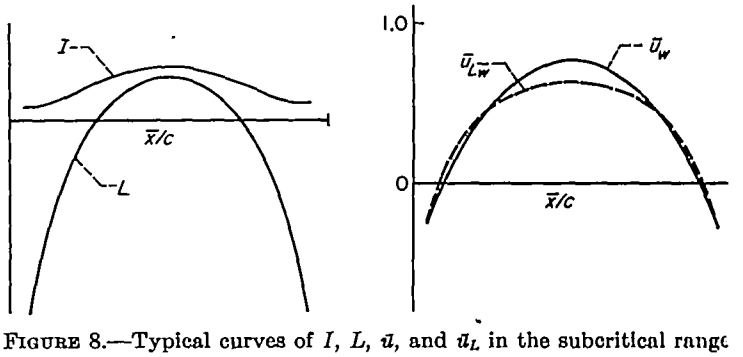

FIGURE 8.—Typical curves of I, L, $\bar{u}$, and $\bar{u}_L$ in the subcritical range

This relation has not been deduced from the foregoing preliminary considerations but is known from many sources in classical subsonic theory. The same result has been found once again in the present work by carrying out an approximate solution of equation (59). The details of these calculations will be described in a later section.

The curves shown in figure 8 are typical of those for all Mach numbers less than the critical Mach number M_{cr}, defined as the lowest free-stream Mach number at which sonic velocity ($\bar{u}_W=1$) occurs somewhere on the wing surface. The aforementioned symmetry properties are preserved for all Mach numbers less than the critical, but the amplitudes of all four curves increase with increasing Mach number. For the symmetrical circular-arc airfoils considered here, the maximum values of $\bar{u}_{L_W}$ and $\bar{u}_W$ and, hence, L and I occur at the 50-percent-chord position for all subcritical Mach numbers. Thus, in addition to the requirement that $I \geq L$ at every point, it is necessary when the Mach number is equal to the critical value, that $I=L$ at the 50-percent-chord position. A rather interesting additional requirement that follows from the quadratic nature of equation (56) together with the assumption that $\bar{u}$ reaches a smooth maximum at the 50-percent-chord station is that the I and L curves have not only the same first derivatives at this station but also identical second derivatives. A typical set of curves for this Mach number is shown in figure 9. It is to be remarked that the minus sign is to be used in equation (59) for all free-stream Mach numbers equal to or less than M_{cr}.

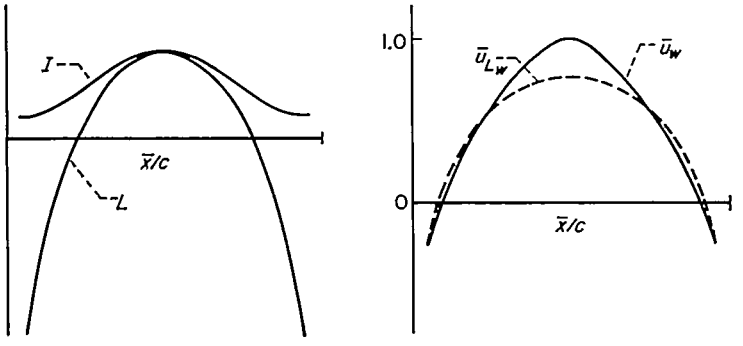

FIGURE 9.—Typical curves of I, L, $\bar{u}$, and $\bar{u}_L$ at the critical Mach number.

It is interesting to contemplate the various possibilities that may occur when the Mach number is increased beyond the critical. Accordingly, let us first consider the implications of assuming that the velocity distribution $\bar{u}_W$ remains symmetrical and continuous across the chord and simply increases in magnitude with increasing Mach number. (This is, in fact, the only type of mixed flow field that the classical iteration methods have indicated, but many doubts have been expressed from time to time regarding the convergence of the methods when $M_o>M_{cr}$.) With such an assumed symmetry of the flow, the four curves will appear qualitatively as shown in figure 10. As may be seen, the curves are all rather similar to those previously discussed for lower Mach numbers. The outstanding difference is the relation between I and L. When $M_o=M_{cr}$, the two curves are tangent at the 50-percent-chord station, and the radius of curvature of the I curve at the same station is equal to that of the L curve. When $M_o>M_{cr}$, tangency occurs at two points, equally spaced before and after the 50-percent-chord station, and the sign in equation (59) is to be changed to plus over the portion of the chord lying between the two points of tangency. In order for $\bar{u}_W$ to attain its maximum value at midchord, as shown in figure 10, the radius of curvature of the I curve must be less than that of the L curve at the 50-percent-chord station. At the tangent or sonic points, it follows from equation (59) and the assumption of smooth acceleration or deceleration through sonic velocity that the second derivative of the I curve is greater than that of the L curve. Similar considerations apply for airfoils that are not symmetrical about the midchord station. The occurrence of shock-free flow would again require that the I curve be tangent to the L curve at two points along the chord.

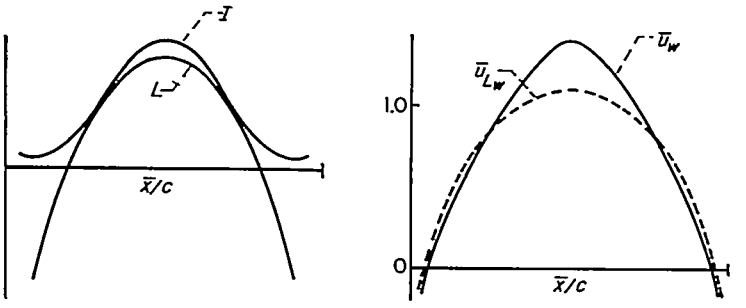

FIGURE 10.—Typical curves of I, L, $\bar{u}$, and $\bar{u}_L$ corresponding to a shock-free supercritical flow, symmeterical solution.

Before leaving this subject, it is interesting to inquire what the result would be of a slight alteration of the airfoil shape, assuming that the original shape was such that the associated flow was of the shock-free mixed type. Consider, for sake of simplicity, that the basic airfoil is symmetrical about the 50-percent-chord station. The assumed shock-free flow is therefore symmetrical about the midchord station and appears as shown in figure 11. In order to preserve the geometrical symmetry, consider that the airfoil shape is changed by the addition to both upper and lower surfaces of small bumps located at the 50-percent-chord station. Since the flow adjacent to the bumps is supersonic, their disturbance pattern is propagated downstream in narrow bands which reflect alternately from the sonic line and the airfoil surface as shown in figure 12. Busemann

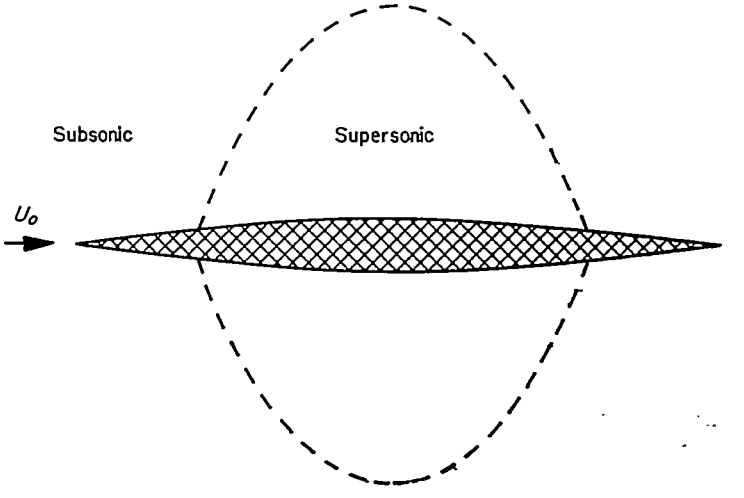

FIGURE 11.—Shock-free transonic flow.

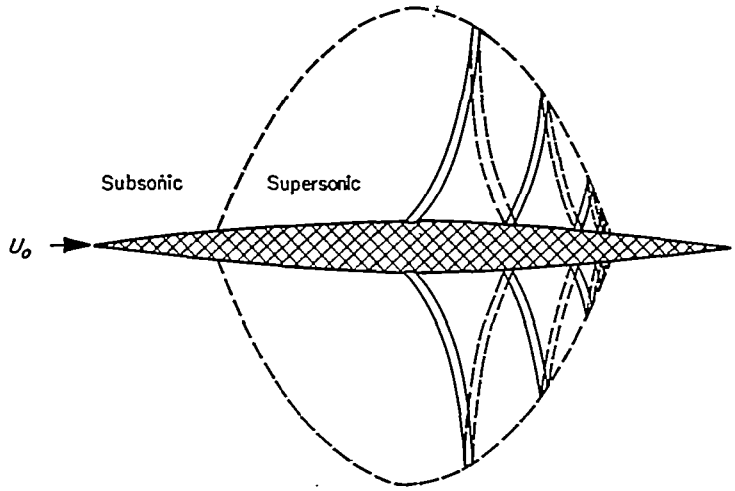

FIGURE 12.—Transonic flow with shock wave.

has pointed out in reference 31 that as the disturbances reach the rear of the supersonic region where the local Mach numbers of the original flow approach unity, the reflections become increasingly concentrated, the disturbances amplify, and finally a shock occurs. It thus appears that there are only a restricted number of shock-free mixed flows and that, in general, the supersonic region terminates with a shock wave.

On the other hand, if the disturbances were propagated forward they would culminate in a shock wave at the forward sonic point. This shock, however, would be an expansion shock in which the velocity jumps from subsonic to supersonic values. As mentioned previously, expansion shocks are forbidden by thermodynamic considerations and, hence, must be excluded from the present analysis. This can be accomplished by stipulating that the transition from subsonic to supersonic velocities at the forward sonic point be smooth, or that the L and I curves retain one point of tangency. In addition to preventing the occurrence of expansion shocks, it appears, on the basis of the foregoing, that this requirement also effectively rules out all the undesired forward propagating disturbances.

The preceding discussion provides an insight into the mechanism for the development of asymmetrical flows about symmetrical airfoils and for the occurrence of shock waves. In the present work, these considerations are reflected in the relation between the I and the L curves. Thus, recall that if the flow is shock free as shown in figure 11, the I and the L curves are both symmetrical as shown previously in figure 10. If the airfoil shape is changed in the manner indicated in figure 12, it is evident that both the I and the L curves will become altered. In so doing, the L curve remains symmetrical about the midchord station, but the asymmetrical nature of the $\bar{u}$ distribution causes the I curve to take on larger values over the rear of the airfoil than over the front. If the flow adjusts itself so that the I curve is tangent to the L curve at a point on the forward half of the airfoil, as it must do to avoid the occurrence of forbidden expansion shock waves, it is likely that the curves will not be tangent at a second point along the rear half of the airfoil. In the application of equation (59), therefore, the sign changes from minus to plus at the point of tangency but may change back to minus at a point where the two curves have different values. As noted previously, such a condition corresponds, in the present analysis, to the occurrence of a shock wave and is associated with a $\bar{u}_W$ curve of the type shown in figure 13.

Since it has been indicated that the shock-free mixed flow is the exception rather than the rule, the curves of figure 13 may be regarded as typical for the supercritical Mach number range. In any event, these curves may be considered as the more general ones since they include the symmetrical curves as a special case. These matters will arise again and be the topic for further discussion in the next section in which an approximate method for the solution of the integral equation for transonic flow will be described.

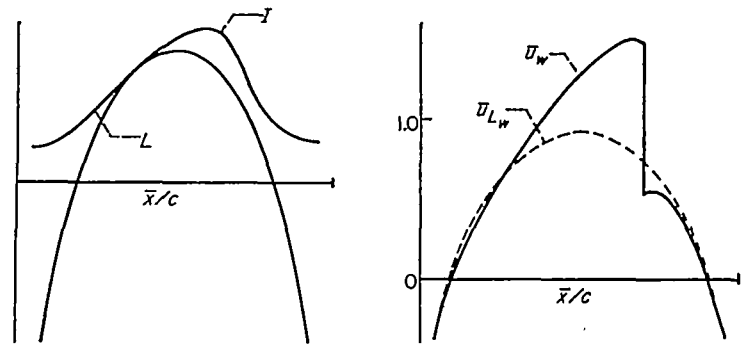

FIGURE 13.—Typical curves of I, L, $\bar{u}$, and $\bar{u}_L$ corresponding to supercritical flow with shock, asymmetrical solution.

SIMPLIFICATION OF THE INTEGRAL EQUATION

The remainder of the present discussion will be concerned with two-dimensional flow about nonlifting symmetrical airfoils of specified geometry under the assumption that any shock waves which may be present are normal shocks situated perpendicular to the x axis. The analysis will be based therefore on equation (54) which, when written in full, is

$$\bar{u}(\bar{x},\bar{z})=\bar{u}_L(\bar{x},\bar{z})+\frac{\bar{u}^2(\bar{x},\bar{z})}{2}-\frac{1}{2\pi}\int_{-\infty}^{+\infty}\int_{-\infty}^{+\infty}\frac{\bar{u}^2(\bar{\xi},\bar{\zeta})}{2}\frac{[(\bar{x}-\bar{\xi})^2-(\bar{z}-\bar{\zeta})^2]}{[(\bar{x}-\bar{\xi})^2+(\bar{z}-\bar{\zeta})^2]^2}\,d\bar{\xi}d\bar{\zeta} \quad (61)$$

Approximate solutions of this equation could conceivably be worked out numerically by starting with a two-dimensional grid of suitably selected values for $\bar{u}(\bar{\xi},\bar{\zeta})$ and iterating until convergence is obtained. Such calculations would proceed by inserting the assumed values for $\bar{u}$ into the double integral and solving to obtain the next approximation for $\bar{u}(\bar{x},\bar{z})$, making use of the tangency condition on the surfaces or functions represented by I and L as discussed in the preceding section. If the first approximation for $\bar{u}$ is taken to be the results given by incompressible or by linearized compressible flow theory, as in the Rayleigh-Janzen and other classical iteration methods, it seems to be the prevailing belief that convergence will be obtained only when the free-stream Mach number is sufficiently small that the flow is subsonic at every point. It is at this point that Oswatitsch (refs. 20 and 21) supplied the important idea that mixed flow fields containing shock waves can be obtained if the starting $\bar{u}$ distri-

bution contains shock waves. Thus, in place of taking the starting solution to be that given by incompressible or linearized compressible flow theory, the idea is to start with a reasonable guess for the values of $\bar{u}$, being sure to include a proper discontinuity complying with the shock relations of equation (52), and then to proceed to the solution. As will be seen in the succeeding sections, it is not necessary to be highly accurate in the initial guess for $\bar{u}$.

A source of difficulty in the numerical solution of equation (61) by an iteration process is the double integral. If it could be reduced to a single integral by introducing a suitable approximation, the entire problem would be greatly simplified. In the present analysis, it is assumed, following Oswatitsch, that approximate knowledge of the velocity distribution is sufficient for providing a working approximation for the double integral. In particular, it is assumed that a sufficiently good approximation to the velocities in the vicinity of the wing can be expressed in terms of the local coordinate $\bar{z}$, the ordinates of the airfoil surface $\bar{z}(\bar{x})$, and the desired but unknown velocity distribution $\bar{u}_W(\bar{x})$ on the airfoil surface. This permits one integration to be performed, thereby reducing the double integral of equation (61) to a single integral.

A number of statements regarding the variation of $\bar{u}$ with $\bar{z}$ over the middle portion of the airfoil can be made immediately. For example, $\bar{u}$ starts from the value $\bar{u}_W$ at the airfoil surface with an intitial rate of change given by the irrotationality condition

$$\left(\frac{\partial \bar{u}}{\partial \bar{z}}\right)_W=\left(\frac{\partial \bar{w}}{\partial \bar{x}}\right)_W \tag{62}$$

and probably vanishes at great distances as $1/\bar{z}^2$. These conditions, of course, are not sufficient to determine completely the variation of $\bar{u}$ with $\bar{z}$, but may be used as the basis for the development of an approximate relation. Oswatitsch (refs. 20 and 21) has already considered this step and has suggested the following relation:

$$\bar{u}(\bar{x},\bar{z})=\frac{\bar{u}_W(\bar{x},o)}{[1+(\bar{z}/b)]^2} \tag{63}$$

where b is a function of $\bar{x}$ so chosen that the irrotationality condition is fulfilled at $\bar{z}=0$. Thus, differentiation of equation (63) with respect to $\bar{z}$ and insertion of the definitions of equation (29) and the boundary condition of equation (14) yield the following:

$$b=-\frac{2\bar{u}_W}{(\partial \bar{u}/\partial \bar{z})_W}=-\frac{2\bar{u}_W}{(\partial \bar{w}/\partial \bar{x})_W}=-\frac{2\beta^3}{k}\frac{\bar{u}_W}{(\partial w/\partial x)_W}$$
$$=-\frac{2\beta^3}{kU_o}\frac{\bar{u}_W}{(\partial^2 \bar{Z}/\partial x^2)}=-\frac{2\bar{u}_W}{(\partial^2 \bar{Z}/\partial \bar{x}^2)} \tag{64}$$

where $\bar{Z}$ represents the reduced ordinates of the airfoil, related to the actual ordinates by

$$\bar{Z}(\bar{x})=\frac{kU_o}{\beta^3}Z(x) \tag{65}$$

Attention is called to the fact that the approximate relation for $\bar{u}(\bar{x},\bar{z})$ given above is not entirely satisfactory. Evidence of this is provided by the fact that $\bar{u}$ is indicated to be zero in the region ahead of the leading edge and behind the trailing edge where b is infinite and that the discontinuities in $\bar{u}$ at the shock surfaces are consistent with the shock relations only at the surface of the airfoil. The errors in the pressures on the airfoil surface resulting from the former are small due to the attenuating influence of distance, and those resulting from the latter have been partially compensated for by a readjustment of the approximation at Mach numbers near unity where the shock strength becomes large.

Substitution of equation (63) into the double integral of equation (61) permits integration with respect to $\bar{\zeta}$. Thus, by performing this integration and setting $\bar{z}=0$, the following approximate integral equation is obtained for $\bar{u}_W$:

$$\bar{u}_W=\bar{u}_{L_W}+\frac{\bar{u}_W^2}{2}-\int_0^c \frac{\bar{u}_W^2}{2b}E\left(\frac{\bar{\xi}-\bar{x}}{b}\right)d\bar{\xi} \tag{66}$$

The function E is

$$E\left(\frac{\bar{\xi}-\bar{x}}{b}\right)=E(X)=\frac{4}{\pi(1+X^2)^5}\left[\frac{\pi}{2}|X|(5-10X^2+X^4)-\right.$$
$$\left.(1-10X^2+5X^4)\ln|X|-\frac{1}{12}(1+X^2)(25-71X^2-X^4-X^6)\right] \tag{67}$$

The nature of $E(X)$ is illustrated graphically in figure 14.

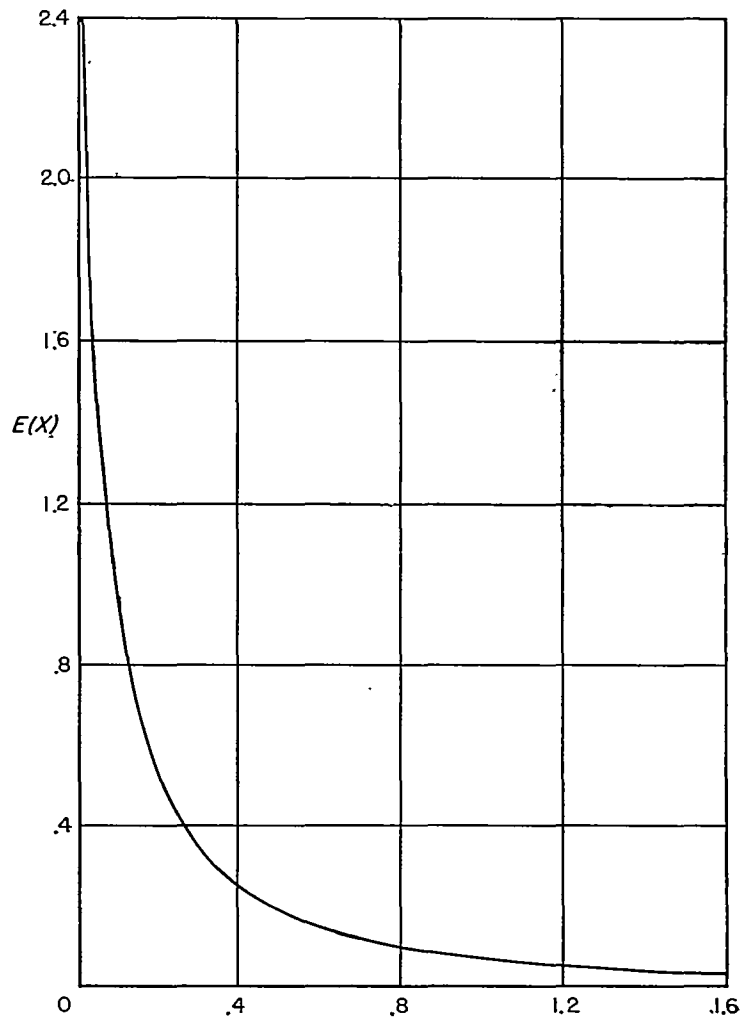

FIGURE 14.—Variation of $E(X)$ with X.

Although the integration interval is indicated in equation (61) to extend from $\bar{\xi}=-\infty$ to $\bar{\xi}=+\infty$, the contribution of the regions ahead of the leading edge and behind the trailing edge is zero since b is infinite. The integration need, therefore, be carried out only over the chord c. It should be noted that the integral in equation (66) corresponds to $I/2$ in equation (56).

Although equation (66) is considerably simpler than equation (61) owing to the replacement of the double integral by a single integral, many of the essential difficulties remain since the integral equation is still nonlinear and the kernel is singular. Since no known methods exist for the solution of such equations, we can only proceed at the present time by introducing additional simplifications. One method proceeds by approximating $\bar{u}_W$ with some simple functions having certain parameters temporarily unspecified. Values for the latter are determined by substituting the functions into the integral equation and satisfying the equation at a limited number of points equal to the number of unspecified parameters. At this point in the analysis, Oswatitsch assumed that the variation of $\bar{u}_W$ across the chord could be represented by a parabola, one or two half-parabolas, or a rectangle combined with a half-parabola, as illustrated in figure 15, all of unspecified height and chordwise extent.

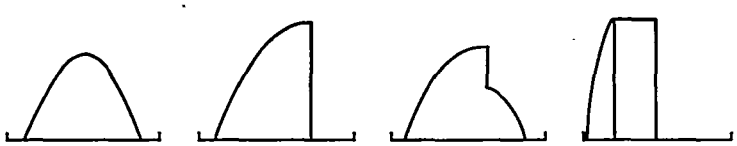

FIGURE 15.—Assumed chordwise variations of $\bar{u}_W$ used by Oswatitsch.

No account was taken in the integral of the influence of the region between the leading edge and the station where $\bar{u}_{L_W}=0$ on the forward part of the airfoil nor between the station where $\bar{u}_{L_W}=0$ on the rear of the airfoil and the trailing edge. Upon inserting a selected combination of the above mentioned elements into equation (66) and integrating, there resulted a system of simultaneous quadratic algebraic equations having as many members as there were elements in the selected general form of solution. In many cases, Oswatitsch used only one element, either a parabola or a half-parabola and assumed a mean value for b for the entire chord. The method included no provision for the improvement of the result through iteration or other means, the only measure of the accuracy being the degree of correspondence between the initial and the final $\bar{u}_W$ distributions. Nevertheless, the results presented in references 20 and 21 were encouraging in that they showed many of the known characteristics of transonic flow about airfoils. In particular, shock waves appeared when the critical Mach number was exceeded and moved rearward with further increases in Mach number. However, because the initial values for $\bar{u}_W$ were generally substituted not only into the integral but also into the term $\bar{u}_W^2/2$ standing outside the integral, and because the tangency requirement on the I and L curves necessary for smooth transition from subsonic to supersonic velocities was not realized, a multiplicity of solutions was often obtained. In one case, three solutions were actually given and more could have been obtained which would have fulfilled equally well the condition of correspondence between initial and final result. In addition, the quality of the results appeared to deteriorate when the Mach number was increased to higher values, the upper limit of acceptability appearing to be a Mach number of about 0.88 for 6-percent-thick airfoils.

The integral equation method has been developed further in references 22 through 25 by Gullstrand. In the first of these, reference 22, equation (61) is simplified to a single integral equation through the use of a more elaborate velocity-distribution function than that given in equation (63), and the resulting equation is solved by an iteration process. The introduction of an iteration procedure makes a marked improvement over the method of Oswatitsch since it then becomes practical to increase greatly the number of elements with which $\bar{u}_W$ is represented. The method is applied to three 6 percent-thick NACA low-drag airfoils and the resulting velocity distributions are given. In common with the original method of Oswatitsch, difficulties occur when the Mach number is too close to unity. The highest Mach number for which results are given is 0.91. More recently, Gullstrand has presented approximate solutions for the velocity distributions on symmetrical airfoils in sonic flow in reference 23.[2] In both of these works, however, the iteration process proceeds by inserting the known values into both the integral and the term $\bar{u}_W^2/2$ standing outside the integral. This procedure is equivalent to replacing the second-degree equation for $\bar{u}_W$ with a linear equation and obscures or loses many of the characteristics of the quadratic solution discussed in the preceding section.

The present analysis also proceeds through the use of an iteration scheme, partly numerical and partly graphical, but the known values are substituted only into the integral at each step of the process. The quadratic nature of the equation is thereby retained and the tangency condition on the I and L curves can be fulfilled. Satisfaction of the latter requirement is essential for uniqueness and convergence. Inasmuch as the calculations for the circular-arc section were well advanced when Gullstrand's papers were received and were producing reasonable results with the simple velocity-distribution function of Oswatitsch, it was decided to continue rather than to start over using a more elaborate velocity-distribution function. It has been found, however, that additional attention must be paid to the influence of the region behind the trailing edge at the higher Mach numbers. Upon observance of these additional refinements, results are obtained for all Mach numbers up to unity. At the lower Mach numbers, these results are in general agreement with those found by the simpler, although more approximate, method of Oswatitsch. The present method carries right on, however, into the higher Mach number range where the simpler method met with difficulties and succeeds in showing the well-known invariance of local Mach number with changes in the free-stream Mach number as the latter approaches unity.

[2] Since equation (61) degenerates at a Mach number of unity where $\beta=0$, the sonic results of reference 23 are obtained by first developing a new double-integral equation to replace equation (61) and then simplifying and solving by an iteration procedure. The integral equation is only used, however, to determine the velocity distribution over the portion of the airfoil forward of the station of maximum thickness. The remainder of the solution is obtained by means of the theory of characteristics.

In the present calculations for circular-arc airfoils, the necessity for additional refinement begins at Mach numbers somewhat greater than that at which the shock wave reaches the trailing edge. Consequently, no attempt is made to account for the influence of the region behind the wing until the Mach number becomes sufficiently large for the shock wave to reach the trailing edge. At higher Mach numbers, the influence of this region is approximated in the following manner. First, it is assumed that the shock wave which stands at the trailing edge remains of the strong family as the free-stream Mach number is increased to unity. It is assumed furthermore that the flow is parallel to the $\bar{x}$ axis at the shock position and that the shock wave is normal to the local flow. With these assumptions, it follows from equation (45) that the values of $\bar{u}$ immediately behind the shock wave are related to those immediately ahead of the shock by

$$\bar{u}_b=2-\bar{u}_a \tag{68}$$

Since $\bar{u}_a$ is given by equation (63), it follows that $\bar{u}_b$ can be expressed in terms of the values of $\bar{u}_W$ and b immediately ahead of the shock wave in the following manner:

$$\bar{u}_b(\bar{z})=2-\frac{\bar{u}_{W_a}}{[1+(\bar{z}/b_a)]^2} \tag{69}$$

Because the shock terminates within a finite distance of the airfoil at all subsonic Mach numbers, equation (69) is appropriate only within a certain range of $|\bar{z}|$, namely, that for which $\bar{u}_a>1$. In the present calculations, the end of the shock occurs at such large $|\bar{z}|$ when the shock is at the trailing edge that equation (69) has been used to represent the values for $\bar{u}$ behind the trailing edge for all $|\bar{z}|$. It is further assumed that the contribution of the region behind the trailing edge can be satisfactorily approximated by equating $\bar{u}$ to $\bar{u}_b$ for all points behind the trailing edge. It is recognized that neither of these assumptions constitutes a good approximation for $\bar{u}$ at great distances from the wing, but the attenuating influence of distance diminishes the error in the values of the integral at points on the airfoil surface. In this way, equation (66) comes to be replaced with the following relation determined from equation (61) by performing an integration with respect to $\bar{\xi}$ under the assumption that the variation of $\bar{u}$ with $\bar{z}$ (or $\bar{\zeta}$) is given by equation (63) for stations ahead of the trailing edge and by equation (69) for stations behind the trailing edge.

$$\bar{u}_W=\bar{u}_{L_W}+\frac{\bar{u}_W^2}{2}-\int_0^c\frac{\bar{u}_W^2}{2b}E\left(\frac{\bar{\xi}-\bar{x}}{b}\right)d\bar{\xi}-\frac{\bar{u}_{W_a}^2}{2b_a}\int_c^{+\infty}E\left(\frac{\bar{\xi}-\bar{x}}{b_a}\right)d\bar{\xi}+\frac{\bar{u}_{W_a}}{2b_a}\int_c^{+\infty}F\left(\frac{\bar{\xi}-\bar{x}}{b_a}\right)d\xi \tag{70}$$

where E is as defined by equation (67) and F is given by

$$F\left(\frac{\bar{\xi}-\bar{x}}{b}\right)=F(X)=\frac{4}{\pi(1+X^2)^3}[\pi|X|(3-X^2)-2(1-3X^2)\ln|X|-(3+2X^2-X^4)] \tag{71}$$

The nature of $F(X)$ is illustrated graphically in figure 16. In this case it is apparent that the three integrals of equation (70) taken together correspond to $I/2$ in equation (56).

To summarize, equation (66) is used in the present calculations when the Mach number is less than that at which the shock wave first reaches the trailing edge, and equation (70) is used for higher Mach numbers. No significant discontinuities are produced in the value of the integrals, however, since the contribution of the additional integrals only becomes significant at Mach numbers greater than that at which the procedure is changed.

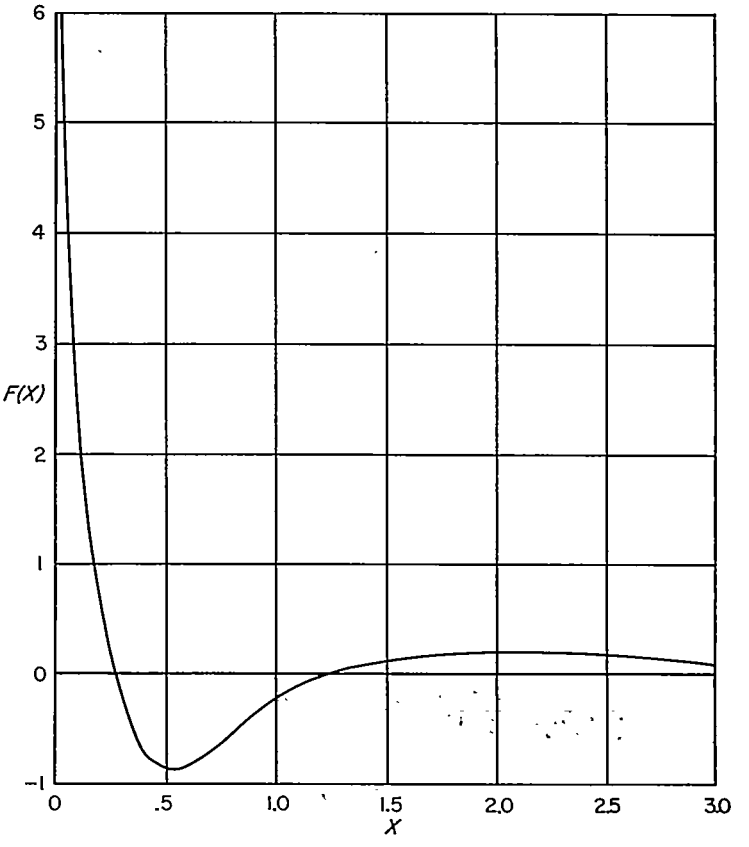

FIGURE 16.—Variation of $F(X)$ with X.

NUMERICAL EVALUATION OF INTEGRAL

One of the principal steps in the iteration method used herein for the solution of equations (66) and (70) is the evaluation of the integrals. Since $\bar{u}_W$ and b are generally prescribed by a set of numerical values rather than by analytical functions, a numerical technique has been used for the integration. This process consists of replacing the prescribed $\bar{u}_W$ distribution with a stepwise approximation as indicated in figure 17, introducing a mean value for b for each of the rectangular elements, integrating to determine the contribution of a single element, and summing the influence of all the elements. The contribution of a single element of width l situated on the airfoil chord, as typified by the shaded area of figure 17, is given by

$$\frac{\bar{u}_{W_i}^2}{2}f_1\left[\left(\frac{\bar{x}-\bar{\xi}_i}{l_i}\right),\left(\frac{2l_i}{b_i}\right)\right]=\frac{\bar{u}_{W_i}^2}{2b_i}\int_{\bar{\xi}_i-\frac{l_i}{2}}^{\bar{\xi}_i+\frac{l_i}{2}}E\left(\frac{\bar{\xi}-\bar{x}}{b_i}\right)d\bar{\xi} \tag{72}$$

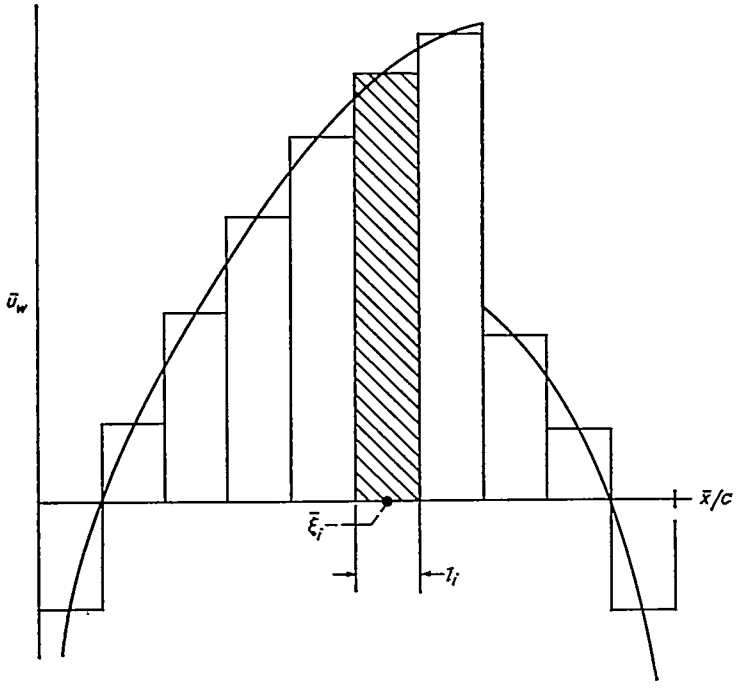

FIGURE 17.—Stepwise approximation used in evaluation of integral when shock wave is forward of trailing edge.

Upon performance of the indicated operations, the following expression is obtained for f_1:

$$\frac{\pi}{4}f_1=\frac{1}{12(1+A^2)^4}\left\{\frac{3\pi}{2}\frac{A}{|A|}[(1+A^2)^4-(1+A^2)^2+8(1+A^2)-8]+12A(A^2-1)\ln|A|-A(1+A^2)[(1+A^2)^2+12]\right\}+\frac{1}{12(1+B^2)^4}\left\{\frac{3\pi}{2}\frac{B}{|B|}[(1+B^2)^4-(1+B^2)^2+8(1+B^2)-8]+12B(B^2-1)\ln|B|-B(1+B^2)[(1+B^2)^2+12]\right\} \quad (73)$$

where

$$\left.\begin{aligned}A&=\frac{l_i+2(\bar{x}-\bar{\xi}_i)}{2b_i}=\frac{1}{4}\left(\frac{2l_i}{b_i}\right)+\frac{1}{2}\left(\frac{\bar{x}-\bar{\xi}_i}{l_i}\right)\left(\frac{2l_i}{b_i}\right)\\B&=\frac{l_i-2(\bar{x}-\bar{\xi}_i)}{2b_i}=\frac{1}{4}\left(\frac{2l_i}{b_i}\right)-\frac{1}{2}\left(\frac{\bar{x}-\bar{\xi}_i}{l_i}\right)\left(\frac{2l_i}{b_i}\right)\end{aligned}\right\} \quad (74)$$

Thus, the integrals in equations (66) and (70) that contain E are approximated as follows:

$$\int\frac{\bar{u}_w^2}{2b}E\left(\frac{\bar{\xi}-\bar{x}}{b}\right)d\bar{\xi}=\sum\frac{\bar{u}_{w_i}^2}{2}f_1\left[\left(\frac{\bar{x}-\bar{\xi}_i}{l_i}\right),\left(\frac{2l_i}{b_i}\right)\right] \quad (75)$$

It is evident from equation (70) that the contribution of a single element of width l situated behind a shock at the trailing edge, as typified by the shaded area of figure 18, is composed of two parts. The first depends on an integral involving $E(X)$ and is evaluated using f_1 in the manner just described for elements on the airfoil. The second depends on an integral involving $F(X)$

$$g_1\left[\left(\frac{\bar{x}-\bar{\xi}_i}{l_i}\right),\left(\frac{2l_i}{b_a}\right)\right]=\frac{1}{b_a}\int_{\bar{\xi}_i-\frac{l_i}{2}}^{\bar{\xi}_i+\frac{l_i}{2}}F\left(\frac{\bar{\xi}-\bar{x}}{b_a}\right)d\bar{\xi} \quad (76)$$

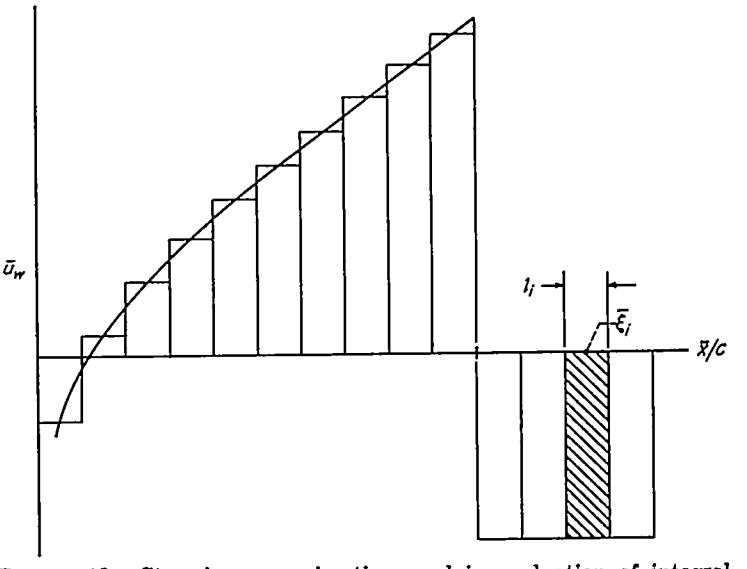

FIGURE 18.—Stepwise approximation used in evaluation of integral when shock wave is at trailing edge.

which, upon evaluation, yields

$$\frac{\pi}{4}g_1=\frac{1}{(1+A^2)^2}\left\{\frac{\pi}{2}\frac{A}{|A|}[(1+A^2)^2+(1+A^2)-2]-2A\ln|A|-A(1+A^2)\right\}+\frac{1}{(1+B^2)^2}\left\{\frac{\pi}{2}\frac{B}{|B|}[(1+B^2)^2+(1+B^2)-2]-2B\ln|B|-B(1+B^2)\right\} \quad (77)$$

where A and B remain as defined in equation (74). Thus, the integral which contains F in equation (70) is approximated as follows:

$$\frac{1}{b_a}\int F\left(\frac{\bar{\xi}-\bar{x}}{b_a}\right)d\bar{\xi}=\sum g_1\left[\left(\frac{\bar{x}-\bar{\xi}_i}{l_i}\right),\left(\frac{2l_i}{b_a}\right)\right] \quad (78)$$

Values of f_1 and g_1 are presented graphically in figures 19 and 20. (It is noted that the graphs in reference 21 that correspond to figure 19 of this report are mislabeled.)

With the simplifications introduced in this section, the function I of equation (56) is approximated by

$$I(\bar{x})=2\sum\frac{\bar{u}_w^2}{2}f_1\left[\left(\frac{\bar{x}-\bar{\xi}_i}{l_i}\right),\left(\frac{2l_i}{b_i}\right)\right] \quad (79)$$

for Mach numbers less than those for which the shock wave is situated at the trailing edge of the airfoil, and

$$I(\bar{x})=2\left\{\sum\frac{\bar{u}_w^2}{2}f_1\left[\left(\frac{\bar{x}-\bar{\xi}_i}{l_i}\right),\left(\frac{2l_i}{b_i}\right)\right]+\frac{\bar{u}_{w_a}^2}{2}\sum f_1\left[\left(\frac{\bar{x}-\bar{\xi}_i}{l_i}\right),\left(\frac{2l_i}{b_i}\right)\right]-\frac{\bar{u}_{w_a}}{2}\sum g_1\left[\left(\frac{\bar{x}-\bar{\xi}_i}{l_i}\right),\left(\frac{2l_i}{b_i}\right)\right]\right\} \quad (80)$$

for larger Mach numbers.

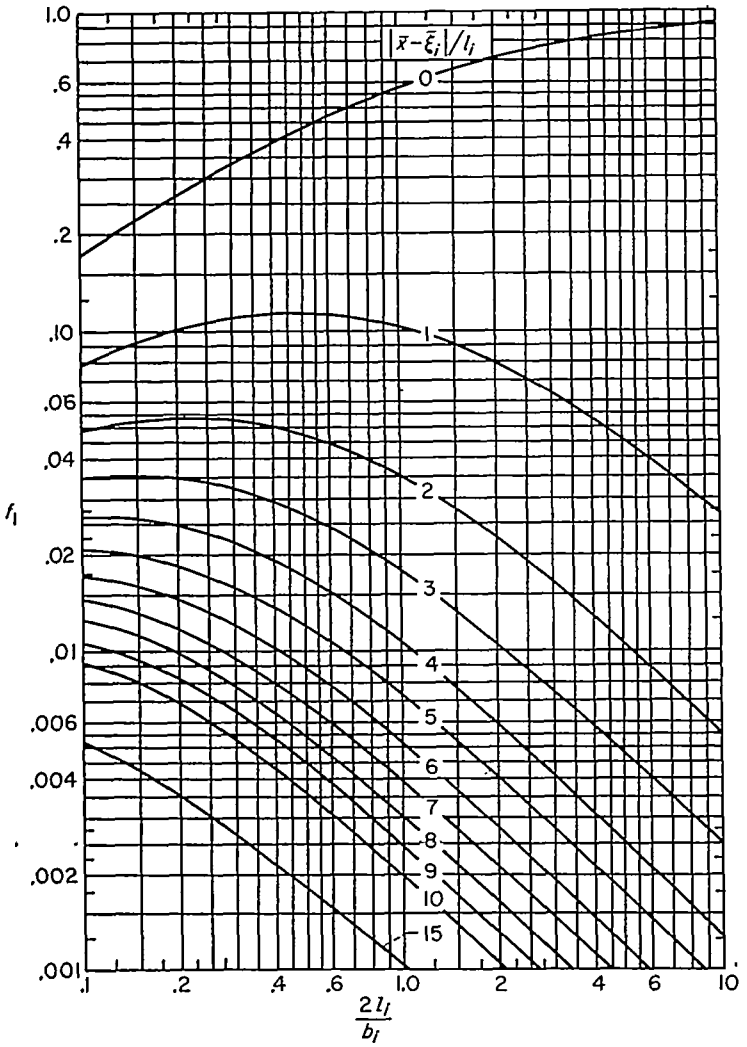

FIGURE 19.—Variation of influence function $f_1\left[\left(\frac{\bar{x}-\bar{\xi}_i}{l_i}\right),\left(\frac{2l_i}{b_i}\right)\right]$ with $\frac{2l_i}{b_i}$ for various values of $\frac{\bar{x}-\bar{\xi}_i}{l_i}$. Computed from equation (73).

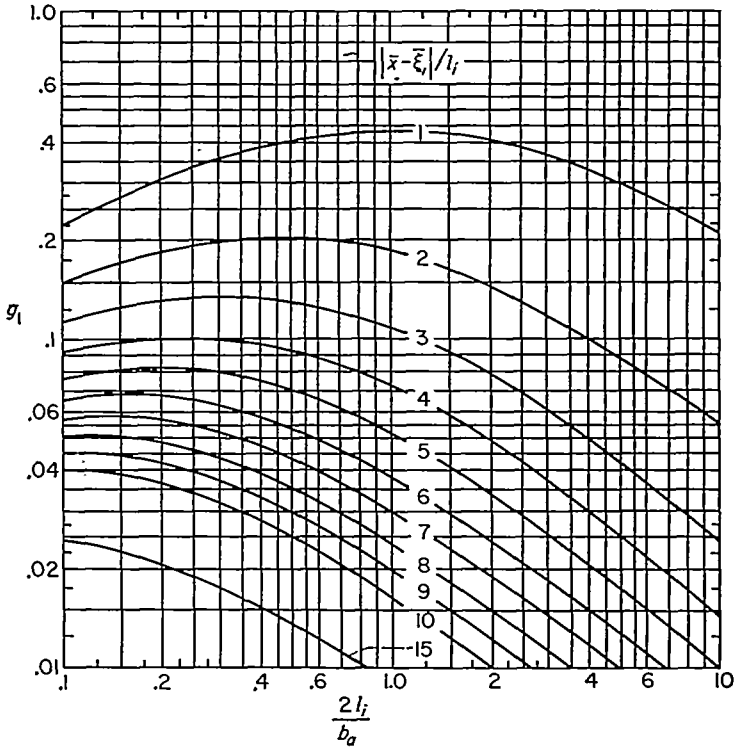

FIGURE 20.—Variation of influence function $g_1\left[\left(\frac{\bar{x}-\bar{\xi}_i}{l_i}\right),\left(\frac{2l_i}{b_a}\right)\right]$ with $\frac{2l_i}{b_a}$ for various values of $\frac{\bar{x}-\bar{\xi}_i}{l_i}$. Computed from equation (77).

DETERMINATION OF $\bar{u}_{L_W}$

The term $\bar{u}_{L_W}$ that appears in the integral equation for transonic flow represents the values for $\bar{u}$ given by linear theory for points on the airfoil surface. Its values can be obtained from the general two-dimensional solution for $\bar{u}_L$ given in equation (47) by performing the indicated operations and setting $\bar{z}=0$. As noted in equation (51), simplification occurs for the symmetrical nonlifting airfoils being considered herein because

$$\Delta\bar{u}=\bar{u}_u-\bar{u}_l=0$$

$$\Delta\frac{\partial\bar{u}_L}{\partial\bar{\zeta}}=\Delta\frac{\partial\bar{w}_L}{\partial}=\frac{k}{\beta^3}\Delta\frac{\partial w_L}{\partial\xi}=2\frac{kU_o}{\beta^3}\frac{d^2Z}{d\xi^2}=2\frac{d^2\bar{Z}}{d\bar{\xi}^2} \tag{81}$$

thus

$$\bar{u}_{L_W}=\lim_{\bar{z}\to 0}\left(-\frac{1}{2\pi}\int_W 2\frac{d^2\bar{Z}}{d\bar{\xi}^2}\ln\frac{1}{r_2}\,d\bar{\xi}\right)$$

$$=\lim_{\bar{z}\to 0}\left(-\frac{1}{\pi}\frac{\partial}{\partial\bar{x}}\int_0^c\frac{d\bar{Z}}{d\bar{\xi}}\ln\frac{1}{r_2}\,d\bar{\xi}\right)=\frac{1}{\pi}\int_0^c\frac{d\bar{Z}_u}{d\bar{\xi}}\frac{d\bar{\xi}}{\bar{x}-\bar{\xi}} \tag{82}$$

The Cauchy principal value is understood in the last integral. The present calculations are for thin circular-arc airfoils for which the reduced ordinates $\bar{Z}_u$ of the upper surface are given by

$$\bar{Z}_u=\frac{kU_o}{\beta^3}Z_u=\frac{kU_o}{\beta^3}\left\{2t\left[\frac{\xi}{c}-\left(\frac{\xi}{c}\right)^2\right]\right\}=2\bar{\tau}c\left[\frac{\xi}{c}-\left(\frac{\xi}{c}\right)^2\right] \tag{83}$$

where $\bar{\tau}$ represents a reduced thickness ratio which is related to the actual thickness ratio as follows:

$$\bar{\tau}=\frac{kU_o}{\beta^3}\frac{t}{c} \tag{84}$$

Performing the indicated operations gives the following expression for $\bar{u}_{L_W}$:

$$\bar{u}_{L_W}=\frac{4}{\pi}\bar{\tau}\left[1+\left(\frac{1}{2}-\frac{\bar{x}}{c}\right)\ln\frac{\bar{x}}{c-\bar{x}}\right] \tag{85}$$

We thus have, by substituting equation (85) into equation (59),

$$L(\bar{x})=2\bar{u}_{L_W}-1=\frac{8}{\pi}\bar{\tau}\left[1+\left(\frac{1}{2}-\frac{\bar{x}}{c}\right)\ln\frac{\bar{x}}{c-\bar{x}}\right]-1 \tag{86}$$

It is seen that $\bar{\tau}$ plays the role of a similarity parameter. Thus, $\bar{u}_{L_W}$ for a family of symmetrical nonlifting airfoils having the same thickness distribution depends only on $\bar{\tau}$ and the position coordinate $\bar{x}/c$. Inspection of the integral equations for transonic flow shows that their solutions for $\bar{u}_W$ also depend only on $\bar{\tau}$ and $\bar{x}/c$.

Many previous papers on transonic flow (e. g., refs. 12, 14, 16, 17, and 18) have used the symbol ξ_o to designate a Mach number thickness ratio parameter different from the parameter $\bar{\tau}$ used herein. The definition of ξ_o, suitably gen-

eralized to allow for various expressions for k, and the relation between ξ_o and τ are as follows:

$$\xi_o=-\frac{1-M_o^2}{[U_o k(t/c)]^{2/3}}=-\left(\frac{1}{\bar{\tau}}\right)^{2/3} \tag{87}$$

The parameter ξ_o possesses the distinct practical advantage of approaching zero rather than infinity as the Mach number approaches unity. The corresponding parameter referring to the local conditions has commonly been designated by the symbol ξ.

$$\xi=-\frac{1-M^2}{[U_o k(t/c)]^{2/3}} \tag{88}$$

where M is the local Mach number. Since the quantity $1-M^2$ is shown in equation (24) to be equivalent, in the present approximation, to $1-M_o^2-ku$, the relation for ξ may be rewritten as

$$\xi=-\frac{1-M_o^2-ku}{[U_o k(t/c)]^{2/3}} \tag{89}$$

which may be expressed in terms of $\bar{u}$ and τ as follows:

$$\xi=\frac{\bar{u}-1}{\bar{\tau}^{2/3}} \tag{90}$$

ITERATION SOLUTION OF INTEGRAL EQUATION

Solutions of the simplified integral equations have been obtained for transonic flow about circular-arc airfoils by using a numerical and graphical process. Four slightly different techniques are used depending on the Mach number or, more precisely, on the value of τ. One procedure is used for the subcritical Mach number range, a second is used in an attempt to find supercritical shock-free solutions, a third to determine supercritical solutions in the range of τ for which the shock position is forward of the trailing edge, and a fourth for still larger values of τ. The latter range extends up to a free-stream Mach number of unity.

Subcritical flows.—Solutions for small Mach numbers can be obtained by a direct iteration process starting with the linear-theory solution. In detail, the calculations proceed in the following manner. The values of $\bar{u}_{L_W}$ corresponding to a given $\bar{\tau}$ (specified thickness ratio and Mach number) are calculated from equation (85). The $\bar{u}_{L_W}$ curve is approximated with a stepwise distribution of ten steps, and the values of the I curve are computed therefrom using equation (79). Knowing the values of $\bar{u}_{L_W}(\bar{x})$ and $I(\bar{x})$, one obtains a first approximation to $\bar{u}_W(\bar{x})$ using equation (59). The process is now repeated using the values for $\bar{u}_W$ to calculate a new I curve, from which a second approximation can be determined for $\bar{u}_W$, etc. A typical set of results illustrating the convergence of the process is shown in figure 21. The process appears to converge rapidly, at least in the present calculations, whenever the Mach number (or more properly $\bar{\tau}$) is sufficiently small that $\bar{u}$ does not exceed unity (or the local velocity does not become supersonic) at any point in the calculation. If $\bar{\tau}$ is increased to a value such that $\bar{u}$ becomes equal to one at any step in the iteration, however, the process terminates abruptly with the appearance of complex values of $\bar{u}$. Since the results of successive iterations oscillate in this Mach number range and since the starting $\bar{u}_L$ distribution provides maximum values that are too small, any such termination occurs in the first iteration step. Such an abrupt termination of the calculations is in marked contrast to the well-known property of the classical iteration methods of producing second- and higher-order solutions indicating shock-free mixed flows. It will be shown in the following discussion that the difference in behavior is not a product of the additional assumptions and approximations introduced herein, but stems directly from the recognition and retention of the quadratic nature of equation (61).

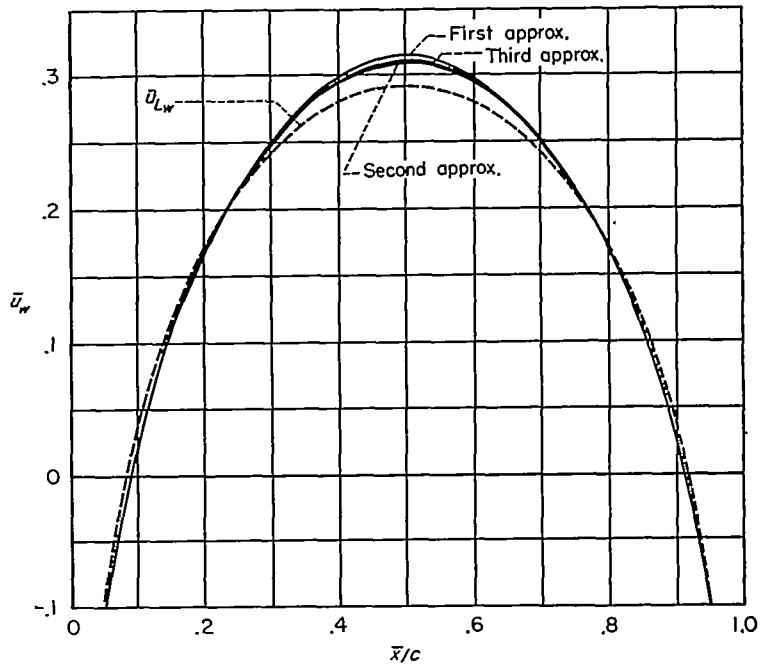

FIGURE 21.—Results of iteration calculations in the subcritical range, $\bar{\tau}=0.229$.

This point can be discussed in greater detail by confining attention to only the first step of the iteration procedure in which the I curve is calculated using $\bar{u}_W=\bar{u}_{L_W}$. If the present iteration procedure is used, if the $\bar{u}_{L_W}$ curve is replaced with ten rectangular steps as shown in figure 17, and if the I curve is calculated using equation (79), then equation (66) yields the following result for $\bar{u}_W$ at the 50-percent-chord station of a circular-arc airfoil:

$$\bar{u}_W\left(\frac{c}{2}\right)=1\pm\sqrt{1-\frac{8}{\pi}\bar{\tau}+1.030\bar{\tau}^2} \tag{91}$$

For low Mach numbers, $\bar{\tau}$ is small, the discriminant is positive, and the first approximation for $\bar{u}_W$ can be readily obtained using the minus sign. As $\bar{\tau}$ increases, the value of the discriminant decreases and becomes negative when $\bar{\tau}$ exceeds 0.490. This value of $\bar{\tau}$, therefore, represents an upper limit for the Mach number at which the present process can lead to a useful result if the starting $\bar{u}_W$ distribution is taken to be that given by linear theory. The value of $\bar{u}_W(c/2)$ given by equation (91) is equal to $(4\bar{\tau}/\pi)$ at small $\bar{\tau}$, and attains a maximum value of unity when $\bar{\tau}=0.490$.

The classical iteration methods of subsonic flow theory have not shown such an abrupt termination of solutions

upon attainment of sonic velocity. The same situation occurs with the present equations if the iteration procedure is altered so as to conform with the classical methods. This change consists simply of substituting $\bar{u}_{L_W}$ into not only the integral of equation (66) but also the term $\bar{u}_W^2/2$ standing outside the integral, thereby converting the quadratic equation for $\bar{u}_W$ into a linear equation. If this procedure is adopted together with the same value for the integral that was used to obtain equation (91), the result of the first iteration is

$$\bar{u}_W\left(\frac{c}{2}\right)=\frac{4}{\pi}\bar{\tau}+0.295\bar{\tau}^2 \tag{92}$$

Since a linear equation is solved at every step of the iteration process, the procedure never terminates. Values for $\bar{u}_W$ in the midchord region become larger with every iteration step, however, and it seems to be the prevailing belief that convergence is obtained only for Mach numbers less than the critical.

It is of interest to compare the approximate results of the first iteration step reviewed above with the exact results for the same airfoil given by Hantzsche and Wendt in reference 32. If the latter results are made comparable to the present results by taking the limiting value corresponding to small-disturbance transonic flow theory, the exact result of the first iteration step is

$$\bar{u}_W\left(\frac{c}{2}\right)=\frac{4}{\pi}\bar{\tau}+\left(\frac{5}{\pi^2}-\frac{1}{4}\right)\bar{\tau}^2=\frac{4}{\pi}\bar{\tau}+0.257\,\bar{\tau}^2 \tag{93}$$

The first term of both equations (92) and (93) is that given by linear theory and is the same in both calculations. The difference in the coefficient of the second term is the result of the errors introduced in the approximate solution of equation (61) (i. e., the velocity-distribution function, finite steps for $\bar{u}_W$, etc.) and is some sort of a measure of the accuracy of the approximate calculations. Just as with equation (92), a value for $\bar{u}_W$ can be calculated for all $\bar{\tau}$, although the question remains of whether the result is a valid first step in a convergent process.

If Hantzsche and Wendt had performed their iteration calculations in a manner comparable to that described herein so that the values of $\bar{u}_L$ are not introduced as an approximation for $\bar{u}$ in determining the important influence of the points lying near P, they would have obtained the following relation (again to the approximation of transonic flow theory) as the result of the first iteration:

$$\bar{u}_W\left(\frac{c}{2}\right)=1\pm\sqrt{1-\frac{8}{\pi}\bar{\tau}+\left(\frac{6}{\pi^2}+\frac{1}{2}\right)\bar{\tau}^2}$$

$$=1\pm\sqrt{1-\frac{8}{\pi}\bar{\tau}+1.108\,\bar{\tau}^2} \tag{94}$$

This result is directly comparable with that given in equation (91) except that the double integral of equation (61) is evaluated exactly rather than approximately. Again, the accuracy of the approximations can be evaluated by comparing the two equations. More important, however, is the fact that the exact results also terminate when $\bar{\tau}$ exceeds a certain value (0.503) and that the corresponding value for $\bar{u}$ is unity. This subject is discussed in greater generality in Appendix B.

As noted above, the first step of the present iteration procedure starting with $\bar{u}_L$ produces maximum values for $\bar{u}$ that are too large. Consequently, the calculations terminate at a value of $\bar{\tau}$ that is somewhat less than corresponds to the true critical Mach number. Solutions can be obtained for the remainder of the subcritical Mach number range, however, if the starting $\bar{u}_W$ is selected having the same general form but larger values than the corresponding $\bar{u}_{L_W}$ distribution. A good starting distribution can be obtained by simply extrapolating the final results for smaller τ.

Calculations of the type just described have been carried through for several values of τ less than the critical value ($\tau_{cr}=0.598$), defined as the smallest value of $\bar{\tau}$ at which sonic velocity ($\bar{u}_W=1$) is attained in the final transonic solution. The results of these calculations are presented in the form of chordwise $\bar{u}_W$ distributions for various $\bar{\tau}$ in figure 22, and in

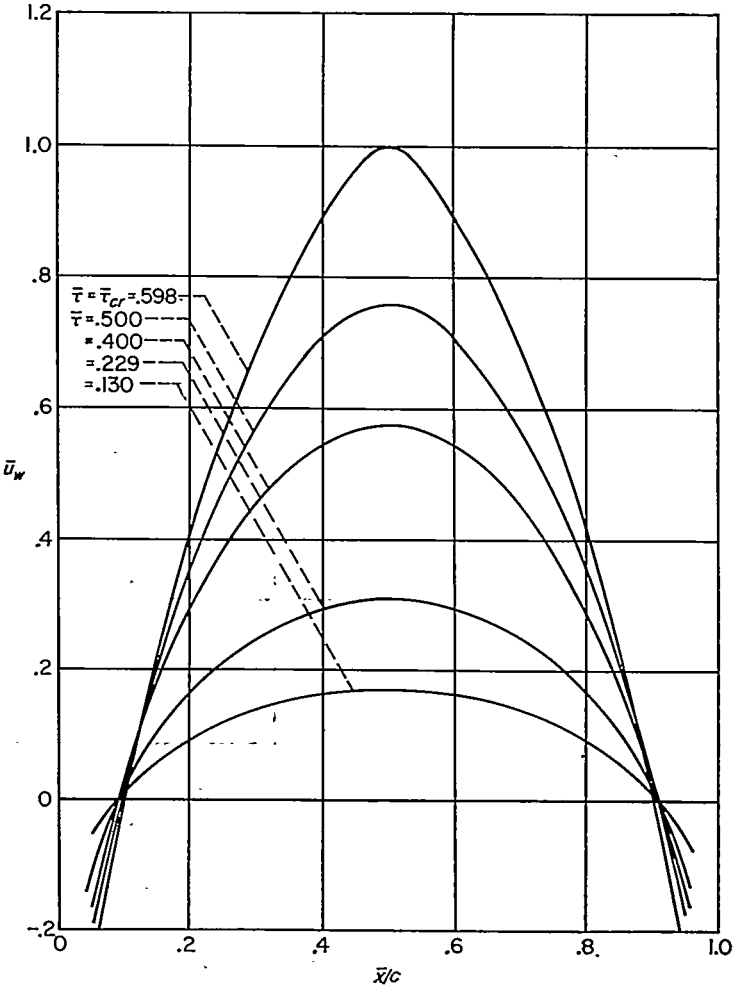

FIGURE 22.—Chordwise variation of $\bar{u}_W$ for various $\bar{\tau}$ in the subcritical range.

the form of curves of $\bar{u}_W$ versus $\bar{\tau}$ for various $\bar{x}/c$ in figure 23.[3] The corresponding values $\bar{u}_{L_W}$ given by linear theory are also shown in figure 23. Comparison of the two sets of curves reveals that the values of $\bar{u}_W$ coincide with those for $\bar{u}_{L_W}$ at

[3] The results for $\bar{\tau}=\bar{\tau}_{cr}$ are also included on these graphs in order to complete the subcritical range, even though they are obtained using a different iteration procedure. Since the procedure is the same as that described in the next section, however, no further comment is necessary at this point.

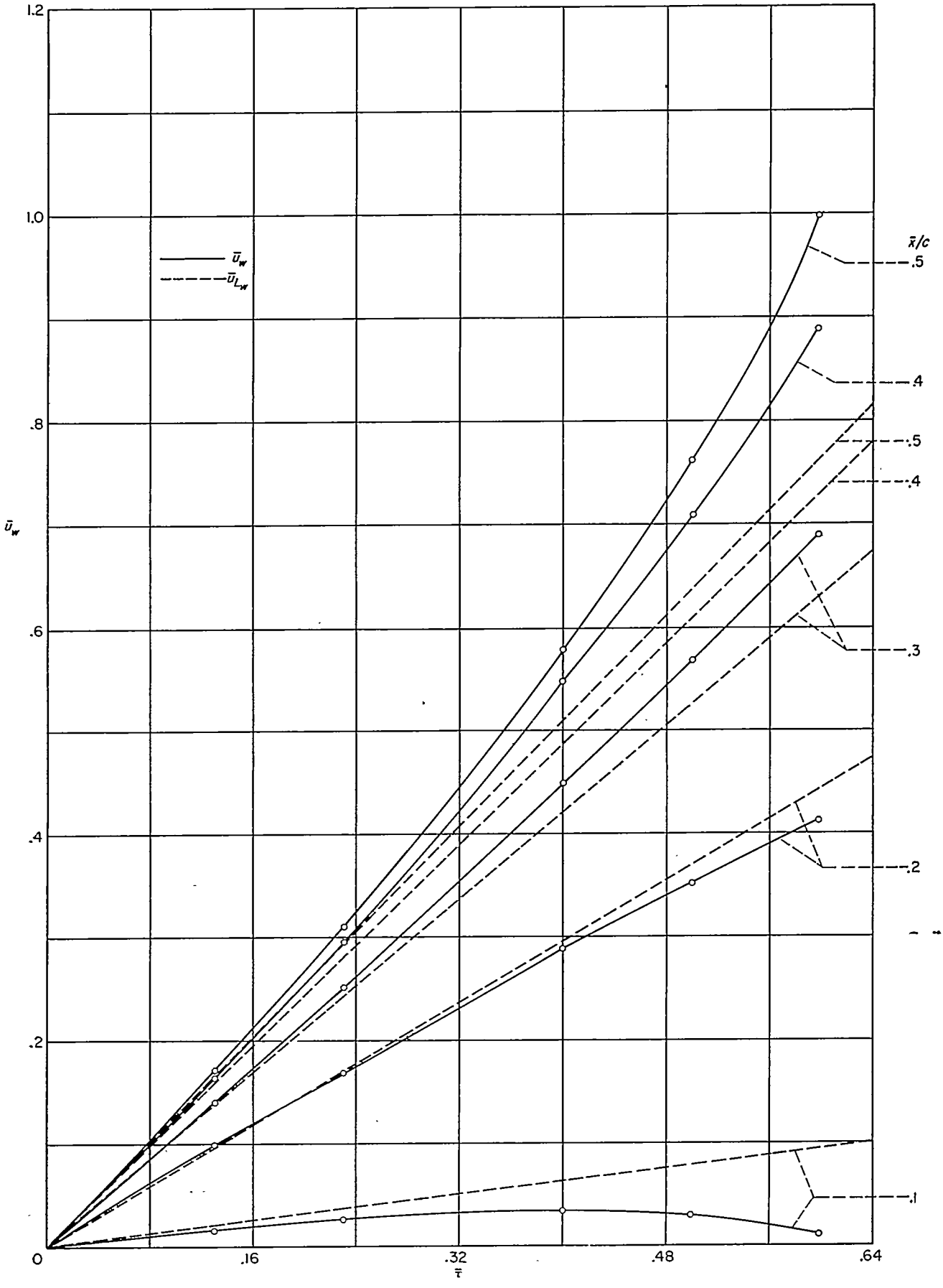

FIGURE 23.—Variation of $\bar{u}_W$ and $\bar{u}_{L_W}$ with $\bar{\tau}$ for various values of $\bar{x}/c$. Subcritical range.

small $\bar{\tau}$ (low Mach number) but become larger than those for $\bar{u}_{L_W}$ at most stations on the airfoil as $\bar{\tau}$ approaches $\bar{\tau}_{cr}$. These trends, which are in accord with generally accepted experimental and theoretical results, will be discussed at greater length in a later section.

Shock-free supercritical flows.—Although it is indicated in the preceding discussion that the present iteration process does not lead to supercritical shock-free flow about airfoils when the starting point for the iteration calculation is $\bar{u}_L$, it is considered of importance and interest to ascertain the behavior of the present approximation when such a solution is deliberately sought by starting with sufficiently large values for $\bar{u}$ that I is greater than L. The interest in this matter is heightened by the fact that the less detailed method used by Oswatitsch leads to such results over a limited range of supercritical Mach numbers. (See figs. 4 (c) and 4 (d) of ref. 20 or figs. 7 (c) and 7 (d) of ref. 21.) Accordingly, iteration calculations have been performed starting with $\bar{\tau}$ greater than $\bar{\tau}_{cr}$ and a symmetrical shock-free $\bar{u}_W$ distribution containing a region of supersonic flow ($\bar{u}_W > 1$) over the middle portion of the chord. A slight change in the iteration procedure is necessary, however, to eliminate the difficulty arising from the requirement described in an earlier section that $I=L$ at the sonic points. To carry out the solution in the same manner as before would require that the $\bar{u}_W$ distribution be found for which the corresponding I curve is tangent to a given L curve. Rather than attempting to find solutions by such indirect means, a method is used in which a new value of $\bar{\tau}$ is determined in such a manner that the tangency condition is fulfilled. In particular, the procedure is to calculate the I curve using equation (79) and the assumed values of $\bar{\tau}$ and $\bar{u}_W$. The next step consists of plotting the I curve and fitting an L curve computed from equation (86) for whatever value of $\bar{\tau}$ is necessary to fulfill the tangency condition as shown in figure 10. A new set of values for $\bar{u}_W$ can now be calculated using equation (59).

$$\bar{u}_W = 1 \pm \sqrt{I - L} \tag{59}$$

where the minus sign is used at stations upstream from the forward sonic point and downstream from the rear sonic point and the plus sign is used for the intermediate stations.

This process has been carried out for a number of assumed initial $\bar{u}_W$ distributions. Figure 24 shows a typical set of results obtained by starting with an initial value for $\bar{\tau}$ of 0.65 and a $\bar{u}_W$ distribution obtained by extrapolating the trends indicated by the solutions for subcritical flows. The assumed initial distribution is indicated by a dotted line in the upper portion of part (a) and the associated I and L curves are shown immediately below. The tangency requirement is fulfilled by taking $\bar{\tau}=0.642$ which compares well with the initial value of 0.65. The corresponding $\bar{u}_W$ distribution calculated therefrom is shown in the upper portion of part (a). Several points of interest are to be noted. The first, of course, is that the assumed and calculated $\bar{u}_W$ distributions

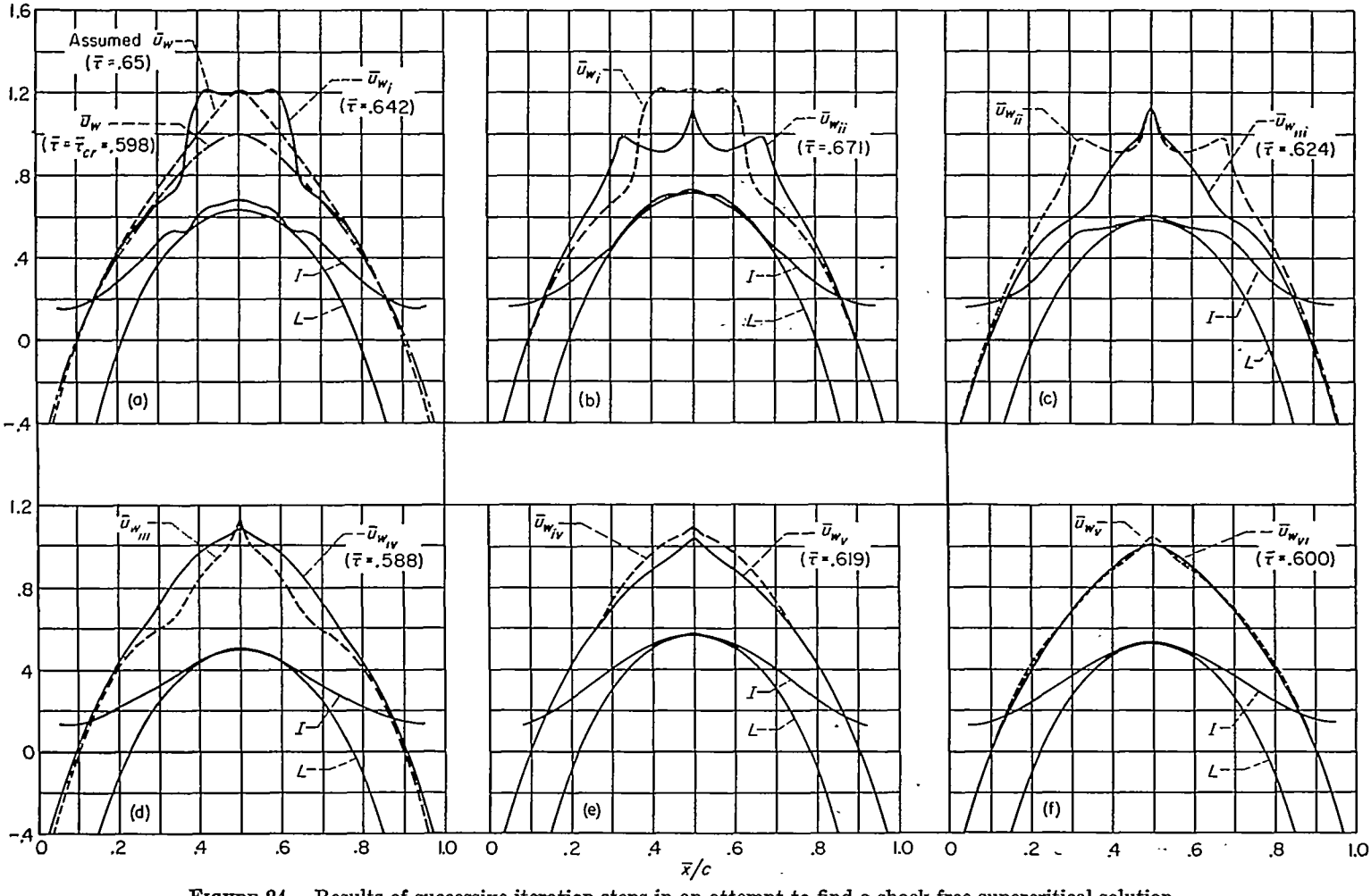

FIGURE 24.—Results of successive iteration steps in an attempt to find a shock-free supercritical solution.

are distinctly dissimilar. The second is that the calculated distribution bears a marked resemblance to a result given by Oswatitsch (see fig. 4(d) of ref. 20 or fig. 7(d) of ref. 21) which may be described as a symmetrical $\bar{u}_W$ distribution containing an abrupt expansion on the front of the airfoil and a compression shock symmetrically situated on the rear of the airfoil.

Since the assumed and calculated $\bar{u}_W$ distributions are too dissimilar to be regarded as solutions, the iteration process was continued, using the calculated results of the first step as the initial values for the second step. The results of this calculation are summarized in part (b). As indicated, $\bar{\tau}$ changes from 0.642 to 0.671 and the new $\bar{u}_W$ distribution is again markedly dissimilar to the initial distribution. The calculations have been carried through several more steps and the results are shown in parts (c) through (f). It can be seen that the initial and calculated $\bar{u}_W$ distributions do not agree, even qualitatively, until several steps of the iteration process have been completed. In the meanwhile, the value of $\bar{\tau}$ has decreased to approximately that for the critical Mach number and the region of supersonic flow has effectively disappeared. The sixth and last step of the iteration calculations presented in figure 24 has produced a value of $\bar{\tau}=0.600$ and a $\bar{u}_W$ distribution nearly identical with that shown in figure 22 for the critical Mach number ($\bar{\tau}_{cr}=0.598$). Although this figure shows the results of only one series of calculations, similar results have been obtained starting with other assumed symmetrical, shock-free, supercritical $\bar{u}_W$ distributions. No case was found in which the calculated values repeated the assumed values until $\bar{\tau}$ had decreased to approximately $\bar{\tau}_{cr}$ and the supersonic zone had vanished.

It should be noted before leaving this section that these results are not presented with the intention of proving or disproving anything about the more fundamental question of the existence or nonexistence of shock-free transonic flows. The purpose, rather, is to illustrate the behavior of the present approximation furnished by the simplified integral equation and the iteration method of solution.

Supercritical flows—shock wave forward of the trailing edge.—The preceding section has shown how the present method of calculating velocity distributions on thin airfoils fails to converge when $\bar{\tau}$ is greater than $\bar{\tau}_{cr}$ and the flow is assumed to be shock free. The identical iteration process will converge rapidly to a solution, however, if the initial $\bar{u}_W$ distribution contains a discontinuity in accord with the shock relations. The method starts by selecting a value for $\bar{\tau}$ and assuming a reasonable distribution for $\bar{u}_W$ over the chord. The main point to observe in the selection of $\bar{u}_W$ is to include a shock wave (a discontinuity in $\bar{u}_W$) through which $\bar{u}_W$ jumps from $1+\Delta$ immediately ahead of the shock to $1-\Delta$ immediately behind the shock. As noted previously, such a jump in $\bar{u}_W$ is consistent with the assumption that the shock wave is a weak normal shock. The next step is to calculate the I curve using equation (79) and the assumed values of $\bar{u}_W$ and $\bar{\tau}$. The I curve is plotted and an L curve is computed using equation (86) and whatever value of $\bar{\tau}$ is necessary to fulfill the tangency condition, as illustrated in figure 13. A new set of values of $\bar{u}_W$ can now be calculated using equation (59), taking proper care to change from the minus to the plus sign at the point of tangency and then return to the minus sign aft of the assumed shock position. In this way, a new approximation for the $\bar{u}_W$ distribution corresponding to the new value for $\bar{\tau}$ is obtained, but the position of the shock wave is unaltered. If the new values for $\bar{\tau}$ and $\bar{u}_W$ are sufficiently close to the assumed values, it is presumed that an approximate solution has been found. In general, however, such a close correspondence is not obtained after the first step, and the entire calculation is repeated using the new values for $\bar{\tau}$ and $\bar{u}_W$ in place of those assumed initially. Throughout the process, the position of the shock wave is kept fixed, and the value of $\bar{\tau}$ is allowed to vary as necessary. In this way, the iteration process selects the solution for a given shock position rather than for a given Mach number. This process was carried out with the shock wave situated at several different stations on the airfoil chord and was found to converge rapidly even when the selected initial values for $\bar{u}_W$ and $\bar{\tau}$ differed considerably from their final values. A typical set of results (namely, that for the shock position fixed at 90-percent-chord station) is shown in figure 25. In common with the rest of the calculations, the initial values for $\bar{u}_W$ and $\bar{\tau}$ were selected by extrapolating

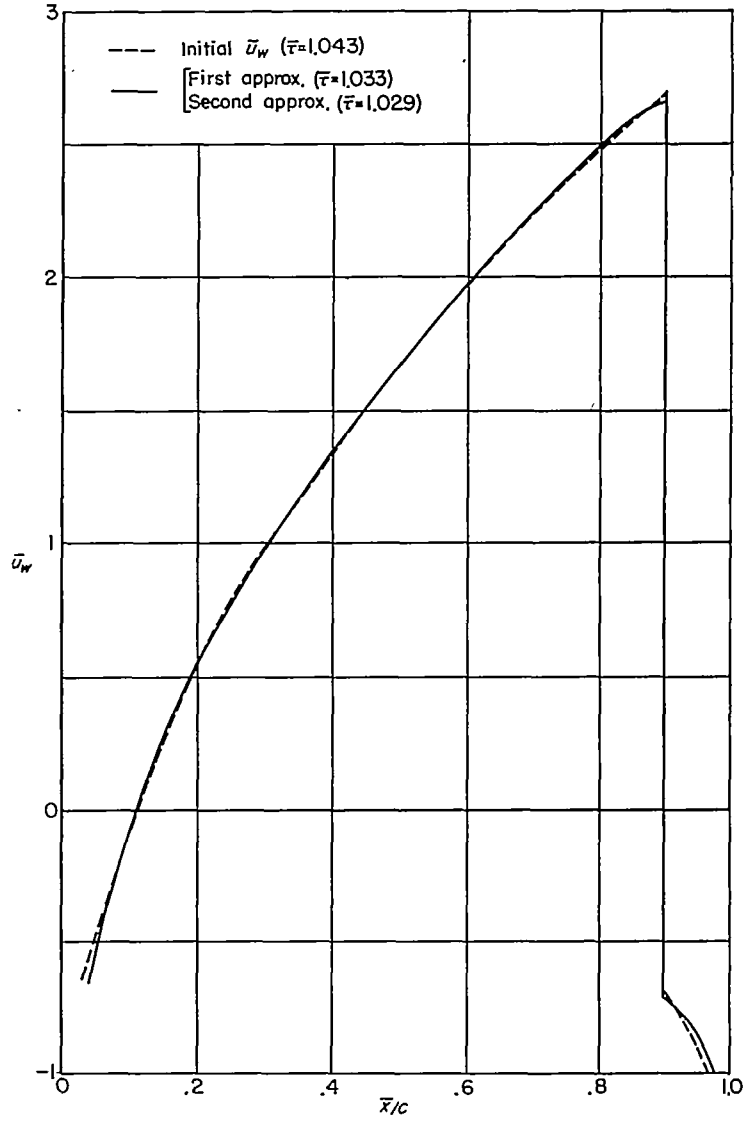

FIGURE 25.—Results of iteration calculations with shock wave at 90-percent chord.

the trends indicated by the calculations for more forward shock positions.

Calculations of the type just described have been carried through with the position of the shock wave fixed at 60-, 70-, 80-, 90-, and 100-percent chord. The results are presented as chordwise $\bar{u}_W$ distributions for various $\bar{\tau}$ in figure 26 and as the variation of $\bar{u}_W$ with $\bar{\tau}$ at selected values of $\bar{x}/c$ in figure 27.

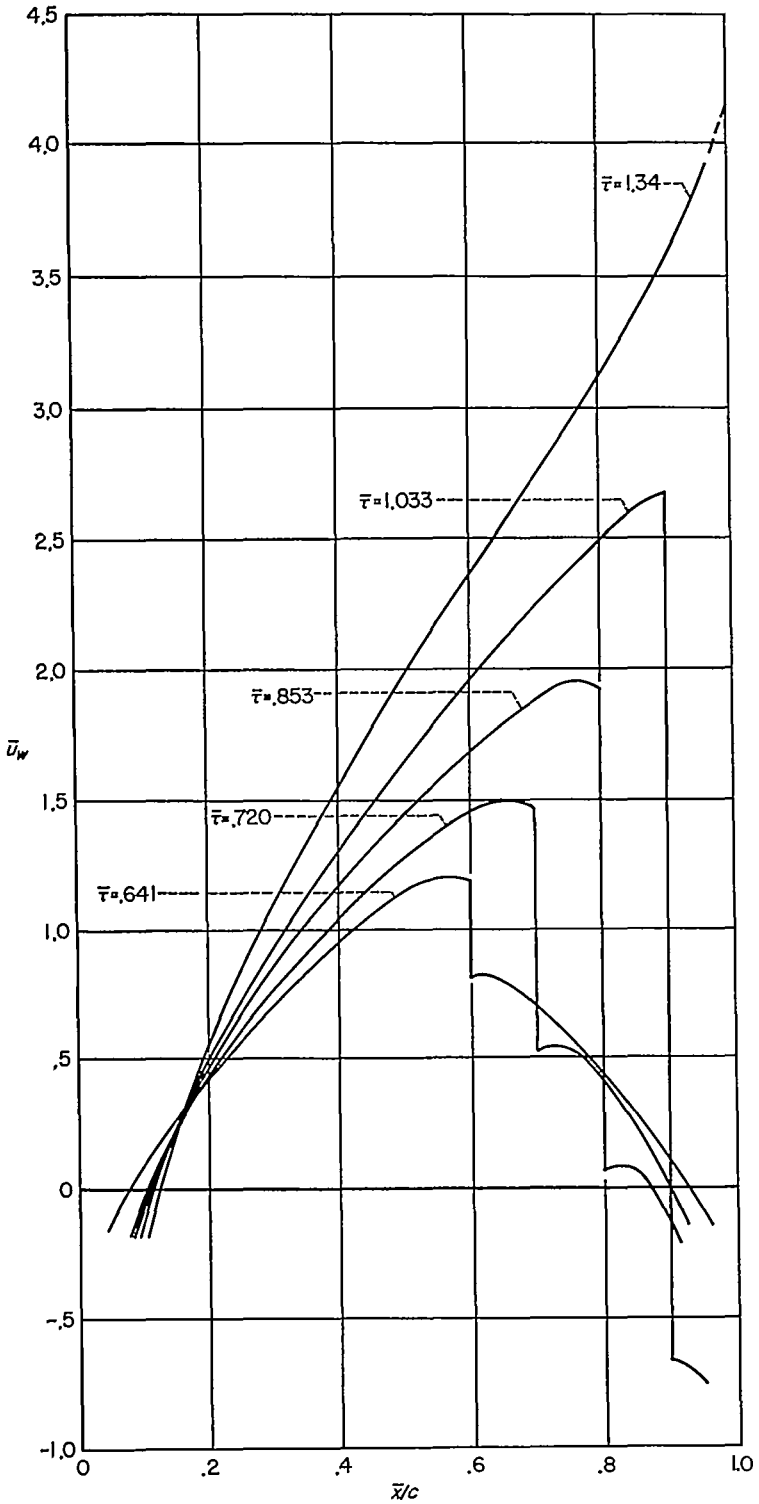

FIGURE 26.—Chordwise variation of $\bar{u}_W$ for various $\bar{\tau}$, shock wave forward of trailing edge.

In order to test the method further, calculations were repeated in many of the cases using a different set of initial values for $\bar{\tau}$ and $\bar{u}_W$. The results of two such calculations for the shock position at the 90-percent-chord station are shown in figure 28. Although the results shown in part (a) were obtained using values for $\bar{u}_W$ that were purposely selected to be too large and those of part (b) to be too small, it can be seen that similar results are obtained after only a few steps of the iteration process. These same results are presented in a second manner in figure 29 wherein the values of $\bar{u}_W$ at several stations on the chord are plotted as a function of $\bar{\tau}$. The final values to which the calculations converge (i. e., those given in fig. 27) are indicated by the solid line. The points connected by the dotted lines are the values obtained at each step of the calculations. It may be seen that the present procedure appears first to place the values of $\bar{u}_W$ and $\bar{\tau}$ on the curve of correct solutions and, subsequently, to converge to the final result.

Supercritical flows—shock wave at the trailing edge.—The calculations just described indicate that the shock wave moves rearward with increasing $\bar{\tau}$ and reaches the trailing edge when $\bar{\tau}=1.34$, corresponding to a Mach number of 0.92 for a 4-percent-thick circular-arc section. The calculations for larger subsonic Mach numbers were performed under the assumption that a strong shock wave remains at the trailing edge. As in the preceding analysis, the shock wave is assumed to stand perpendicular to the x axis, and the flow is assumed to be normal to the shock wave, even though these conditions cannot be correct at the base of the shock wave since the flow must turn through a finite angle.

The method of calculation used for the higher Mach number range where the shock wave stands at the trailing edge is essentially the same as that used for mixed flows at lower Mach numbers. A slight modification enters in that the I curve is calculated by means of equation (80) rather than (79). This change is made because the contribution of the region immediately behind the trailing edge becomes of increasing significance as the Mach number approaches unity. Since the contribution is small at the lowest Mach number for which the shock wave is situated at the trailing edge, no significant discontinuity is produced in the results by this change in procedure. A difficulty arises in the iteration process, however, because there is no longer any distinguishing feature to fix the value of $\bar{\tau}$ for which the solution is being sought. To review, for pure subsonic flows, $\bar{\tau}$ itself can be maintained at a fixed value from step to step in the iteration process. At Mach numbers somewhat greater than the critical, where the shock wave stands on the airfoil, the tangency requirement makes it difficult to prescribe $\bar{\tau}$ directly but a satisfactory method is obtained by fixing the shock position and carrying out the iteration process until the associated value for $\bar{\tau}$ is found. At still larger Mach numbers, the first method is of no avail and the second method cannot produce a unique result since the shock wave is considered to be fixed at the trailing edge over the rest of the range of subsonic free-stream Mach numbers. For lack of a better method, the calculations were carried out for this range using a procedure that might be described as

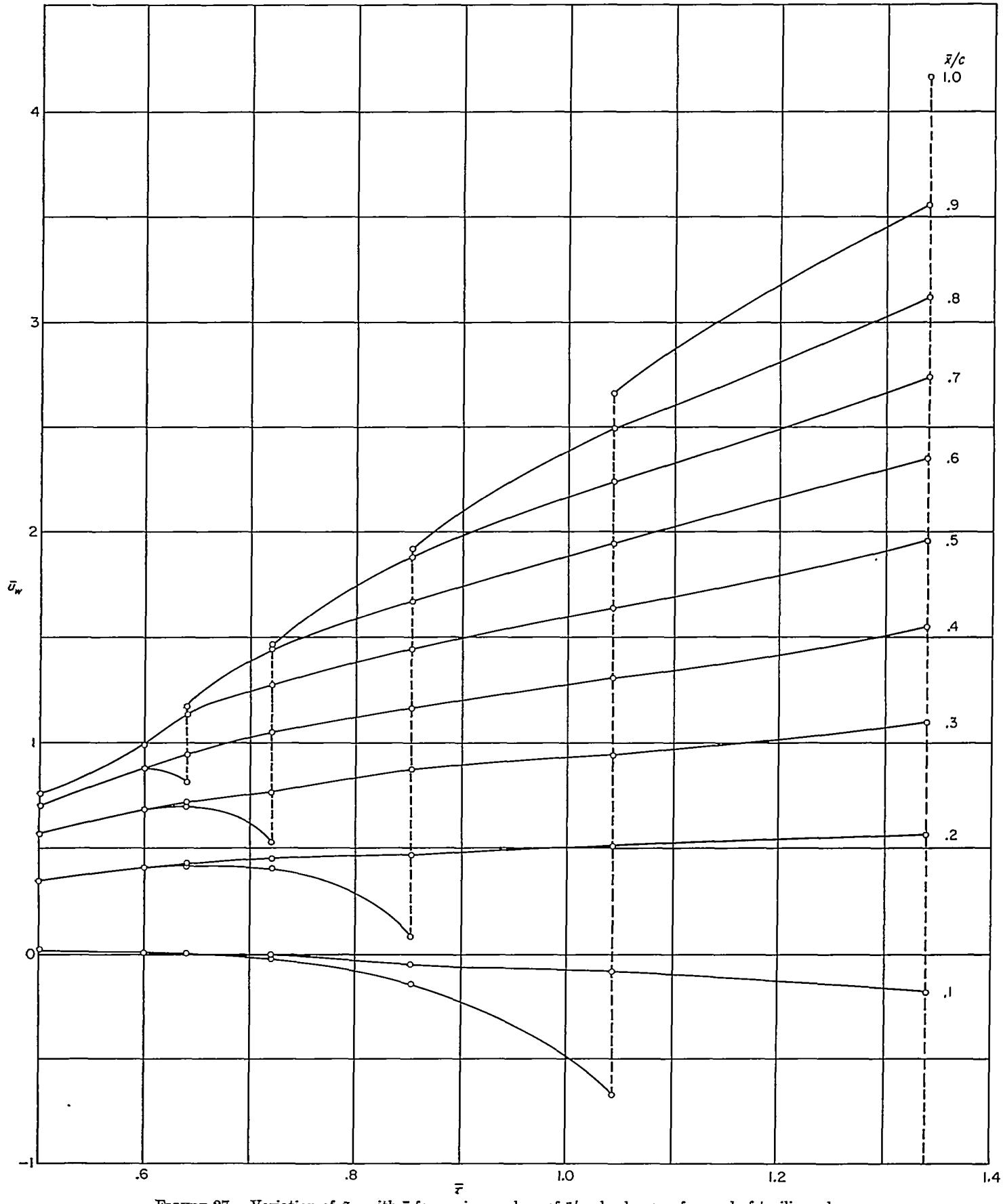

FIGURE 27.—Variation of $\bar{u}_w$ with $\bar{\tau}$ for various values of $\bar{x}/c$, shock wave forward of trailing edge.

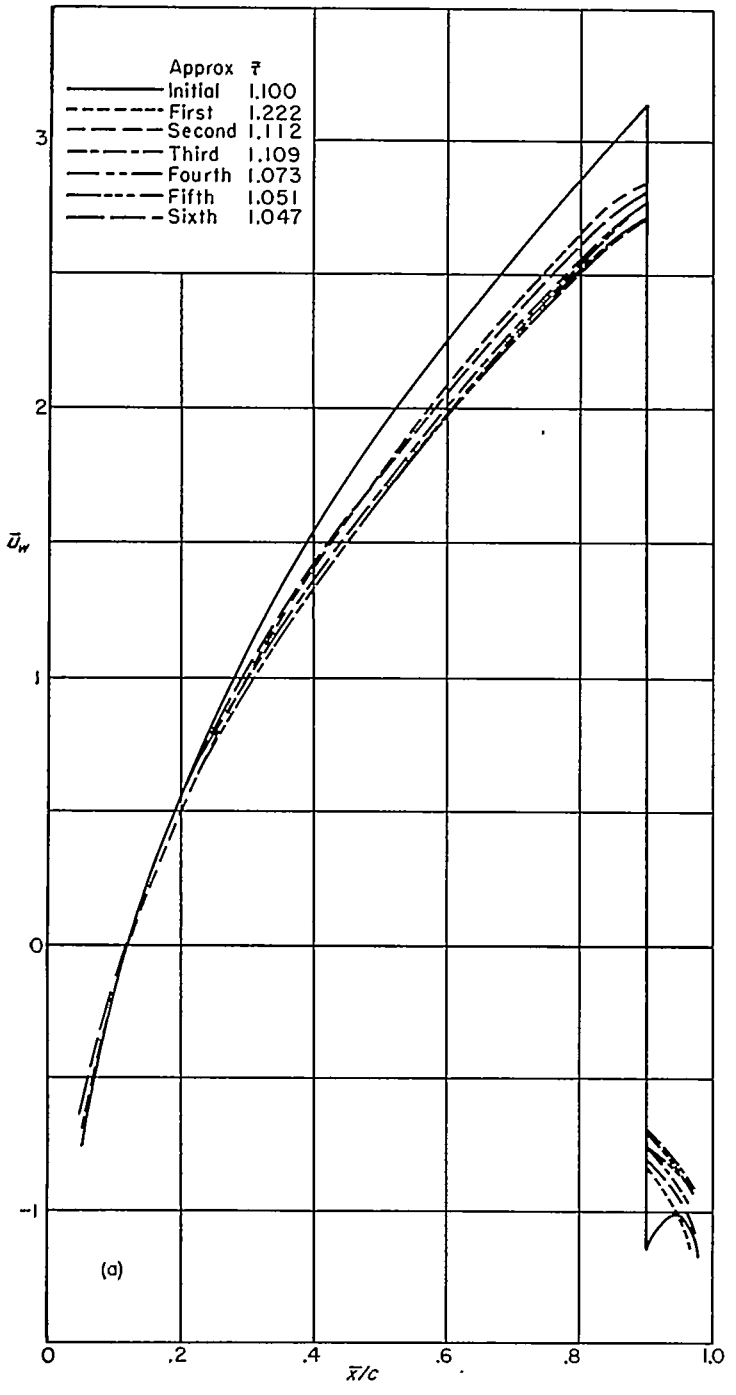

(a) Initial $\bar{u}_W$ too large.

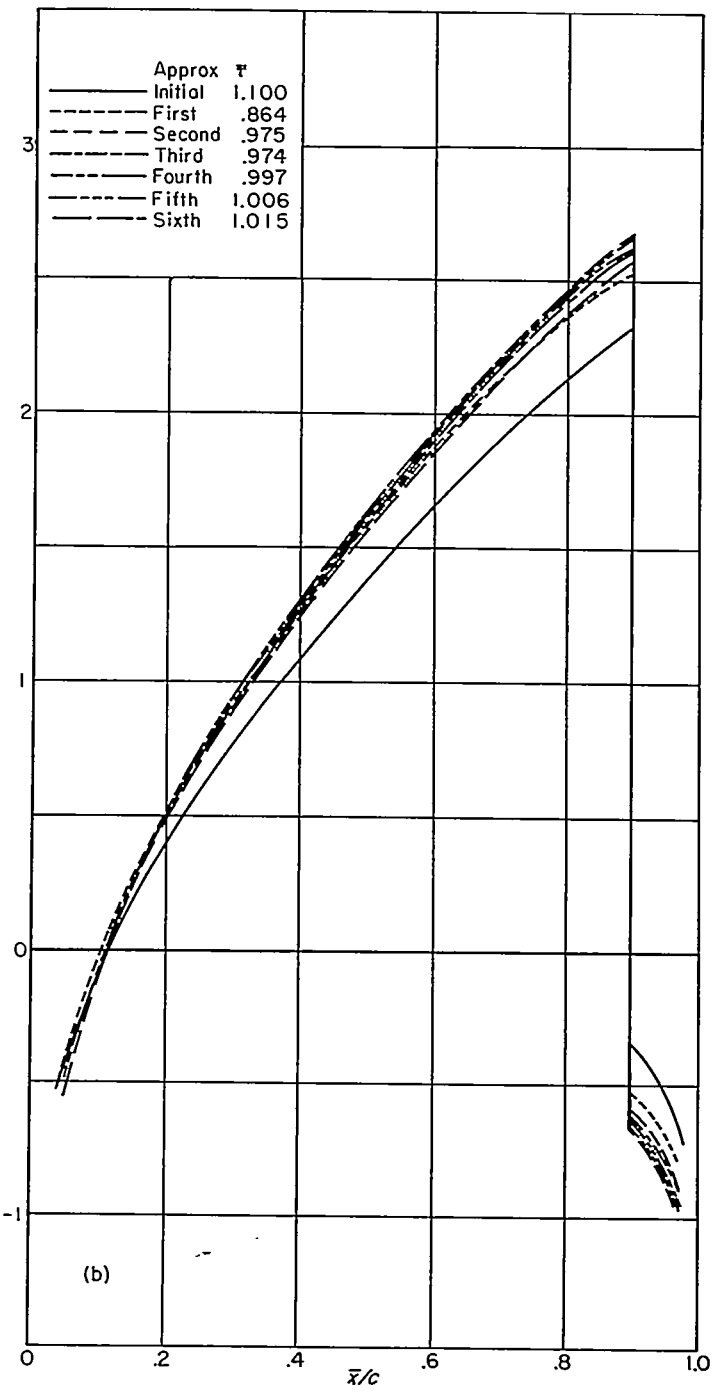

(b) Initial $\bar{u}_W$ too small.

FIGURE 28.—Results of iteration calculations started with deliberately poor assumption for $\bar{u}_W$, shock wave at 90-percent chord.

being partly iteration and partly trial and error. The calculations proceed as follows: A value of $\bar{\tau}$ is selected and an estimate made for the associated $\bar{u}_W$ distribution. On the basis of these values, calculations are performed resulting in a new set of values for $\bar{\tau}$ and $\bar{u}_W$. Similar calculations are repeated on a trial-and-error basis using the same $\bar{u}_W$ distribution but various values for $\bar{\tau}$ until the resulting $\bar{\tau}$ is equal to the assumed value. These values are then plotted on a graph of $\bar{u}_W$ versus $\bar{\tau}$. If these values were an actual solution of the integral equation, the resulting values of $\bar{u}_W$ would also be equal to the assumed values. In the present calculations, however, the resulting values of $\bar{u}_W$ are generally found to be somewhat smaller than the assumed values. These new values for $\bar{u}_W$, together with a smaller value for $\bar{\tau}$, are next taken as the starting values for a second series of trial-and-error calculations. Again, the $\bar{u}_W$ distribution is held fixed as various values are tried for $\bar{\tau}$. The calculations are again terminated when the value of $\bar{\tau}$ is so selected that it repeats itself. The values of $\bar{u}_W$ and $\bar{\tau}$ are then plotted on the graph. Unfortunately, it was not found possible in the present calculations to determine a set of values for $\bar{u}_W$ and $\bar{\tau}$ that would repeat themselves precisely. In all cases investigated, the values of $\bar{u}_W$ and $\bar{\tau}$ were found to diminish somewhat in successive iteration steps. The source of this difficulty has not been ascertained at the present time. It could be due to one or

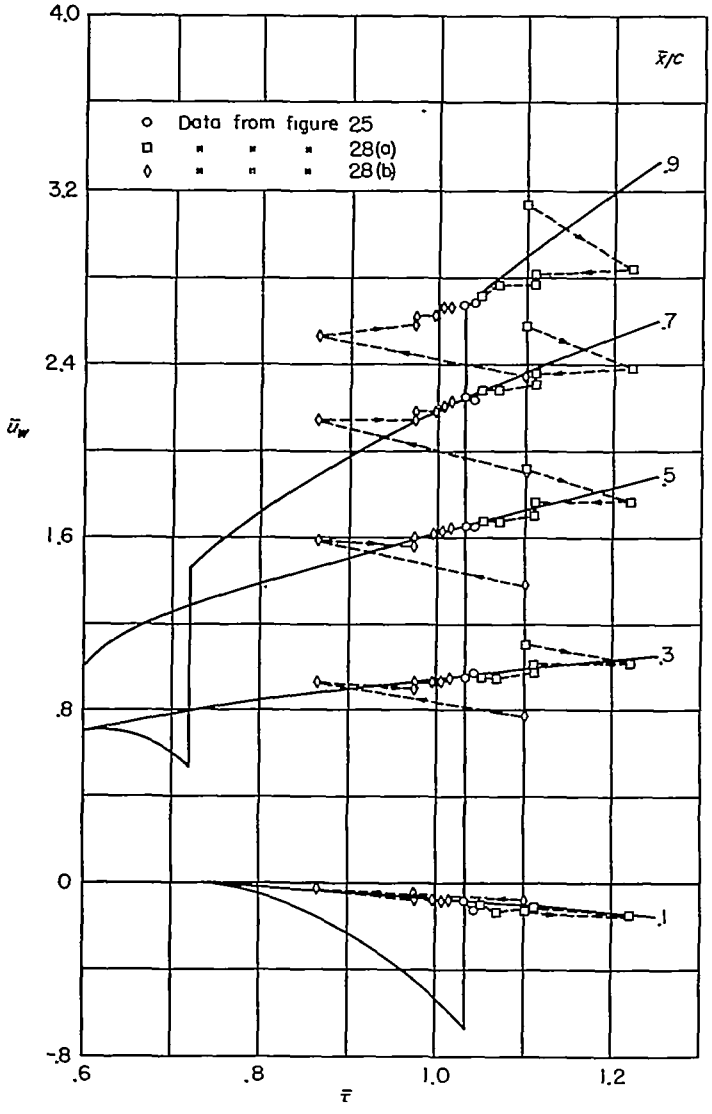

FIGURE 29.—Results of calculations with shock wave at 90-percent chord. (Cross plot of data in figures 25 and 28.)

more of the simplifying assumptions introduced in the approximate calculations or it could be due to the fact that an iteration process was not devised which would lead to a definite result, as at smaller $\bar{\tau}$.

There are a number of points, however, which tend to indicate that the successive values of $\bar{u}_w$ and $\bar{\tau}$ obtained after the first few iteration steps may be regarded as near solutions. One of these concerns the fact that calculations made starting with different initial values for $\bar{u}_w$ and $\bar{\tau}$ converge to a common result after the first few iteration steps. To illustrate, results of typical series of calculations starting with $\bar{\tau}$ of about 20 and three different $\bar{u}_w$ distributions are shown in figure 30. It can be seen that the three sets of calculations all converge to determine a single line after the first few iterations. In order to promote insight into the significance of the indicated variation of $\bar{\tau}$ from step to step of the iteration process, the corresponding Mach numbers for a 4-percent-thick section are also shown. Comparison on this basis shows that the variation of Mach number from step to step of the iteration process is very small.

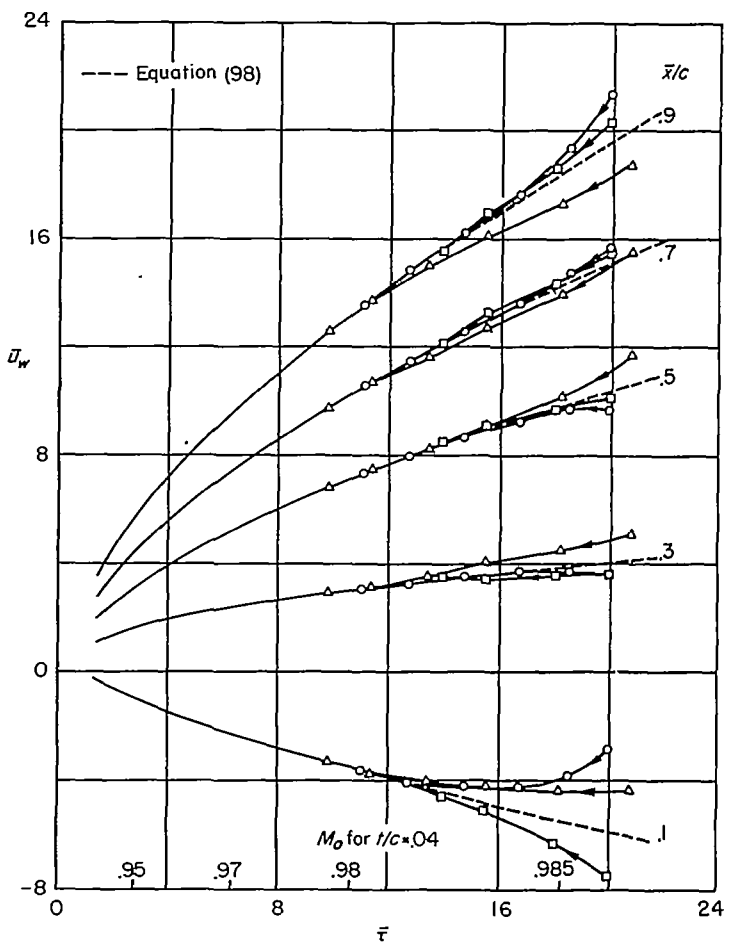

FIGURE 30.—Results of iteration calculations started with deliberately poor assumption for $\bar{u}_w$, shock wave at trailing edge.

An additional factor lending credence to the applicability of the solutions for large $\bar{\tau}$ is provided by the phenomenon of the Mach number freeze wherein the local Mach number is invariant with changes in the free-stream Mach number when the latter is near unity or, more precisely,

$$\left(\frac{dM}{dM_o}\right)_{M_o=1}=0 \tag{95}$$

It is known from the papers of Vincenti and Wagoner (ref. 14), Liepmann and Bryson (refs. 28 and 29), and others that the corresponding approximate relation yielded by the small-disturbance transonic theory is

$$\left(\frac{d\xi}{d\xi_o}\right)_{\xi_o=0}=0 \tag{96}$$

If the parameter k involved in the definitions of ξ is independent of M_o, as is the case when k is taken to be as given in equation (17), and if the local Mach number M is calculated using equation (24), the above two relations are completely equivalent. If k contains M_o, however, as it does in the preferred definition given in equation (7), dM/dM_o only vanishes when M, as well as M_o, equals unity. If it is assumed that the freeze extends over a finite range of Mach numbers, the variation of $\bar{u}$ with $\bar{\tau}$ must obey the following relation for large $\bar{\tau}$:

$$\xi=\frac{\bar{u}-1}{\bar{\tau}^{2/3}}=\text{const.} \tag{97}$$

Equation (97) has been used to compute a curve of $\bar{u}_W$ versus $\bar{\tau}$ under the assumption that the freeze extends at least to as small a value of $\bar{\tau}$ as 10, which corresponds to a Mach number of 0.978 for a 4-percent-thick section. These lines, which all have the characteristic form

$$\frac{\bar{u}_W-1}{(\bar{u}_W)_{\bar{\tau}=10}-1}=\left(\frac{\bar{\tau}}{10}\right)^{2/3} \tag{98}$$

are also shown in figure 30. It can be seen that the lines so determined are almost identical with those determined previously after the first few steps of the iteration process. This comparison shows that the solutions obtained by the iteration process possess the phenomenon of the Mach number freeze. A further check was made by extrapolating the curves of $\bar{u}_W$ versus $\bar{\tau}$ to $\bar{\tau}=40$ with the aid of equation (98) and using the values thus obtained as the initial values for an iteration calculation. It is found that these values nearly satisfy the integral equation although the values of $\bar{u}_W$ and $\bar{\tau}$ diminish slightly from step to step during the iteration process, just as at the smaller values of $\bar{\tau}$. The significance, in terms of Mach number, of these changes is even smaller than at lower Mach numbers. For example, the changes produced in the values of $\bar{u}$ and $\bar{\tau}$ in the first step of the iteration process correspond, for a 4-percent-thick section, to an indiscernible change in the local Mach number and a change in the free-stream Mach number of less than 0.001. On the basis of these results, it appears proper to extrapolate the curves of $\bar{u}_W$ versus $\bar{\tau}$ to values of $\bar{\tau}$ approaching infinity, corresponding to a Mach number of unity, by using equation (98).

The results of the calculations for the range of $\bar{\tau}$ for which the shock wave is at the trailing edge are summarized in figures 31 and 32.

RESULTS

RESULTS IN TERMS OF REDUCED QUANTITIES

The calculations described in the preceding sections have produced values for the velocity distributions at the surface of thin circular-arc airfoils in flows having free-stream Mach numbers ranging from zero to unity. These results are presented in graphical form in figures 22, 23, 26, 27, 31 and 32 in terms of the reduced quantities $\bar{u}$ and $\bar{\tau}$ defined in equations (29) and (84) and repeated below.

$$\bar{u}=\frac{k}{1-M_o^2}u, \qquad \bar{\tau}=\frac{U_o k}{(1-M_o^2)^{3/2}}\frac{t}{c}$$

where k represents the coefficient of the nonlinear term in the approximate differential equation for φ (eq. (6)).

The results of a number of previous investigations of transonic-flow theory have been presented in terms of the quantities ξ_o and ξ defined in equations (87) and (88)

$$\xi_o=-\frac{1-M_o^2}{[U_o k(t/c)]^{2/3}}, \qquad \xi=-\frac{1-M^2}{[U_o k(t/c)]^{2/3}}$$

The relations between the two sets of quantities are given by equations (87) and (90)

$$\xi_o=-\left(\frac{1}{\bar{\tau}}\right)^{2/3}, \qquad \xi=\frac{\bar{u}-1}{\bar{\tau}^{2/3}}$$

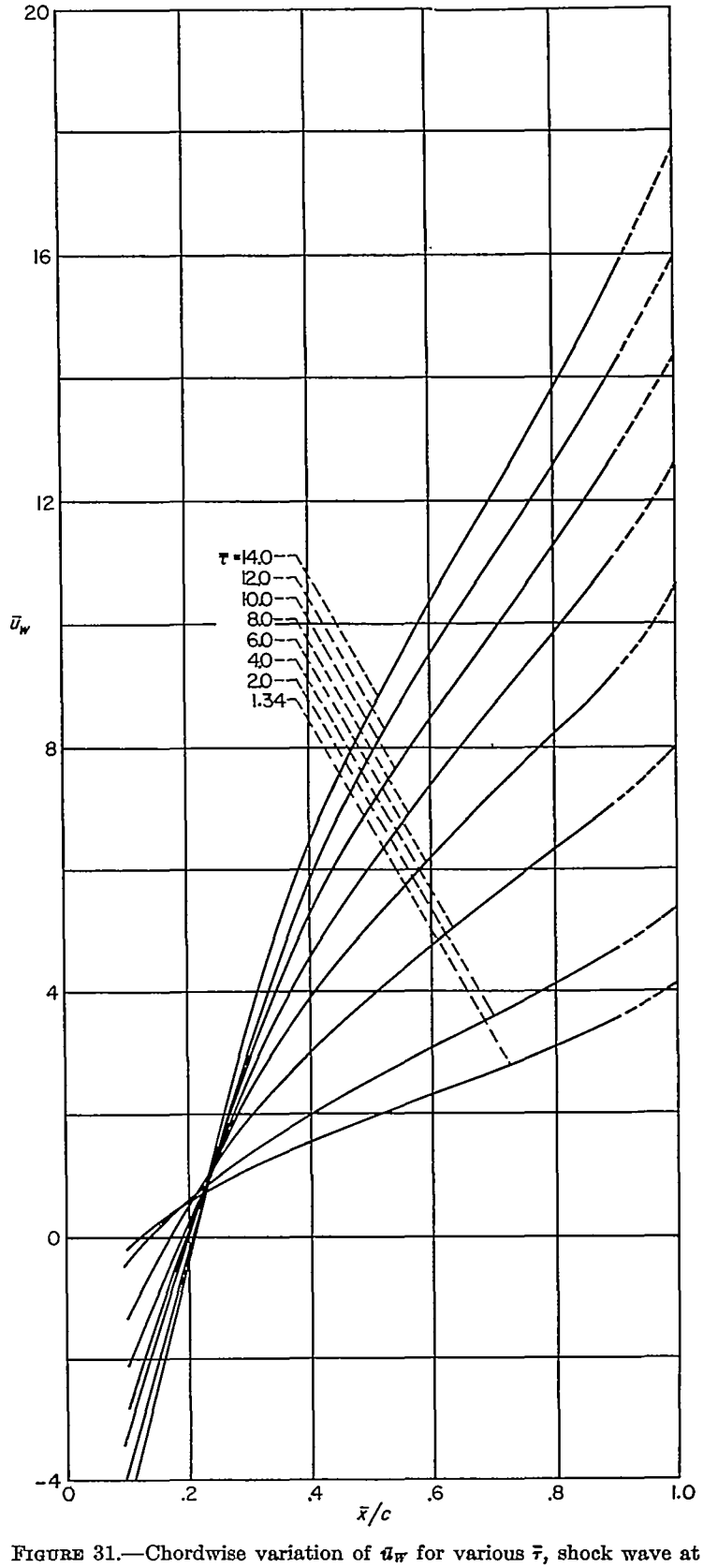

FIGURE 31.—Chordwise variation of $\bar{u}_W$ for various $\bar{\tau}$, shock wave at trailing edge.

Pressure distribution.—In many applications, the quantity of prime interest is the pressure distribution rather than the velocity or Mach number distribution. Because of the simple relation between the pressure coefficient and the perturbation velocity provided by equation (16), however,

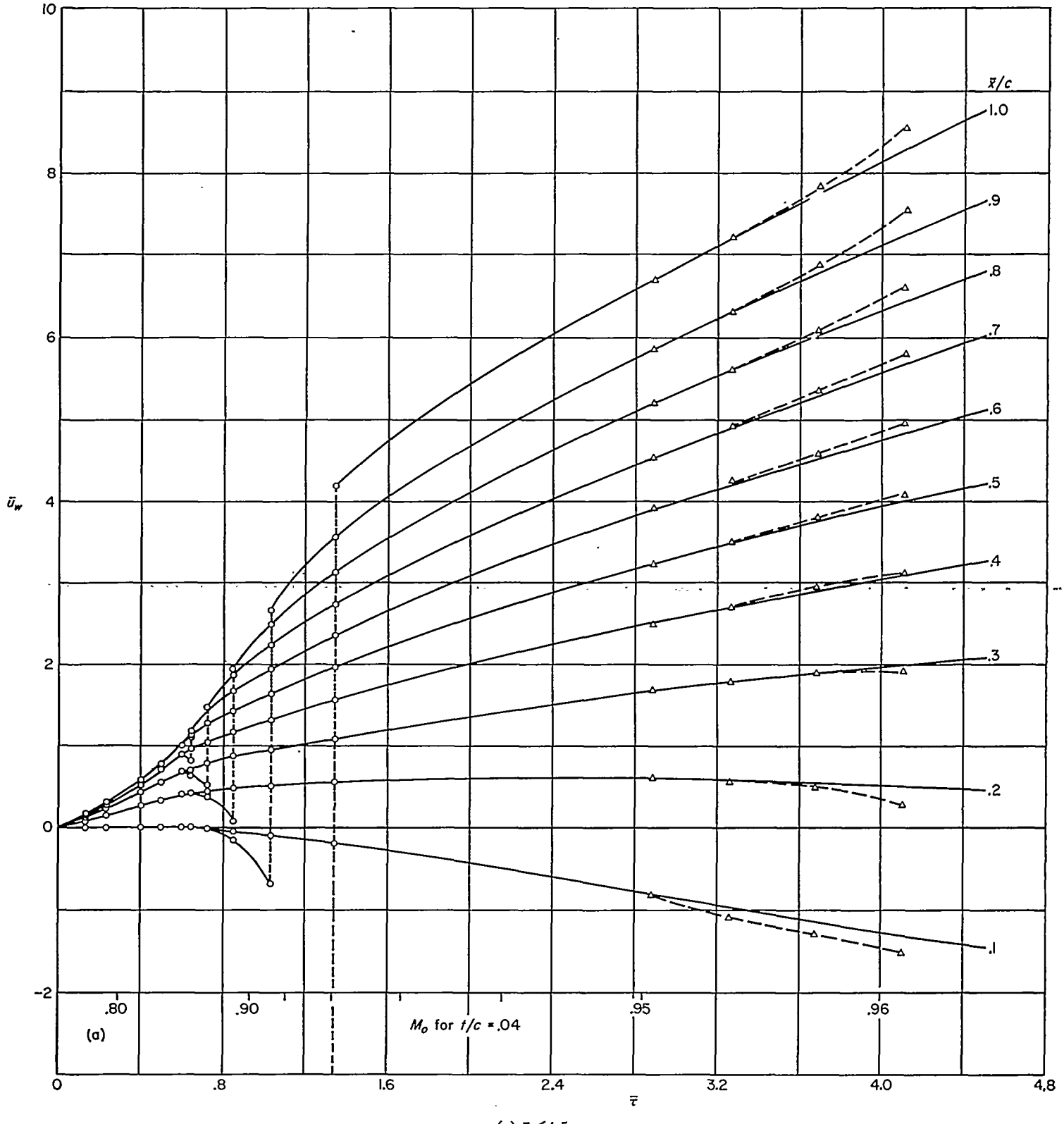

(a) $\bar{\tau}<4.5$

FIGURE 32.—Variation of $\bar{u}_w$ with $\bar{\tau}$ for various values of $\bar{x}/c$, shock wave at trailing edge.

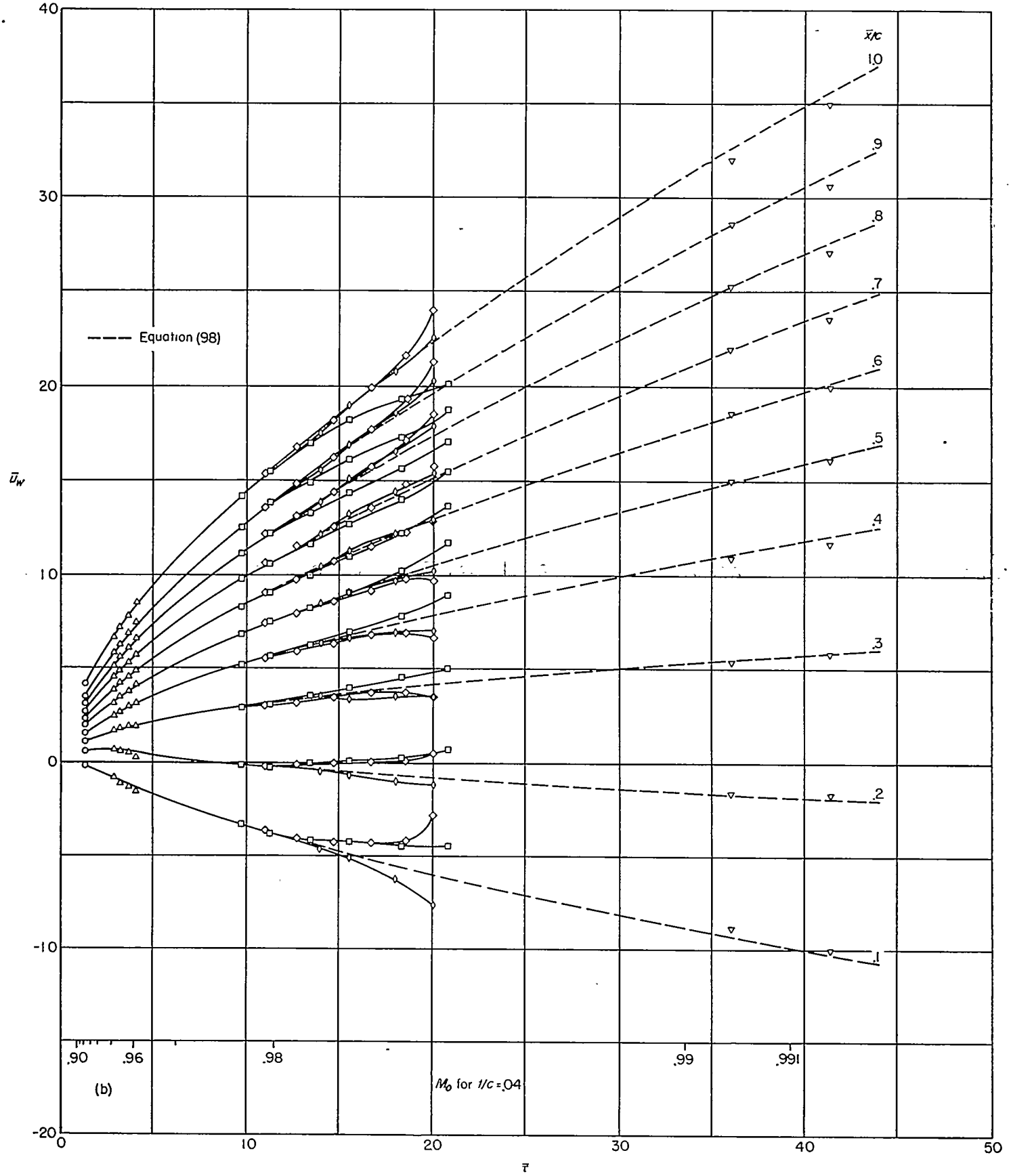

(b) Large $\bar{r}$.

FIGURE 32.—Concluded.

it is a simple matter to determine the pressure distribution once the velocity distribution is known; thus,

$$C_p=-\frac{2u}{U_o}=-\frac{2(1-M_o^2)}{U_o k}\bar{u}=-\frac{2(t/c)^{2/3}}{(U_o k)^{1/3}}\left(\frac{\bar{u}}{\bar{\tau}^{2/3}}\right) \tag{99}$$

The latter expression for C_p suggests the introduction of a reduced pressure coefficient $\overline{C_p}$ defined by

$$\overline{C_p}=\frac{(U_o k)^{1/3}}{(t/c)^{2/3}}C_p=-2\left(\frac{\bar{u}}{\bar{\tau}^{2/3}}\right) \tag{100}$$

Equation (100) may be rewritten in terms of ξ_o and ξ as follows:

$$\overline{C_p}=-2(\xi-\xi_o) \tag{101}$$

The foregoing results have been used to calculate $\overline{C_p}$ for numerous stations on the airfoil chord for various ξ_o (or $\bar{\tau}$). The results so obtained are presented in figure 33 in the form of chordwise pressure distributions ($\overline{C_p}$ vs. $\bar{x}/c$) for various ξ_o. This figure is presented in three parts: Part (a) contains the results for subcritical Mach numbers, part (b) for slightly supercritical Mach numbers for which the shock wave stands on the airfoil surface, and part (c) for still larger Mach numbers for which the shock wave is at the trailing edge.

The same results are presented in another manner in figure 34 in which the variation of $\overline{C_p}$ with ξ_o is plotted for various stations $\bar{x}/c$ along the airfoil chord. This form of presentation is the counterpart, in terms of reduced quantities, of the plots commonly found in many experimental investigations showing the variation of pressure coefficient C_p with free-stream Mach number M_o at prescribed points on the surface of wings and bodies. The corresponding curves given by

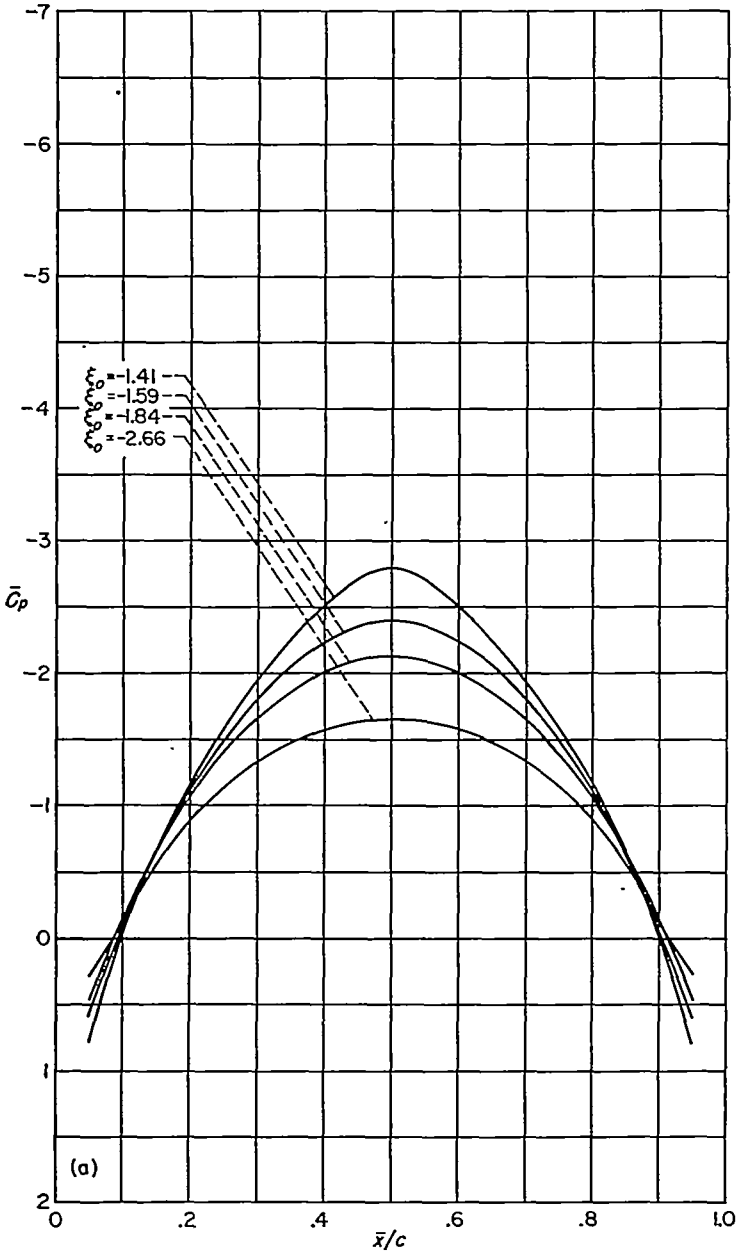

(a) Subcritical.

FIGURE 33.—Chordwise variation of $\overline{C_p}$ for various ξ_o.

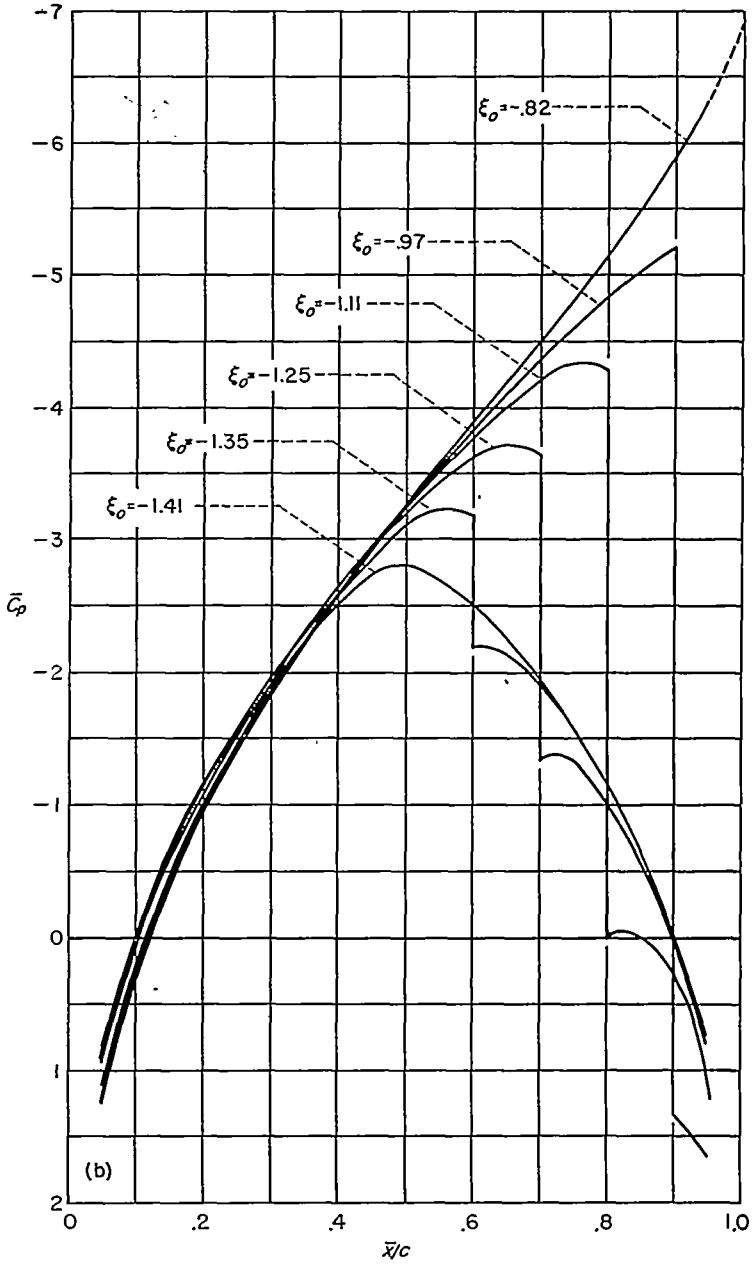

(b) Shock wave forward of trailing edge.

Figure 33.—Continued.

linear theory are shown in figure 34 by dotted lines. These curves are computed using the equation

$$\overline{C}_{p_L}=-\frac{8}{\pi\sqrt{-\xi_o}}\left[1+\left(\frac{1}{2}-\frac{\bar{x}}{c}\right)\ln\frac{\bar{x}}{c-\bar{x}}\right] \tag{102}$$

obtained by direct substitution of equations (87) and (100) into equation (85). It can be seen that the present results and those of linear theory are in good agreement for values of ξ_o considerably less than zero. For ξ_o near to zero, however, the present results display a behavior completely different from that indicated by linear theory. This is as it should be since it is well known that linear theory is totally inadequate for the analysis of steady two-dimensional flows about airfoils when the Mach number approaches unity, or, in the present notation, when ξ_o approaches zero.

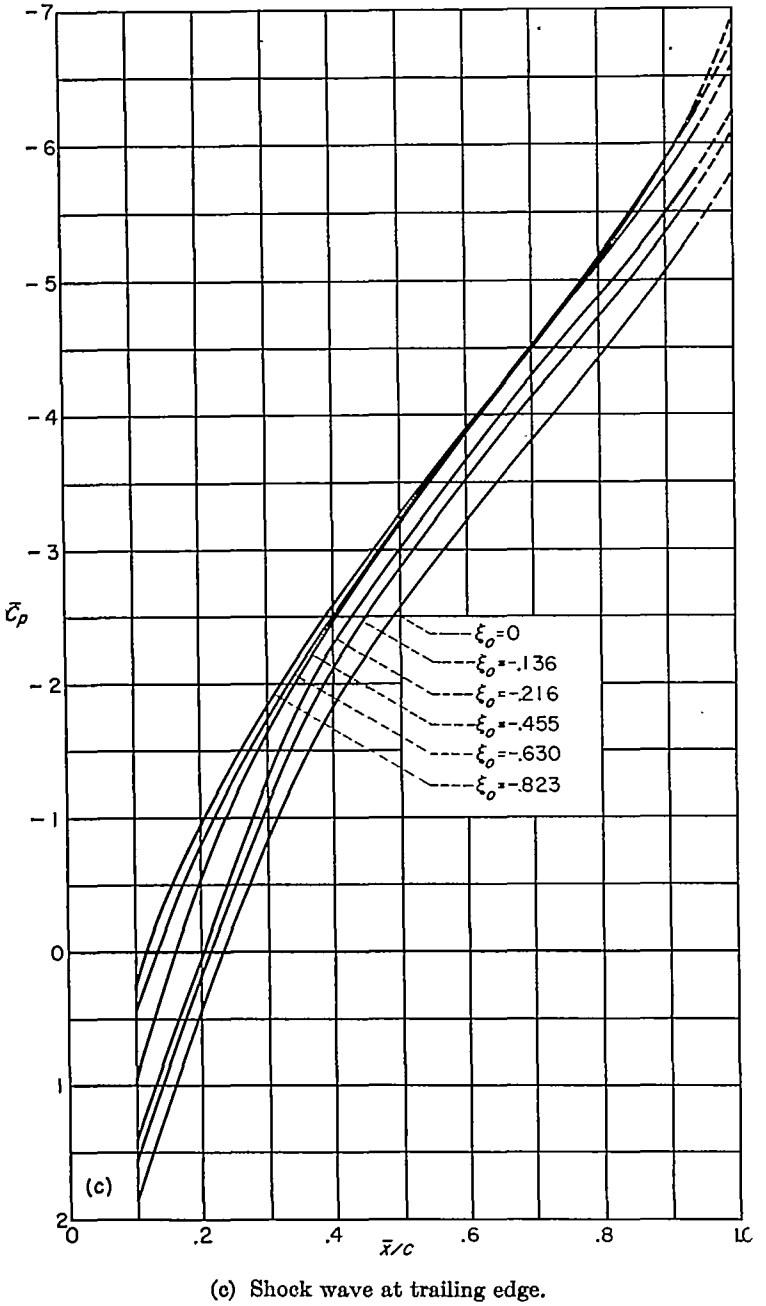

(c) Shock wave at trailing edge.

FIGURE 33.—Concluded.

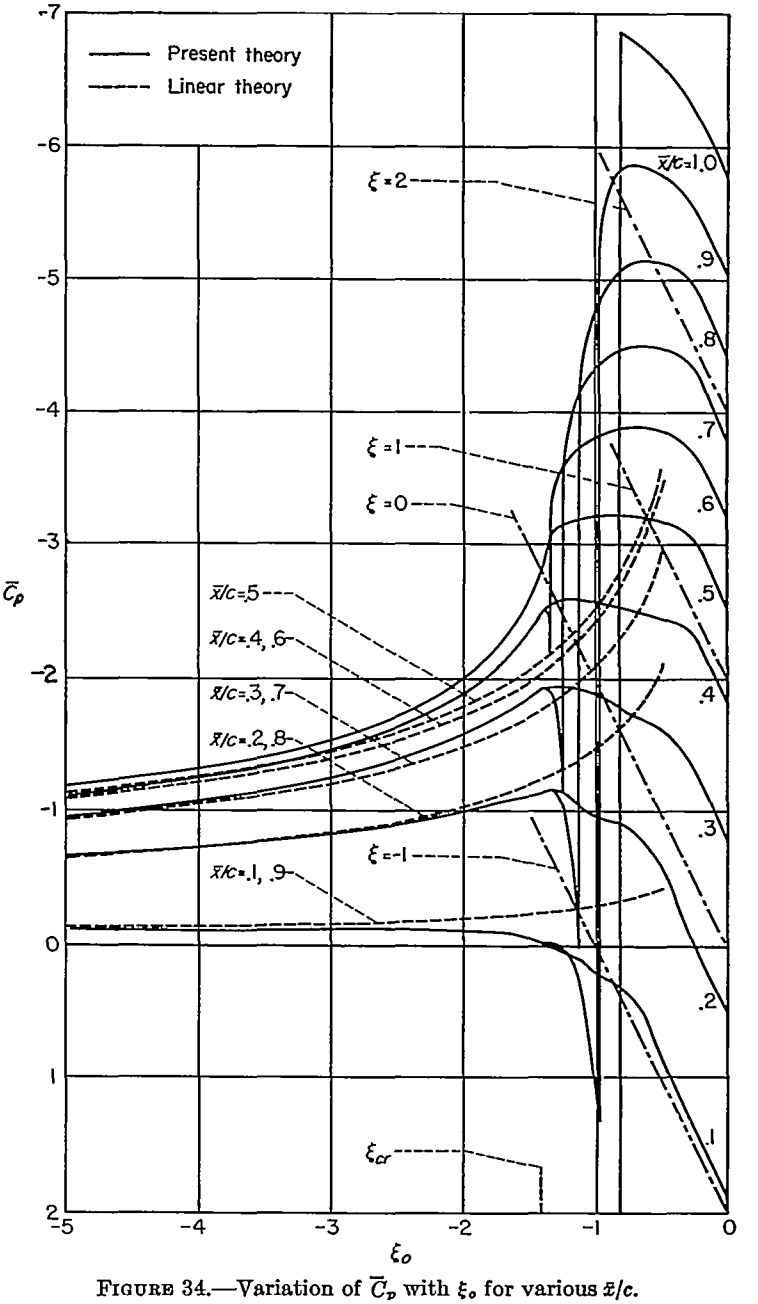

FIGURE 34.—Variation of $\overline{C}_p$ with ξ_o for various $\bar{x}/c$.

In order to provide further information regarding the significance of the indicated variations of $\overline{C}_p$ with ξ_o, lines of constant ξ have also been included in figure 34. The local velocities are subsonic if ξ is negative and are supersonic if ξ is positive. The Mach number freeze is indicated in figure 34 by the curve representing the variation of $\overline{C}_p$ with ξ_o at a given station $\bar{x}/c$ becoming parallel to a line of constant ξ. It can be seen from this figure that such behavior occurs at all stations on the airfoil for ξ_o near zero.

Pressure drag.—The foregoing paragraphs have been concerned with the determination of pressure distributions on thin nonlifting circular-arc airfoil sections. Once these results are known, it is a simple matter to determine the section pressure drag coefficient c_d

$$c_d=\frac{d}{\frac{\rho_o}{2}U_o^2 c}=\frac{2}{c}\int_0^c C_p\frac{dZ_u}{dx}dx \tag{103}$$

It is convenient at this point to introduce a reduced section drag coefficient $\bar{c}_d$ defined in terms of reduced quantities, thus

$$\bar{c}_d=\frac{2}{c}\int_0^c \bar{C}_p \frac{d(\bar{Z}_u/\bar{\tau})}{d\bar{x}}d\bar{x} \tag{104}$$

It is clear from the definitions of $\bar{C}_p$, $\bar{\tau}$, $\bar{Z}$, and $\bar{x}$ that the relation between c_d and $\bar{c}_d$ is

$$\bar{c}_d=\frac{(U_o k)^{1/3}}{(t/c)^{5/3}}\frac{2}{c}\int_0^c C_p\frac{dZ_u}{dx}dx=\frac{(U_o k)^{1/3}}{(t/c)^{5/3}}c_d \tag{105}$$

It should be remarked that some additional error is incurred in the present calculations of drag because the pressures are large and only poorly determined in the vicinity of the leading and trailing edges.

The variation of $\bar{c}_d$ with ξ_o has been computed and the results are shown in figure 35. It can be seen that $\bar{c}_d$ is zero for ξ_o less than -1.418 (corresponding to the critical Mach number). The rapid rise of $\bar{c}_d$ as ξ_o is increased beyond the critical is associated with the rearward movement of the shock and terminates abruptly when the shock reaches the trailing edge at $\xi_o=-0.825$. The drag coefficient continues to increase slowly with further increases of ξ_o although at a much reduced rate; and, finally, at a value of ξ_o somewhat less than zero, $\bar{c}_d$ becomes invariant with further changes in ξ_o. This latter behavior is associated with the Mach number freeze, thus,

$$\left(\frac{d\bar{c}_d}{d\xi_o}\right)_{\xi_o=0}=\frac{2}{c}\int_0^c\left(\frac{d\bar{C}_p}{d\xi_o}\right)_{\xi_o=0}\frac{d(\bar{Z}_u/\bar{\tau})}{d\bar{x}}d\bar{x}$$

$$=-\frac{4}{c}\int_0^c\left(\frac{d\xi}{d\xi_o}-1\right)_{\xi_o=0}\frac{d(\bar{Z}_u/\bar{\tau})}{d\bar{x}}d\bar{x} \tag{106}$$

Since the Mach number freeze corresponds, in the approximate theory to $(d\xi/d\xi_o)_{\xi_o=0}=0$, equation (106) may be simplified to the following form:

$$\left(\frac{d\bar{c}_d}{d\xi_o}\right)_{\xi_o=0}=\frac{4}{c}\int_0^c\frac{d(\bar{Z}_u/\bar{\tau})}{d\bar{x}}d\bar{x}=\frac{4}{c}\left[\frac{(\bar{Z}_u)_{TE}-(\bar{Z}_u)_{LE}}{\bar{\tau}}\right]$$

$$=4\left[\frac{(Z_u)_{TE}-(Z_u)_{LE}}{t}\right] \tag{107}$$

where $(Z_u)_{LE}$ and $(Z_u)_{TE}$ refer to the ordinates of the upper surface at the leading edge and trailing edge, respectively. Since both of these quantities are zero for the circular-arc airfoils treated herein, it follows that

$$\left(\frac{d\bar{c}_d}{d\xi_o}\right)_{\xi_o=0}=0 \tag{108}$$

The corresponding results for symmetrical double-wedge profiles given in references 17, 13, and 14 by Trilling, Guderley and Yoshihara, and Vincenti and Wagoner, respectively, are also shown in figure 35. Except for the value of $\bar{c}_d$ at $\xi_o=0$, the two sets of results bear only a qualitative resemblance. In some cases, the reason for the difference is clear; in other cases, the reasons are more obscure. An example of the former concerns the result that the drag of the circular-arc section is zero for ξ_o less than -1.408, whereas the drag of the double-wedge section remains finite for all ξ_o. The latter behavior results from the fact that the critical Mach number is zero for the double-wedge section. The reasons for the pronounced difference in shape between the two curves for drag at subsonic speeds are not so clear. The immediate explanation is that the shock wave moves rearward across the chord of the circular-arc airfoil at a more rapid rate than it does with the double-wedge airfoil. For the circular-arc airfoil, the shock wave has moved to the

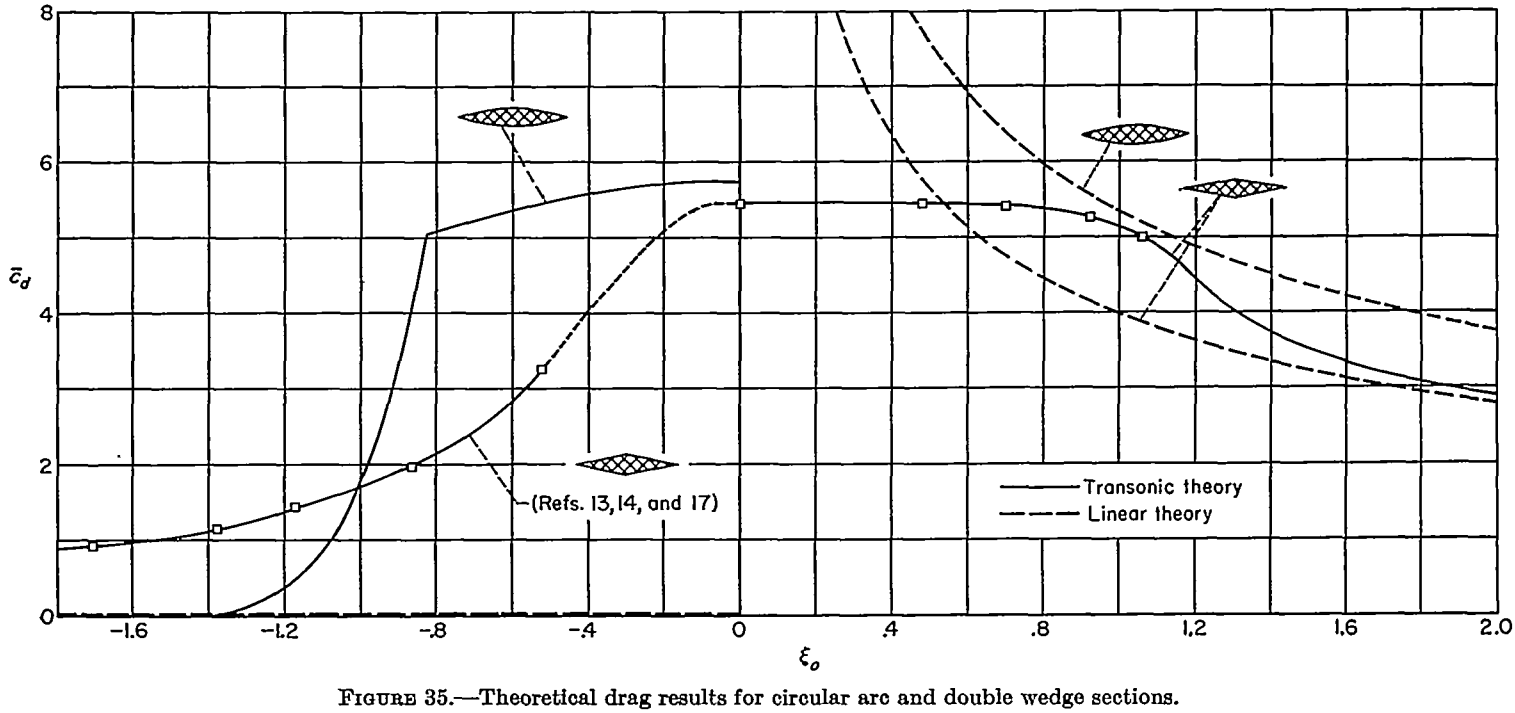

FIGURE 35.—Theoretical drag results for circular arc and double wedge sections.

trailing edge when ξ_o equals -0.825. This condition marks the end of the rapid increase in drag. On the other hand, Trilling's results for the double-wedge airfoil indicate that the shock wave does not reach the trailing edge until the free-stream Mach number is unity, or $\xi_o=0$. Whether this difference is an actual property of the solutions of transonic small-disturbance theory for these two profiles, or the result of simplifying assumptions introduced in either the present analysis or that of Trilling remains an unanswered question at the present time.

RESULTS IN TERMS OF PHYSICAL QUANTITIES

The preceding section has summarized the results of the present calculations of the pressure distribution and drag of thin circular-arc airfoils in flows having free-stream Mach numbers up to unity. These results are given in terms of the reduced parameters $\overline{C}_p$, $\overline{c}_d$, and ξ_o, which possess the advantage of condensing the information for all thickness ratios onto a single curve, but the disadvantage of being somewhat complicated and unfamiliar. Consequently, it is the aim of this section to re-express these results in terms of the more conventional quantities C_p, c_d, M_o, and t/c.

Critical Mach number.—An airfoil property that is always of interest is the critical Mach number, M_{cr}. The variation of the critical Mach number with thickness ratio can be readily determined from the result that $\xi_{cr}=-1.408$, thus,

$$\xi_{cr}=-\frac{1-M_{cr}^2}{[U_o k(t/c)]^{2/3}}=-1.408 \qquad (109)$$

In this and in the remainder of the discussion, it is assumed whenever the results of numerical computations are presented that k is as defined in equation (7) and that γ is equal to 1.4. Figure 36 shows a plot of the results of these calculations together with the corresponding results obtained using (a) linear theory and (b) thin-airfoil theory for incompressible flow together with the Kármán-Tsien rule to account for the effect of compressibility. In both of the latter calculations, the variation of $C_{p_{cr}}$ with M_o was determined using equation (23), as is customary in engineering practice. It can be seen that the present calculations indicate that the critical Mach number is somewhat less than given by either linear theory or by the Kármán-Tsien method. This is in accord with the results found when the more exact theories are applied to thin airfoils.

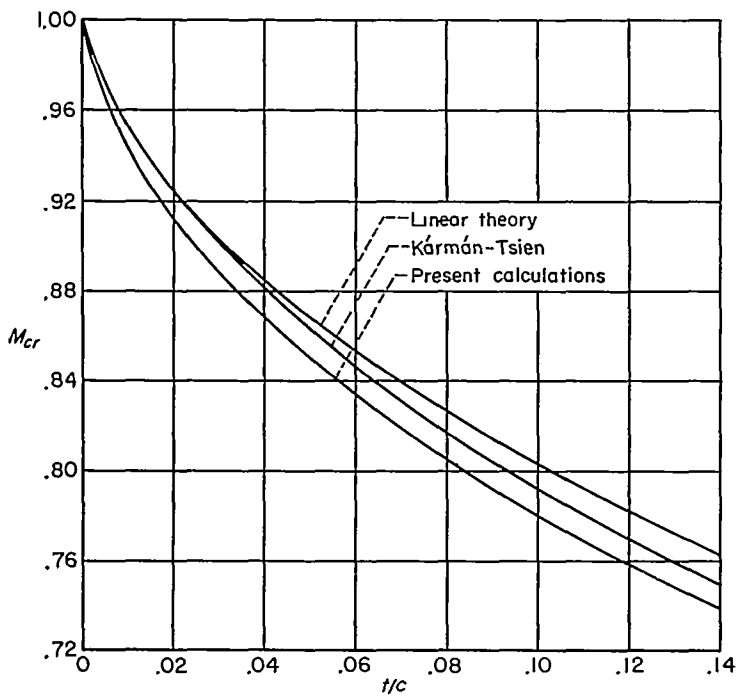

FIGURE 36.—Variation of critical Mach number with thickness ratio for circular-arc airfoil.

Pressure distribution.—The foregoing general results have been applied to determine the pressure distributions on a 4-percent-thick circular-arc profile. These results are presented in two alternative forms in figures 37 and 38. The first of these shows the chordwise variation of C_p for various free-stream Mach numbers and illustrates the development and rearward movement of the shock wave as the free-stream Mach number increases beyond the critical. The second form shows the variation of C_p with M_o for selected points x/c on the airfoil chord. Three sets of auxiliary lines are also shown; they are (a) lines of constant local Mach number computed using equations (24) and (25) and (b) lines showing the variation of C_p with M_o at selected points on the airfoil chord computed using thin-airfoil theory for incompressible flow together with the Kármán-Tsien rule. At Mach numbers less than the critical, it can be seen that the pressure coefficient at a given point on the airfoil surface varies with Mach number in a manner similar to that predicted by the Kármán-Tsien rule. It is also apparent, as was pointed out earlier in connection with equations (22) and (23) and figure 2, that the value to be taken for the critical Mach number differs slightly depending on whether the lines of constant local Mach number are computed by the present approximation (eq. (24)) or by the exact isentropic relation (eq. (25)). The irregular behavior of the pressures on the rear half of the airfoil at supercritical Mach numbers is associated with the passage of the shock wave. At Mach numbers near unity, a completely different behavior is evidenced in which the values of C_p change with M_o in such a manner that the local Mach number remains essentially constant. Direct calculation shows that the present theory implies the following approximate relation for dC_p/dM_o at a free-stream Mach number of unity.[4]

$$\left(\frac{dC_p}{dM_o}\right)_{M_o=1}=\frac{4}{\gamma+1}\frac{2}{3}(C_p)_{M_o=1}, \qquad k=M_o^2\left(\frac{\gamma+1}{U_o}\right) \qquad (110)$$

This may be compared with the exact relation given by Vincenti and Wagoner in reference 14.

$$\left(\frac{dC_p}{dM_o}\right)_{M_o=1}=\frac{4}{\gamma+1}\frac{2}{\gamma+1}(C_p)_{M_o=1} \qquad (111)$$

[4] It might be noted here that numerous investigators have given the approximate relation

$$\left(\frac{dC_p}{dM_o}\right)_{M_o=1}=\frac{4}{\gamma+1}, \qquad k=\frac{\gamma+1}{U_o}$$

rather than that given in equation (110). As indicated by the auxiliary equations, the relations for dC_p/dM_o at $M_o=1$ follow directly from the particular definition of k. It is interesting to observe that the expression for k given in equation (7) provides the more accurate relation for $(dC_p/dM_o)_{M_o=1}$, even though, as noted in connection with the discussion of equation (96), it provides the lesser accuracy in the determination of $(d\Lambda/dM_o)_{M_o=1}$.

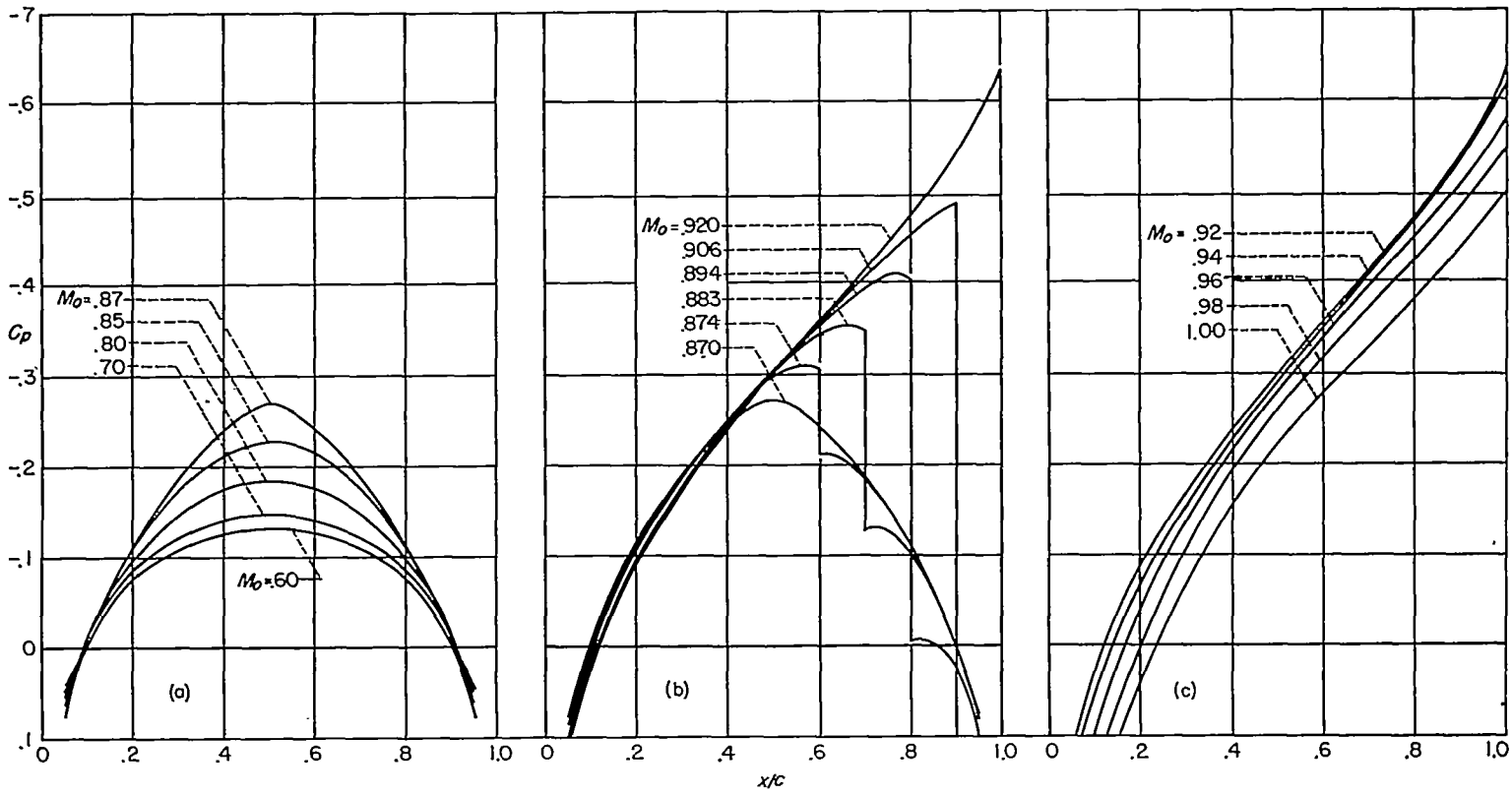

(a) Subcritical. (b) Shock wave forward of trailing edge. (c) Shock wave at trailing edge.

FIGURE 37.—Chordwise variation of C_p for varous free-stream Mach numbers, 4-percent-thick circular-arc airfoil.

Pressure drag.—The variation of the section pressure drag coefficient c_d with M_o has also been calculated for the 4-percent-thick circular-arc airfoil and the results are shown in figure 39. The general features of this curve are very similar to those discussed previously in connection with the corresponding curve of figure 35 for the reduced quantities. The major point of difference concerns the slope of the curve at a Mach number of unity. Thus, the preceding discussion has disclosed that $d\overline{c_d}/d\xi_o$ is zero at a Mach number of unity; whereas figure 39 shows that dc_d/dM_o is negative at $M_o=1$. Direct substitution gives the following value for this slope:

$$\left(\frac{dc_d}{dM_o}\right)_{M_o=1}=-\frac{2}{3}(c_d)_{M_o=1} \tag{112}$$

Vincenti and Wagoner have shown in reference 14 that the exact relation for flow about a closed airfoil is

$$\left(\frac{dc_d}{dM_o}\right)_{M_o=1}=-\frac{2}{\gamma+1}(c_d)_{M_o=1} \tag{113}$$

The negative value of the slope given in equation (112) arises from the fact that the quantity k which appears in all the reduced parameters ($\overline{c_d}$, $\overline{C_p}$, ξ_o, etc.) is a function of M_o. If, as in many other papers, k is equated to $(\gamma+1)/U_o$ and is thus independent of M_o, the value of the slope is zero, thus

$$\left(\frac{dc_d}{dM_o}\right)_{M_o=1}=0, \qquad k=\frac{\gamma+1}{U_o} \tag{114}$$

COMPARISON WITH EXPERIMENT

Inasmuch as the results described in the preceding sections were calculated after making numerous simplifications and approximations, not the least of which is the assumption of inviscid flow, it is desirable to include some comparisons with experiment. This is particularly true for the present problem since it is well known that phenomena outside the scope of potential theory, such as separation, boundary-layer shock-wave interaction, etc. are prominent features of transonic flow about airfoils. Since it is indicated in the preceding discussion that the present results are in general accord with the proven Prandtl-Glauert and Kármán-Tsien results in the subcritical Mach number range, the following remarks will be confined to the supercritical range.

There are at least three papers available which present results of detailed measurements of flow at high subsonic velocities about symmetrical circular-arc airfoil sections, namely, reference 33 by Liepmann, reference 34 by Liepmann, Ashkenas, and Cole, and reference 35 by Wood and Gooderum. The first two of these are concerned primarily with boundary-layer shock-wave interaction and contain statements casting doubt on the accuracy of the values indicated for the free-stream Mach number, a quantity of only secondary interest in their investigations. In general, it appears that values given for M_o in these two papers are somewhat too great. The more recent investigation of Wood and Gooderum appears to be better in this particular and possesses the advantage of being made with an interferometer so that knowledge is gained about the entire flow

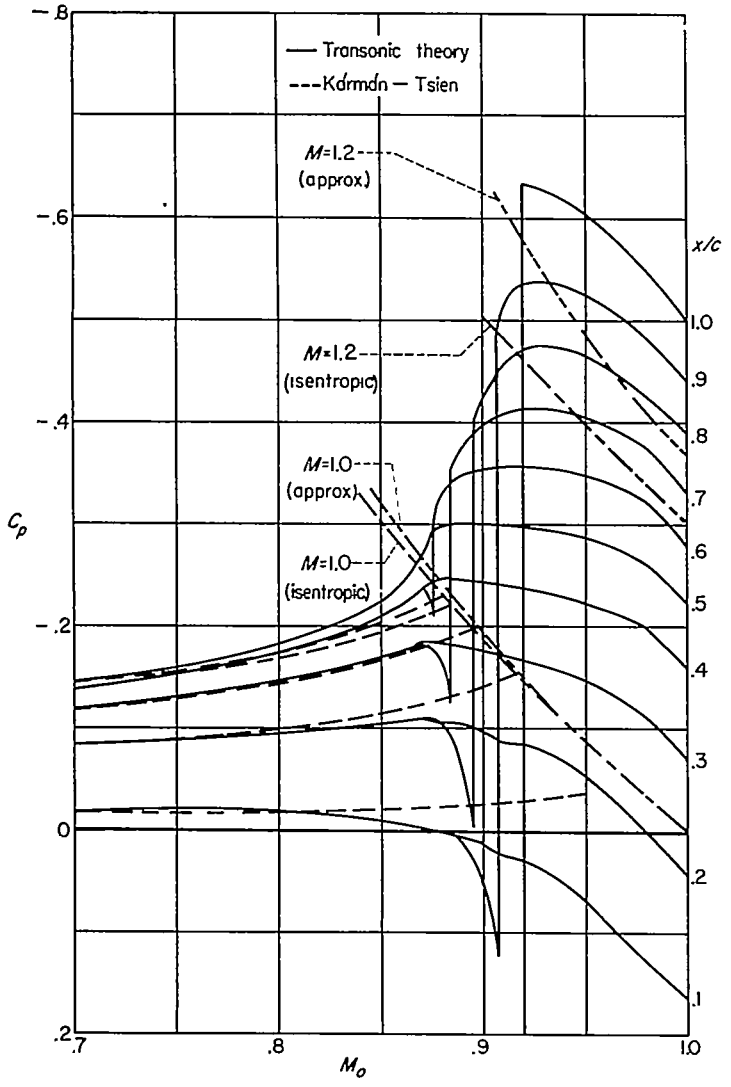

FIGURE 38.—Variation of C_p with M_o for various values of x/c, 4-percent thick circular-arc airfoil.

field. A disadvantage, however, is that the tests were made using a 12-percent-thick model, which severely strains the assumptions of transonic small-disturbance theory. Nevertheless, the comparisons will be made with the data of reference 35.

The studies of Liepmann (ref. 33), Ackeret, Feldmann, and Rott (ref. 36), and others have shown that the boundary layer can have a profound influence on a transonic flow field. This immediately raises a question regarding the usefulness of a potential-flow theory, such as the present, which disregards the boundary layer completely. In order to illustrate better the nature of these effects, two interferograms of the flow about 12-percent-thick circular-arc airfoils are reproduced from reference 35 and shown in figure 40. The free-stream Mach number is 0.88, and the Reynolds number based on the chord is 600,000 for both photographs. The conditions for the two flows differ in that the boundary layer is laminar in the flow pictured on the left and turbulent in that pictured on the right. The interferogram for the laminar case shows that the shock waves are of the λ type and that the flow separates near the midchord station. When the boundary layer is turbulent, however, it may be seen that the shock wave is of the simple single wave type,

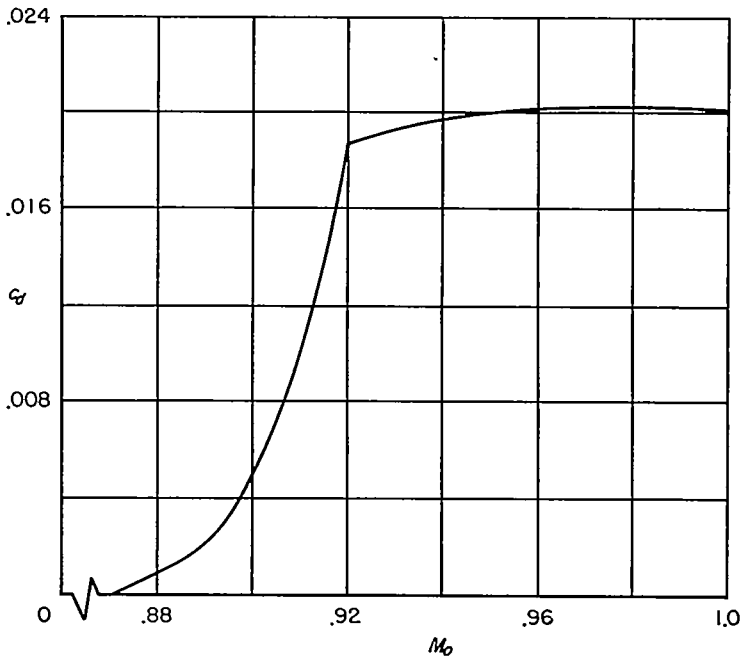

FIGURE 39.—Variation of c_d with M_o, 4-percent-thick circular-arc airfoil.

and that the extent of the region of separated flow is greatly diminished. From this pair of photographs, it is apparent that two of the simplifying assumptions introduced in the course of the present analysis (i. e., (a) no flow separation occurs and (b) the shock wave is a single normal wave) are in better accord with the physical phenomenon if the boundary layer is turbulent ahead of the shock wave than if it is laminar. Figure 41 shows experimental pressure distributions determined from the two interferograms of figure 40 together with the corresponding theoretical results. Because of difficulties in interpreting the interferograms, the experimental pressure distributions presented in reference 35 and reproduced in figure 41 are terminated at the separation point. It can be seen that the theoretical results are in substantial agreement with the experimental data available for the portion of the airfoil forward of the separation point. Although the experimental and theoretical pressure distributions matched equally well for all the test data of reference 35, the degree of correspondence must be attributed, in part, to a fortunate cancellation of errors since individual components involved in the perturbation analysis (e. g., the relation between w and dZ/dx, C_p and the perturbation velocity components, etc.) contain appreciable errors when applied to such a thick airfoil. Although the corresponding experimental values are not available for the pressures at stations aft of the separation point, it is presumed from other experimental data that the pressures reach their maximum negative value in the vicinity of the separation point and return toward the free-stream value at stations farther aft on the airfoil, rather than varying in the manner indicated by the calculated results.

Before leaving this topic, the following remarks should be made concerning experimental factors which may affect these conclusions. The first is that the authors of reference 35 do not consider the data for the turbulent boundary layer to be as reliable as that for the laminar boundary

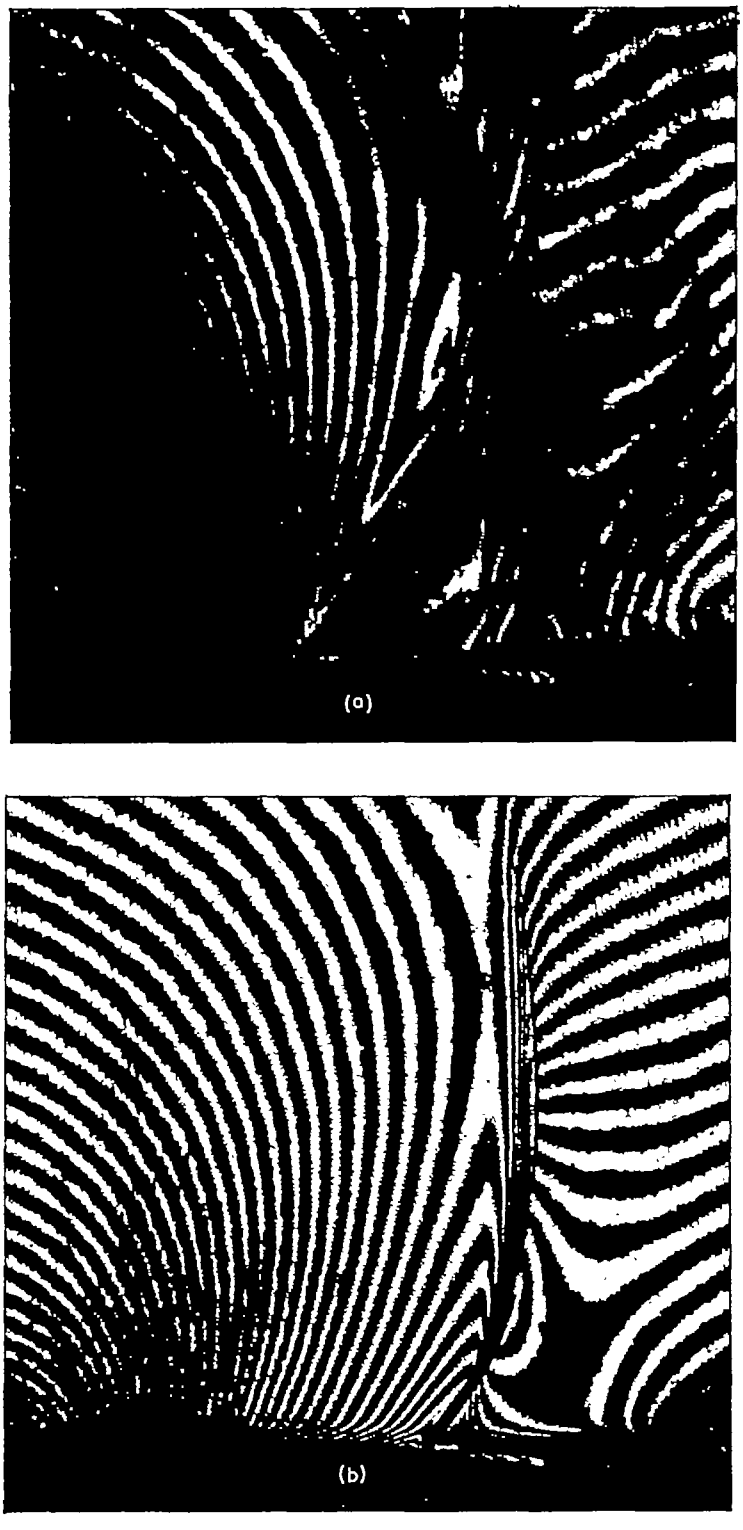

(a) Laminar boundary layer.
(b) Turbulent boundary layer.

FIGURE 40.—Interferograms of flow about 12-percent-thick circular-arc airfoil at a Mach number of 0.88 and a Reynolds number of 600,000. From reference 35.

layer. The reason for this is that the method used to make the boundary layer turbulent (the upper half of the airfoil was mounted on a flat plate which extended one chord length forward of the leading edge of the airfoil) produced such a thick boundary layer that difficulties were encountered in correctly extrapolating the lines of the interferograms to the airfoil surface.[5] The differences in boundary-layer thickness are clearly evident in the interferograms shown in figure 40. The second stems from the fact that the tests were conducted with a 12-percent-thick airfoil. Comparisons of theory and experiment for such thick airfoils not only strain the small-disturbance assumptions of the theory but also emphasize unduly such features of the flow as the curvature of the shock wave and boundary-layer separation which are disregarded completely in the theory. The third is concerned with the fact that results of a recent flight investigation by Harrin (ref. 37) have shown that, at Reynolds numbers of the order of 20,000,000, there is very little difference in pressure distribution with laminar and turbulent boundary layers. In particular, it is found that the λ type shock and large region of separated flow commonly associated with laminar boundary layers do not occur. If this result is substantiated by further experiments, it will be of particular significance in work such as the present where some assumption has to be made about the nature of the shock system, and the assumption that the shock wave is a single wave leads to the greatest simplification.

The principal discrepancy between calculated pressure distributions and those measured with a turbulent boundary layer stems from the fact that the shock wave meets the airfoil surface at a station farther forward than calculated. The interferograms of figure 40 show that a substantial portion of the forward shift is due to a pronounced curvature of the shock wave near the airfoil. This suggests a comparison of the calculated shock positions with not only the positions observed at the airfoil surface but also at some distance, say a half chord length, away from the airfoil. The results of such a comparison with the data for turbulent boundary layers given in reference 35 are shown in figure 42. It can be seen that the calculated shock positions vary with M_o in a manner which parallels the experimental results at $z/c=0.5$ but not those at the airfoil surface. It is almost certain that the details of this phenomenon are greatly influenced by separation and by interaction of the shock wave and boundary layer, and are, hence, beyond the reach of separation-free potential theory for transonic flow. Since the pressure gradients and shock strength increase with airfoil thickness, it might be presumed that these effects would be greater for thick airfoils than for thin airfoils. An indication of such a trend is furnished by the pressure-distribution data of Göthert (ref. 38) for NACA 0006, 0009, 0012, 0015, and 0018 airfoils. Figure 43 shows a plot of the variation with ξ_o of the shock position at the surface of each of these airfoils. If the shock positions were changing in accord with the similarity rules of transonic flow theory, these results would all fall on a single curve. It can be seen, however, that this is not the case and that the shock moves rearward across the chord at a slower rate for the thick airfoils than for the thin ones. It appears, therefore, that at best, the calculated shock positions will only agree with those found experimentally for very thin airfoils.

[5] Results are also given in reference 35, although not for a Mach number of 0.88, in which the boundary layer is made turbulent by a wire stretched across the test section one chord length ahead of the leading edge. When these results are plotted in the form shown in figure 39, they fall about half way between the calculated results and those obtained with the half model mounted on a plate.

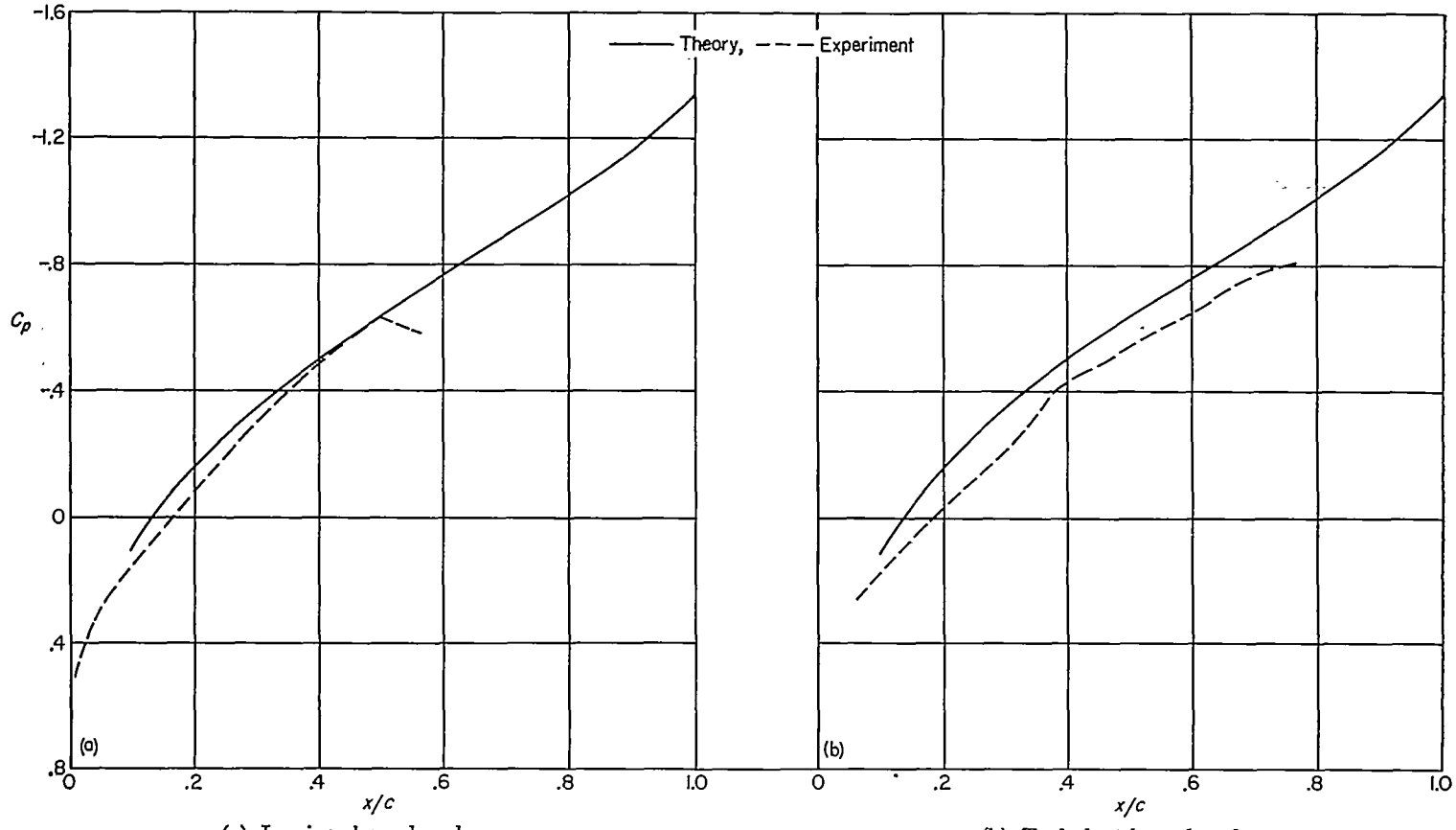

(a) Laminar boundary layer. (b) Turbulent boundary layer.

FIGURE 41.—Comparison of theoretical and experimental chordwise pressure distributions for a 12-percent-thick circular-arc airfoil at a Mach number of 0.88. Experimental data from reference 35 for a Reynolds number of 600,000.

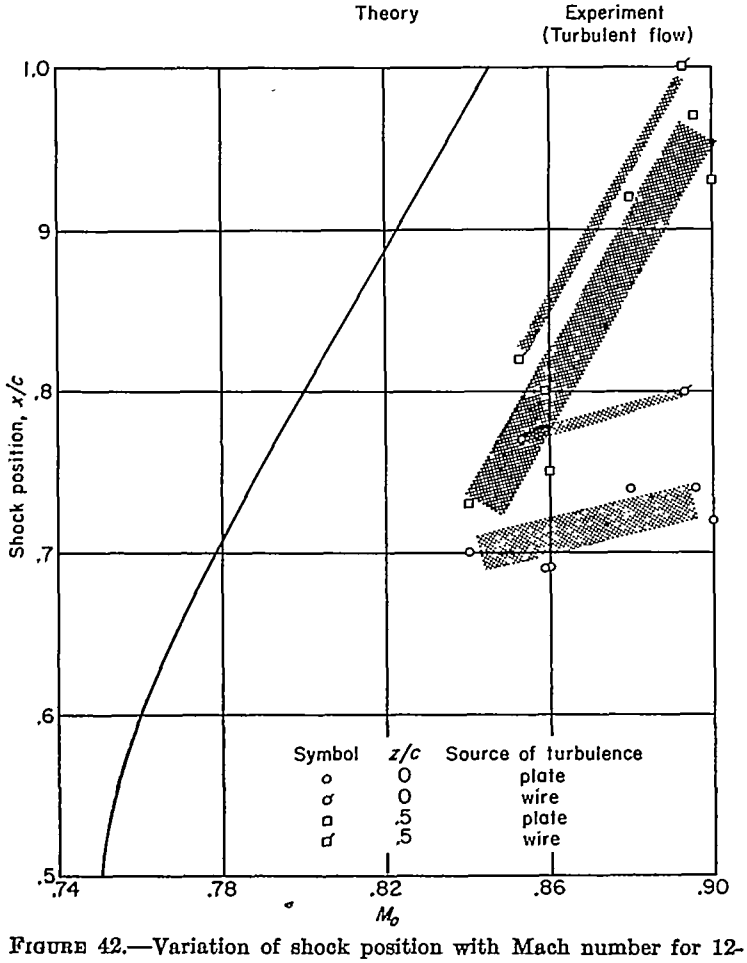

FIGURE 42.—Variation of shock position with Mach number for 12-percent-thick circular-arc airfoil.

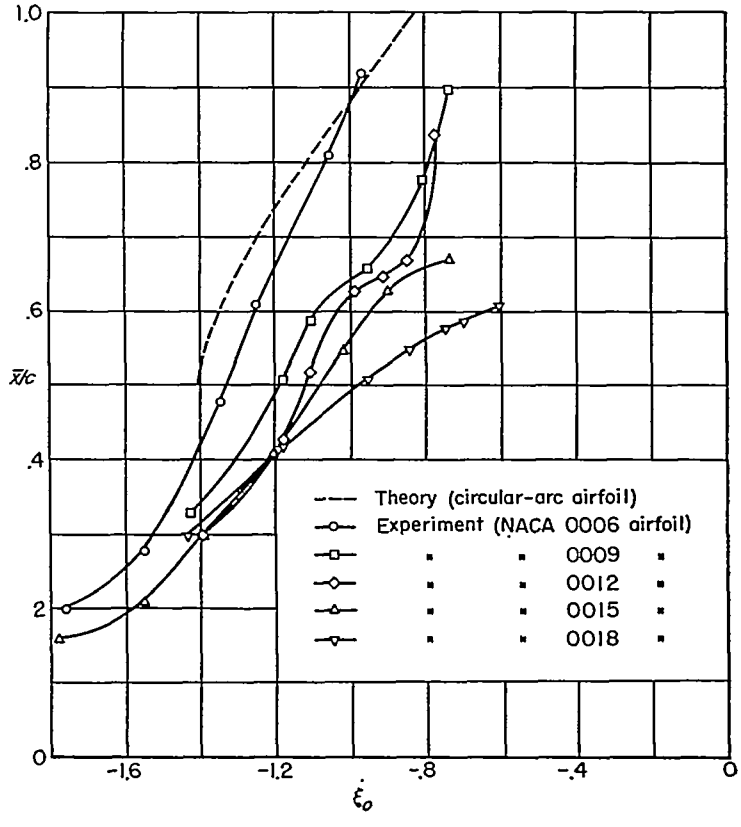

FIGURE 43.—Effect of thickness on shock position.

It is apparent that changes in the shock position will be accompanied, in many cases, by substantial changes in the pressure drag of the airfoil. In particular, the forward shift of the shock noted for the thick airfoils will diminish the region of high negative pressures on the rear of the airfoil, thereby decreasing the drag. These effects will, of course, be zero until the critical Mach number is exceeded, will increase as the shock moves across the airfoil, and may diminish somewhat again as sonic free-stream velocity is approached, since the actual, as well as calculated, shock position then approaches the trailing edge. These effects would probably alter the curve for the pressure drag of a thick airfoil so that it would appear somewhat like that illustrated in figure 44.

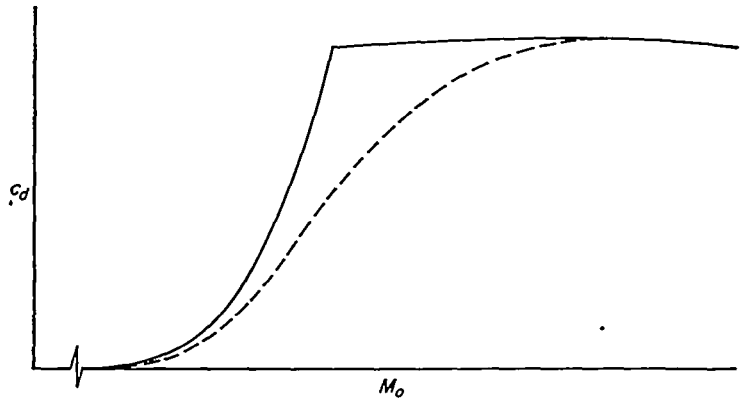

FIGURE 44.—Presumed drag results for a thick airfoil.

CONCLUDING REMARKS

The foregoing results are encouraging in that they show that the introduction of a small number of rough, although reasonable, assumptions leads to a relatively simple method for the calculation of pressure distributions on thin circular-arc airfoils at all Mach numbers up to unity. Perhaps the most important aspect of the present work is the recognition of the quadratic nature of the integral equation and the retention of this feature in the iteration solution. With the knowledge that acceptable results can be obtained without excessive effort, it appears worthwhile to re-examine the approximate solution of the equations with an eye toward improvement, or elimination, of the simplifying assumptions. Probably one of the weakest elements of the present method is the velocity-distribution function introduced in equation (63). This particular function is used to determine the entire flow field but, actually, only insures that the velocity and velocity gradient have the correct value at the airfoil surface and that the velocity diminishes toward zero at infinity as $1/z^2$. As can be seen by comparing the experimental and calculated results shown in figure 45, this function succeeds reasonably well for circular-arc airfoils. On the other hand, such a simple function cannot be expected to give good results for all airfoils. For instance, the present velocity-distribution function cannot be expected to provide good results for airfoils having flat surfaces over a substantial part of the chord (e. g., wedge airfoils, etc.) since it indicates no attenuation with distance above an element of the airfoil where the radius of curvature of the surface is infinite. Gullstrand (ref. 22) has proposed a different velocity-distribution function which satisfies one more known requirement, but it has not been established as yet whether or not it is sufficiently general to cover all interesting cases.

AMES AERONAUTICAL LABORATORY
NATIONAL ADVISORY COMMITTEE FOR AERONAUTICS
MOFFETT FIELD, CALIF., *Nov. 19, 1953*

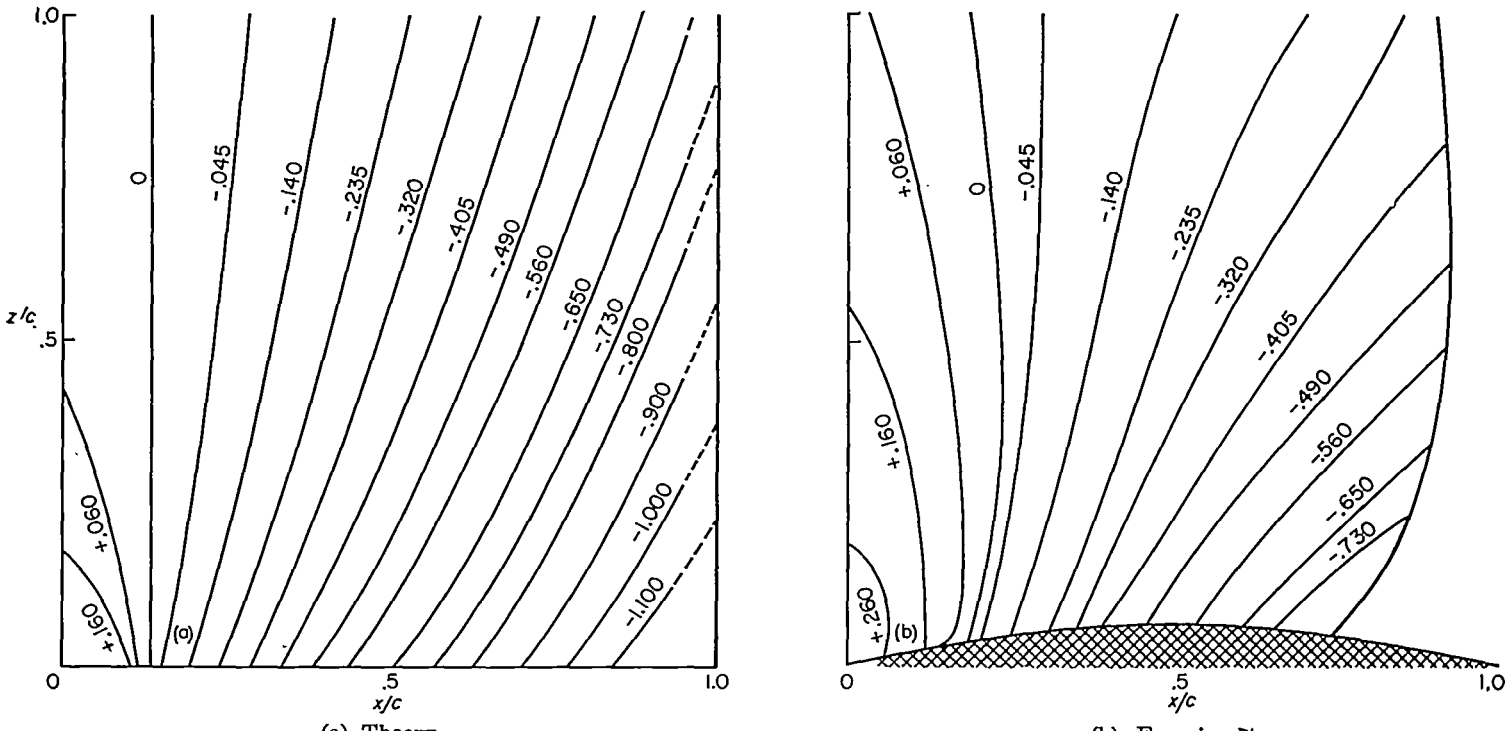

(a) Theory. (b) Experiment.

FIGURE 45.—Comparison of theoretical and experimental lines of constant C_p around a 12-percent-thick circular-arc airfoil at a Mach number of 0.88. Experimental data from reference 35 for Reynolds number of 600,000. Turbulent boundary layer.

APPENDIX A

PRINCIPAL SYMBOLS

a	speed of sound
a_o	speed of sound in the free stream
a^*	critical speed of sound
b	function defined in equations (63) and (64)
C_p	pressure coefficient, $\frac{p-p_o}{\frac{\rho_o}{2}U_o^2}$
$\overline{C_p}$	$\frac{(U_o k)^{1/3}}{(t/c)^{2/3}} C_p$
c	chord
c_d	section pressure drag coefficient, $\frac{d}{\frac{\rho_o}{2}U_o^2 c}$
$\overline{c_d}$	$\frac{(U_o k)^{1/3}}{(t/c)^{5/3}} c_d$
d	pressure drag
E	function defined in equation (67)
F	function defined in equation (71)
f_1	function defined in equations (72) and (73)
g_1	function defined in equations (76) and (77)
I	function defined in equations (57) and (58)
k	coefficient of nonlinear term of differential equation for φ (See eqs. (7), (17), (18), and (21).)
L	$2\bar{u}_L - 1$
l	width of element used in approximating the chordwise velocity distribution
M	local Mach number
M_{cr}	critical Mach number
M_o	free-stream Mach number
n	inward normal to surface enclosing R
P	arbitrary point x, y, z
p	static pressure
p_o	free-stream static pressure
R	region of integration
r_2	$\sqrt{(\bar{x}-\bar{\xi})^2+(\bar{z}-\bar{\zeta})^2}$
r_3	$\sqrt{(\bar{x}-\bar{\xi})^2+(\bar{y}-\bar{\eta})^2+(\bar{z}-\bar{\zeta})^2}$
S	surface of shock wave
s	wing semispan
t	maximum thickness of profile
U_o	free-stream velocity
u, v, w	perturbation velocity components parallel to x, y, z axes, respectively
$\bar{u}$	$\frac{k}{\beta^2}u$
$\bar{v}$	$\frac{k}{\beta^3}v$
$\bar{w}$	$\frac{k}{\beta^3}w$
$\tilde{u}, \tilde{v}, \tilde{w}$	Cartesian velocity components on the two sides of a shock wave, with $\tilde{u}$ being parallel to the flow direction ahead of the shock
X	$\frac{\bar{\xi}-\bar{x}}{b}$
x, y, z	Cartesian coordinates where x extends in the direction of the free-stream velocity
$\bar{x}$	x
$\bar{y}$	βy
$\bar{z}$	βz
Z	ordinates of wing profiles
$\overline{Z}$	$\frac{kU_o}{\beta^3}Z$
β	$\sqrt{1-M_o^2}$
γ	ratio of specific heats, for air $\gamma=1.4$
Δ	difference between values of quantity on the upper and lower sides of the xy plane
$\bar{\xi}, \bar{\eta}, \bar{\zeta}$	variables of integration corresponding to $\bar{x}, \bar{y}, \bar{z}$
ξ_o	$-\frac{1-M_o^2}{[U_o k(t/c)]^{2/3}}$
ξ	$-\frac{1-M^2}{[U_o k(t/c)]^{2/3}}$
ρ_o	free-stream density of air
Σ	surface enclosing volume R
$\bar{\tau}$	$\frac{kU_o}{\beta^3}\frac{t}{c}$
Φ	velocity potential
φ	perturbation velocity potential
$\bar{\varphi}$	$\frac{k}{\beta^2}\varphi$
ψ	$\frac{1}{r_3}\frac{\partial^2}{\partial\bar{\xi}^2}\left(\frac{\bar{u}^2}{2}\right)$

Subscripts

a	values ahead of shock wave
b	values behind shock wave
cr	conditions associated with the critical Mach number
L	values given by linear theory
LE	leading edge
l	values on the lower surface of wing or wake
$M_o=1$	values at $M_o=1$
P	values at arbitrary point P
S	values along shock wave
TE	trailing edge
u	values on the upper surface of wing or wake
W	values at the wing surface

413672—57——17

APPENDIX B

DISCUSSION OF CERTAIN PROPERTIES OF THE QUADRATIC ITERATION METHOD

INTRODUCTION

The present results are obtained using an iteration process which differs from that of previous workers in that the quadratic nature of the integral equation is recognized and retained throughout the analysis. This appendix is concerned with an investigation of certain properties of the two methods and a discussion of the applicability of each method to transonic-flow problems. Certain other problems will be avoided by confining attention to symmetrical nonlifting wings with sufficiently smooth entries at leading and trailing edges that there are no stagnation points.[1] Methods of handling stagnation points are discussed in references 39 and 40.

The fundamental relations for the following discussion, equations (41) and (43), can be written in the following more abbreviated form

$$\bar{u}=\bar{u}_L-I_1 \tag{B1}$$

$$\bar{u}=\bar{u}_L+\frac{\bar{u}^2}{2}-\frac{I_2}{2} \tag{B2}$$

where I_1 and I_2 refer to the integrals over R and S in equations (41) and (43), respectively, and $\bar{u}_L$ is the linear-theory solution given by equation (42). As is evident from the derivation in the text, equations (B1) and (B2) are totally equivalent since the latter is derived from the former by partial integration such that

$$I_1=\frac{I_2}{2}-\frac{\bar{u}^2}{2} \tag{B3}$$

Since methods for inverting, or solving, nonlinear integral equations such as equations (B1) and (B2) are not known, the present analysis, in common with many previous analyses, seeks an approximate solution by iteration. These methods proceed, in general, by substituting a known function for $\bar{u}$ into the integrals, integrating, and solving the resulting algebraic equation for a new approximation for $\bar{u}$, which is in turn substituted into the integrals, etc. The procedure employed in the present analysis differs from that traditionally employed in that it is based on equation (B2) rather than equation (B1). The most obvious difference between the two procedures is that the algebraic equation to solve for the new $\bar{u}$ is linear in the traditional analysis and quadratic in the present analysis. Although solutions of equations (B1) and (B2) must actually be identical, it is shown in equations (91) through (94) that this is not always the case for the results indicated by a partially completed iteration calculation. Since the linear iteration method is accepted universally for purely subsonic flow, and by some for mixed flows, it is important that we examine the relation between the results of the two procedures in greater detail.

SHOCK-FREE FLOW

Shock-free flow will be considered first. The integrals I_1 and I_2 are then simply

$$I_1=\frac{1}{4\pi}\iiint_R \frac{1}{r_3}\frac{\partial^2}{\partial\bar{\xi}^2}\left(\frac{\bar{u}^2}{2}\right)d\bar{\xi}\,d\bar{\eta}\,d\bar{\zeta} \tag{B4}$$

$$I_2=2\left[\frac{1}{4\pi}\iiint_R \frac{\bar{u}^2}{2}\frac{\partial^2}{\partial\bar{\xi}^2}\left(\frac{1}{r_3}\right)d\bar{\xi}\,d\bar{\eta}\,d\bar{\zeta}\right] \tag{B5}$$

and will be designated $I_1(\bar{u}^2)$ and $I_2(\bar{u}^2)$ to call attention to the fact that they involve the square of $\bar{u}$. The linear-theory solution $\bar{u}_L$ has the form

$$\bar{u}_L=\bar{\tau}a_1(\bar{x},\bar{y},\bar{z})=a_1\bar{\tau} \tag{B6}$$

where a_1 is a known function. Both the linear and quadratic iteration procedures can be started by letting $\bar{u}=0$ and designating this approximation by $\bar{u}_0$.

The results for successive iteration steps using the linear iteration method are determined by solving

$$\bar{u}_{n+1}=\bar{u}_L-I_1(\bar{u}_n^2) \tag{B7}$$

In this way we obtain

$$\bar{u}_0=0$$

$$\bar{u}_1=\bar{u}_L=a_1\bar{\tau}$$

$$\bar{u}_2=\bar{u}_L-I_1(\bar{u}_1^2)=\bar{u}_L-\bar{\tau}^2I_1(a_1^2)=a_1\bar{\tau}+a_2\bar{\tau}^2$$

$$\bar{u}_3=\bar{u}_L-I_1(\bar{u}_2^2)=a_1\bar{\tau}+a_2\bar{\tau}^2+a_3\bar{\tau}^3+0(\bar{\tau}^4)$$

. . . . . .

$$\bar{u}_n=\sum_{n=1}^{n}a_n\bar{\tau}^n+0(\bar{\tau}^{n+1}) \tag{B8}$$

where $a_n=a_n(\bar{x},\bar{y},\bar{z})$ are functions of the wing geometry, and ultimately therefore of a_1. This procedure has the interesting property that one and only one additional term in the power series expansion for $\bar{u}$ is determined in its final form with each iteration step. That is

$$\bar{u}_n=\bar{u}_{n-1}+a_n\bar{\tau}^n+0(\bar{\tau}^{n+1}) \tag{B9}$$

Note that a single expression is obtained for all Mach numbers and thickness ratios, and that the magnitudes of these parameters are reflected solely in the value for $\bar{\tau}$. The principal question concerns the range of convergence of the series. It is evident that the series cannot continue to converge as M_o approaches unity because $\bar{\tau}$ approaches infinity, but the precise bound on the radius of convergence is difficult to establish at this point.

The results for successive iteration steps using the quadratic method are determined by solving

$$\bar{u}_{n+1}-\frac{\bar{u}_{n+1}^2}{2}=\bar{u}_L-\frac{I_2(\bar{u}_n^2)}{2} \tag{B10}$$

Thus

$$\bar{u}_{n+1}=1\pm\sqrt{1-2\bar{u}_L+I_2(\bar{u}_n^2)}$$
$$=1\pm\sqrt{1-\chi_n} \tag{B11}$$

where

$$\chi_n=2\bar{u}_L-I_2(\bar{u}_n^2)$$

and

$$\chi_n<1$$

if $\bar{u}_{n+1}$ is to remain real. The minus sign is associated with local velocities that are subsonic and the plus sign with those that are supersonic. This result can be made more nearly comparable with the power series representation provided by the linear iteration method by expanding the radical of equation (B11) under the assumption that $|\chi_n|<1$, whereby we obtain

$$\bar{u}_{n+1}=1\pm\left[1-\frac{1}{2}\chi_n-\frac{1}{2}\left(\frac{1}{4}\right)\chi_n^2-\right.$$
$$\left.\frac{1}{2}\left(\frac{1}{4}\right)\left(\frac{3}{6}\right)\chi_n^3-\frac{1}{2}\left(\frac{1}{4}\right)\left(\frac{3}{6}\right)\left(\frac{5}{8}\right)\chi_n^4-\ldots\right] \tag{B12}$$

Consider first purely subsonic flow. Then successive iterations yield the following results

$$\bar{u}_0=0$$

$$\bar{u}_1=\bar{u}_L+0(\bar{u}_L^2)=a_1\bar{\tau}+0(\bar{\tau}^2)$$

$$\bar{u}_2=\bar{u}_L-\frac{I_2(\bar{u}_1^2)}{2}+\frac{\bar{u}_L^2}{2}+0(\bar{u}_L^3)=\bar{u}_L-I_1(\bar{u}_n^2)+0(\bar{u}_L^3)$$
$$=a_1\bar{\tau}+a_2\bar{\tau}^2+0(\bar{\tau}^3)$$

$$\ldots\ldots\ldots\ldots\ldots\ldots\ldots\ldots$$

$$\bar{u}_n=\sum_{n=1}^{n}a_n\bar{\tau}^n+0(\bar{\tau}^{n+1}) \tag{B13}$$

where the a_n have the same values as in equation (B8). This series and that given by equation (B8) are the same since they can be made to agree to any arbitrary number of terms. Thus the two methods lead to the same result for purely subsonic flow. Whereas there is some doubt about the range of convergence of equation (B8), it is clear that equation (B13) only applies to purely subsonic flow. This is evident, first of all, from the use of the minus sign in equation (B11). Moreover, since the series only converges for $|\chi_n|<1$, the largest value for $\bar{u}$ which can be represented by equation (B13) is unity. Since $\bar{u}$ equals unity when the local velocity is sonic, this result can be interpreted as indicating that equation (B8) converges for purely subsonic flow, but diverges for mixed flow.

There also exists a range in which the expression given in equation (B12) applies using the plus sign for certain regions of the flow field. The resulting series expansion for $\bar{u}$, however, does not lead to that given by equation (B8) or (B13), inasmuch as the first term is independent of $\bar{\tau}$.

FLOW WITH SHOCK WAVES

Although many of the general notions described for shock-free flow carry over into the analysis of transonic flows with shock waves, certain changes must be introduced. It is clear, for instance, that the linear iteration method cannot be used with the starting $\bar{u}$ distribution taken as zero or $\bar{u}_L$, because then equation (B8) would be reproduced and no discontinuities or shock waves would ever appear. On the other hand, it might seem reasonable to suppose that a successful iteration calculation could be accomplished using a starting $\bar{u}$ distribution containing a shock wave and estimated to be close to the correct solution. This is, in fact, what is done in the present analysis, but using the quadratic, rather than linear, iteration method. Although, as shown in the preceding section, there is no essential difference between the results of the two iteration methods in the subcritical range, the quadratic method emerges as definitely superior when the free-stream Mach number approaches unity. Its decisive advantage lies in the fact that small errors in the estimated $\bar{u}$ distribution lead only to finite errors in the calculated $\bar{u}$ as M_o approaches unity, whereas infinite errors can result from the calculations performed by the linear iteration method. The means by which small errors can be magnified in the linear iteration process can be seen by examining equation (B1) together with the definition of $\bar{u}$ and $\bar{u}_L$.

$$\bar{u}=\frac{k}{\beta^2}u;\qquad \bar{u}_L=\frac{k}{\beta^2}u_L$$

Thus equation (B1) can be rewritten as follows:

$$u=u_L-\bar{I}_1$$

where

$$\bar{I}_1=\frac{\beta^2}{k}I_1$$

Now, as M_o approaches unity, u remains finite but u_L approaches infinity. The largest values of u_L are attained on the airfoil surface where u_L approaches infinity as $1/\beta$ in two-dimensional flow and $\ln\beta$ in three-dimensional flow. This means, in the linear iteration method, that the desired solution u must be determined from the small difference between two large numbers. Since $\bar{I}_1$ is only evaluated approximately in an iteration method by substituting a function for u which differs from the exact function by a finite amount, it is apparent that very large or infinite errors may result as M_o approaches unity. On the other hand, equation (B2), which is used in the quadratic iteration method, can be rewritten as follows:

$$\frac{\beta^2}{k}u-u^2=\frac{\beta^2}{k}u_L-\frac{\bar{I}_2}{2}$$

where

$$\bar{I}_2=\frac{\beta^4}{k^2}I_2$$

Now in this case the term containing u_L becomes indefinitely small compared with u^2 as the Mach number approaches unity, and only finite errors result when an approximation is substituted for u in I_2.

REFERENCES

1. Oswatitsch, K., und Wieghardt, K.: Theoretische Untersuchungen über stationäre Potentialströmungen und Grenzschichten bei hohen Geschwindigkeiten. Lilienthal-Gesellschaft für Luftfahrtforschung, Bericht S 13/1d, 1942, S. 7–24. (Also available as NACA TM 1189, 1948)
2. Busemann, A., and Guderley, K. Gottfried: The Problem of Drag at High Subsonic Speeds. British Ministry of Aircraft Production, Völkenrode, Rep. and Trans. No. 184, Mar. 1947.
3. Guderley, K. Gottfried: Considerations of the Structure of Mixed Subsonic-Supersonic Flow Patterns. Tech. Rep. F–TR–2168–ND, AAF, Air Materiel Command, Wright Field, 1947.
4. Guderley, K. Gottfried: On the Transition from a Transonic Potential Flow to a Flow with Shocks. Tech. Rep. F–TR–2160–ND, AAF, Air Materiel Command, Wright Field, Aug. 1947.
5. von Kármán, Theodore: The Similarity Law of Transonic Flow. Jour. Math. and Phys., vol. XXVI, no. 3, Oct. 1947, pp. 182–190.
6. Kaplan, Carl: On Similarity Rules for Transonic Flows. NACA Rep. 894, 1948. (Supersedes NACA TN 1527)
7. Berndt, S. B.: Similarity Laws for Transonic Flow Around Wings of Finite Aspect Ratio. KTH Aero TN 14, Royal Inst. Tech., Stockholm, Sweden, 1950.
8. Oswatitsch, K., and Berndt, S. B.: Aerodynamic Similarity at Axisymmetric Transonic Flow Around Slender Bodies. KTH Aero TN 15, Royal Inst. Tech., Stockholm, Sweden, 1950.
9. Spreiter, John R.: Similarity Laws for Transonic Flow About Wings of Finite Span. NACA TN 2273, 1951.
10. Busemann, Adolf: Application of Transonic Similarity. NACA TN 2687, 1952.
11. Harder, Keith C.: Transonic Similarity Rules for Lifting Wings. NACA TN 2724, 1952.
12. Spreiter, John R.: On the Application of Transonic Similarity Rules. NACA Rep. 1153, 1953 (Supersedes TN 2726)
13. Guderley, Gottfried, and Yoshihara, Hideo: The Flow Over a Wedge Profile at Mach Number 1. Jour. Aero. Sci., vol. 17, no. 11, Nov. 1950, pp. 723–735.
14. Vincenti, Walter G., and Wagoner, Cleo B.: Transonic Flow Past a Wedge Profile With Detached Bow Wave—General Analytical Method and Final Calculated Results. NACA TN 2339, 1951.
15. Guderley, Gottfried, and Yoshihara, Hideo: Two-Dimensional Unsymmetric Flow Patterns at Mach Number 1. Jour. Aero. Sci., vol. 20, no. 11, Nov. 1953.
16. Cole, Julian D.: Drag of Finite Wedge at High Subsonic Speeds. Jour. Math. and Phys., vol. 30, no. 2, July 1951, pp. 79–93.
17. Trilling, Leon: Transonic Flow Past a Wedge at Zero Angle of Attack. Z. a. M. P., vol. IV, Fasc. 5, Sept. 1953.
18. Vincenti, Walter G., and Wagoner, Cleo B.: Theoretical Study of the Transonic Lift of a Double-Wedge Profile With Detached Bow Wave. NACA TN 2832, 1952.
19. Kaplan, Carl: A Review of Approximate Methods in Subsonic Compressible Flow. NACA-University Conference on Aerodynamics, 1948.
20. Oswatitsch, K.: Die Geschwindigkeitsverteilung bei lokalen Überschallgebieten an flachen Profilen. Zeitschrift für Angewandte Mathematik und Mechanik, Bd. 30, Nr. 1/2, Jan./Feb. 1950, S. 17–24.
21. Oswatitsch, K.: Die Geschwindigkeitsverteilung an symmetrischen Profilen beim Auftreten lokaler Überschallgebiete. Acta Physica Austriaca, Bd. 4, Nr. 2–3, Dec. 1950, S. 228–271.
22. Gullstrand, Tore R.: The Flow Over Symmetrical Aerofoils without Incidence in the Lower Transonic Range. KTH Aero TN 20, Royal Inst. Tech., Stockholm, Sweden, 1951.
23. Gullstrand, Tore R.: The Flow Over Symmetrical Aerofoils without Incidence at Sonic Speed. KTH Aero TN 24, Royal Inst. Tech., Stockholm, Sweden, 1952.
24. Gullstrand, Tore R.: A Theoretical Discussion of Some Properties of Transonic Flow Over Two-Dimensional Symmetrical Aerofoils at Zero Lift with a Simple Method to Estimate the Flow Properties. KTH Aero TN 25, Royal Inst. Tech., Stockholm, Sweden, 1952.
25. Gullstrand, Tore R.: The Flow Over Two-Dimensional Aerofoils at Incidence in the Transonic Speed Range. KTH Aero TN 27, Royal Inst. Tech., Stockholm, Sweden, 1952.
26. Sauer, Robert: Introduction to Theoretical Gas Dynamics. J. W. Edwards, Ann Arbor, 1947.
27. Liepmann, H. W., and Puckett, A. E.: Introduction to Aerodynamics of a Compressible Fluid. John Wiley & Sons, Inc., New York, 1947.
28. Liepmann, H. W., and Bryson, A. E., Jr.: Transonic Flow Past Wedge Sections. Jour. Aero. Sci., vol. 17, no. 12, Dec. 1950, pp. 745–755.
29. Bryson, Arthur Earl, Jr.: An Experimental Investigation of Transonic Flow Past Two-Dimensional Wedge and Circular-Arc Sections Using a Mach-Zehnder Interferometer. NACA TN 2560, 1951.
30. Heaslet, Max. A., and Lomax, Harvard: The Use of Source-Sink and Doublet Distributions Extended to the Solution of Arbitrary Boundary Value Problems in Supersonic Flow. NACA Rep. 900, 1948. (Formerly NACA TN 1515)
31. Busemann, Adolf: The Drag Problem at High Subsonic Speeds. Jour. Aero. Sci., vol. 16, no. 6, June 1949, pp. 337–344.
32. Hantzsche, W., und Wendt, H.: Der Kompressibilitätseinfluss für dünne wenig gekrümmte Profile bei Unterschallgeschwindigkeit. Z. a. M. M., Bd. 22, Nr. 2, Apr. 1942, S. 72–86.
33. Liepmann, H. W.: The Interaction Between Boundary Layer and Shock Waves in Transonic Flow. Jour. Aero. Sci., vol. 13, no. 12, Dec. 1946.
34. Liepmann, H. W., Ashkenas, Harry, and Cole, Julian D.: Experiments in Transonic Flow. Tech. Rep. No. 5667, Air Materiel Command, U. S. Air Forces, Feb. 1948.
35. Wood, George P., and Gooderum, Paul B.: Investigation With an Interferometer of the Flow Around a Circular-Arc Airfoil at Mach Numbers Between 0.6 and 0.9. NACA TN 2801, 1952.
36. Ackeret, J., Feldmann, F., und Rott, N.: Untersuchungen an Verdichtungsstössen und Grenzschichten in schnell bewegten Gasen. Mitteilungen aus dem Institut für Aerodynamik. Nr. 10, Zurich 1946. (Also available as NACA TM 1113, 1947.)
37. Harrin, Eziaslav N.: A Flight Investigation of the Effect of Shape and Thickness of the Boundary Layer on the Pressure Distribution in the Presence of Shock. NACA TN 2765, 1952.
38. Göthert, B.: Druckverteilungs und Impulsverlustschaubilder für das Profil NACA 0 00 06 (bis 0 00 18)—1,130 bei hohen Unterschallgeschwindigkeiten. FB 1505/1 bis 5, 1941. (Also available as Tech. Trans. TT–25 through 29, Nat. Research Council of Canada, 1947.)
39. Van Dyke, Milton D.: Subsonic Edges in Thin-Wing and Slender-Body Theory. NACA TN 3343, 1954.
40. Lighthill, M. J.: Higher Approximations. Sec. E of General Theory of High Speed Aerodynamics. Vol. VI of High Speed Aerodynamics and Jet Propulsion, W. R. Sears, ed., Princeton Univ. Press, 1954.